การสังเคราะห์อนุภาคแม่เหล็กที่เคลือบด้วยพอลิสไตรีนซึ่งดัดแปรด้วย
2-(3-(2-แอมิโนเอทิลไทโอ)โพรพิลไทโอ)เอทานามีนสำหรับสกัดไอออนปรอทและเงิน

นายคุณาวุฒิ ใจแน่

วิทยานิพนธ์นี้เป็นส่วนหนึ่งของการศึกษาตามหลักสูตรปริญญาวิทยาศาสตรมหาบัณฑิต
สาขาวิชาปิโตรเคมีและวิทยาศาสตร์พอลิเมอร์
คณะวิทยาศาสตร์ จุฬาลงกรณ์มหาวิทยาลัย
ปีการศึกษา 2552

SYNTHESIS OF POLYSTYRENE-COATED MAGNETIC PARTICLES MODIFIED

WITH 2-(3-(2-AMINOETHYLTHIO)PROPYLTHIO)ETHANAMINE FOR

EXTRACTION OF Hg(II) AND Ag(I) IONS

Mr. Kunawoot Jainae

A Thesis Submitted in Partial Fulfillment of the Requirements

for the Degree of Master of Science Program in Petrochemistry and Polymer Science

Faculty of Science

Chulalongkorn University

Academic Year 2009

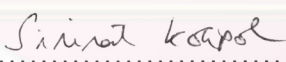|	
Thesis Title	SYNTHESIS OF POLYSTYRENE-COATED MAGNETIC PARTICLES MODIFIED WITH 2-(3-(2-AMINOETHYLTHIO) PROPYLTHIO)ETHANAMINE FOR EXTRACTION OF Hg(II) AND Ag(I) IONS
By	Mr. Kunawoot Jainae
Field of Study	Petrochemistry and Polymer Science
Thesis Advisor	Assistant Professor Fuangfa Unob, Ph.D.
Thesis Co-Advisor	Nipaka Sukpirom, Ph.D.

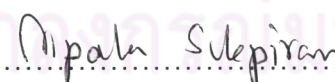Accepted by the Faculty of Science, Chulalongkorn University in Partial Fulfillment of the Requirements for the Master's Degree

………………………………………… Dean of the Faculty of Science
(Professor Supot Hannongbua, Dr.rer.nat.)
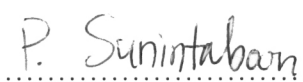
THESIS COMMITTEE

………………………………………… Chairman
(Associate Professor Sirirat Kokpol, Ph.D.)

………………………………………… Thesis Advisor
(Assistant Professor Fuangfa Unob, Ph.D.)

………………………………………… Thesis Co-Advisor
(Nipaka Sukpirom, Ph.D.)

………………………………………… Examiner
(Assistant Professor Warinthorn Chavasiri, Ph.D.)

………………………………………… External Examiner
(Panya Sunintaboon, Ph.D.)

คุณาวุฒิ ใจแน่ : การสังเคราะห์อนุภาคแม่เหล็กที่เคลือบด้วยพอลิสไตรีนซึ่งดัดแปรด้วย 2-(3-(2-แอมิโนเอทิลไทโอ)โพรพิลไทโอ)เอทานามีนสำหรับสกัดไอออนปรอทและเงิน. (SYNTHESIS OF POLYSTYRENE-COATED MAGNETIC PARTICLES MODIFIED WITH 2-(3-(2-AMINOETHYLTHIO)PROPYLTHIO)ETHANAMINE FOR EXTRACTION OF Hg(II) AND Ag(I) IONS) อ.ที่ปรึกษาวิทยานิพนธ์หลัก: ผศ.ดร. เฟื่องฟ้า อุ่นอบ, อ.ที่ปรึกษาวิทยานิพนธ์ร่วม: อ.ดร.นิปกา สุขภิรมย์, 167 หน้า.

สังเคราะห์ตัวดูดซับไอออนปรอท(II) และเงิน(I) จากอนุภาคแม่เหล็กโคบอลต์เฟอร์ไรท์ และเคลือบด้วยพอลิสไตรีนที่สังเคราะห์ด้วยปฏิกิริยาอะตอมทรานสเฟอร์แรดิคัลพอลิเมอไรเซชัน เพื่อเพิ่มความอยู่ตัวของอนุภาคแม่เหล็กในสารละลายที่มีภาวะเป็นกรดสูง จากนั้นดัดแปรพื้นผิว อนุภาคที่เคลือบด้วยพอลิสไตรีนด้วยลิแกนด์ 2-(3-(2-แอมิโนเอทิลไทโอ)โพรพิลไทโอ)เอทานามีน เพื่อเพิ่มประสิทธิภาพในการสกัดและความจำเพาะต่อไอออนปรอท(II) และเงิน(I) พิสูจน์เอกลักษณ์ ตัวดูดซับที่สังเคราะห์ได้ด้วยเทคนิคอินฟราเรด เทคนิคการเลี้ยวเบนของรังสีเอกซ์ เทคนิคการ เปลี่ยนแปลงน้ำหนักโดยอาศัยคุณสมบัติทางความร้อน เทคนิคกล้องจุลทรรศน์อิเล็กตรอนแบบ ส่องกราด และเทคนิคการตรวจวัดพื้นที่ผิว พบว่ามีพอลิสไตรีนและลิแกนด์บนพื้นผิวอนุภาค แม่เหล็ก ศึกษาปัจจัยที่มีผลต่อการสกัดไอออนโลหะทั้งสองชนิด เช่น พีเอชของสารละลาย เวลาใน การสกัด ความแรงไอออนและไอออนรบกวนในสารละลาย พบว่า พีเอชในช่วง 7 ถึง 8 และ 5 ถึง 8 เป็นภาวะที่เหมาะสมในการสกัดไอออนปรอท(II) และเงิน(I) ตามลำดับ เมื่อใช้เวลาในการสกัด เท่ากับ 60 นาที ความแรงไอออนและไอออนรบกวนในสารละลายไม่มีผลต่อการสกัด ยกเว้น ไอออนคลอไรด์ ไอโซเทอร์มของการดูดซับเป็นไปตามไอโซเทอร์มแบบแลงเมียร์ และ จลนพลศาสตร์การดูดซับเป็นไปตามจลนพลศาสตร์อันดับสองเทียม ค่าความจุการดูดซับสูงสุด สำหรับไอออนปรอท(II) และเงิน(I) เท่ากับ 0.42 และ 0.44 มิลลิโมลต่อกรัม ตามลำดับ ไอออนปรอท (II) และเงิน(I)ที่ถูกดูดซับสามารถชะออกได้โดยใช้ไทโอยูเรีย 0.5 และ 1.0 โมลต่อลิตรใน 1 เปอร์เซ็นต์กรดไนตริก ตามลำดับ เมื่อใช้เวลาในการชะเท่ากับ 60 นาที ตัวดูดซับที่สังเคราะห์ได้ให้ ประสิทธิภาพการสกัดไอออนเงิน(I)สูงสุดในครั้งแรกของการสกัด ขณะที่สามารถใช้ในการสกัด ไอออนปรอท(II)ได้อย่างน้อย 10 ครั้งโดยประสิทธิภาพการสกัดยังไม่เปลี่ยนแปลง นอกจากนี้พบว่า ตัวดูดซับสามารถสกัดไอออนปรอท(II) และเงิน(I)ในน้ำตัวอย่างจริงได้

สาขาวิชา ปิโตรเคมีและวิทยาศาสตร์พอลิเมอร์ ลายมือชื่อนิสิต ....

ปีการศึกษา 2552 ลายมือชื่อ อ.ที่ปรึกษาวิทยานิพนธ์หลัก ....

ลายมือชื่อ อ.ที่ปรึกษาวิทยานิพนธ์ร่วม ....

507 22274 23 : MAJOR PETROCHEMISTRY AND POLYMER SCIENCE

KEY WORD : MAGNETIC PARTICLES / ATOM TRANSFER RADICAL POLYMERIZATION

EXTRACTION / Hg(II) / Ag(I)

KUNAWOOT JAINAE: SYNTHESIS OF POLYSTYRENE-COATED MAGNETIC PARTICLES MODIFIED WITH 2-(3-(2-AMINOETHYLTHIO)PROPYLTHIO) ETHANAMINE FOR EXTRACTION OF Hg(II) AND Ag(I) IONS. THESIS ADVISOR: ASST.PROF. FUANGFA UNOB, Ph.D., THESIS CO-ADVISOR: NIPAKA SUKPIROM, Ph.D., 167 pp.

A new adsorbent for mercury(II) and silver(I) extraction from aqueous solution was prepared using cobalt ferrite magnetic particles. To improve the stability of the particles in acidic solution, the cobalt ferrite particles were coated with polystyrene via atom transfer radical polymerization. The ligand 2-(3-(2-aminoethylthio)propylthio)ethanamine (AEPE) was further grafted on the polystyrene-coated particles to improve the extraction efficiency and selectivity toward Hg(II) and Ag(I) ions. The obtained adsorbents were characterized by Fourier transform infrared spectroscopy, X-ray diffraction spectroscopy, thermogravimetric analysis, scanning electron microscopy and surface area analysis. The results from characterization indicated the presence of the desired molecules on the magnetic particles surface. The extraction efficiency of adsorbent was evaluated using batch method. The effect of solution pH, extraction time, ionic strength and coexisting ions were investigated. The optimal pH for Hg(II) and Ag(I) extraction were pH 7-8 and pH 5-8, respectively, using the extraction time of 60 minutes. The ionic strength and coexisting ions in solution did not affect the extraction efficiency, except for chloride ions. The adsorption isotherm and adsorption kinetics for the two metals followed Langmuir isotherm and pseudo-second order kinetics, respectively. The maximum adsorption capacities were 0.42 and 0.44 mmol g^{-1} for Hg(II) and Ag(I), respectively. The suitable eluent for the desorption of Hg(II) and Ag(I) were 0.5 M thiourea in 1% HNO_3 and 1.0 M thiourea in 1% HNO_3, respectively, using the elution time of 60 minutes. The adsorbent gave the highest extraction efficiency for Ag(I) extraction only for the first time application. On the other hand, the adsorbent could be used to extract Hg(II) at least 10 times. Moreover, the adsorbent could also extract Hg(II) and Ag(I) ions in real wastewater samples.

Field of Study : Petrochemistry and Polymer Science Student's Signature _Kunawoot Jainae_

Academic Year 2009 Advisor's Signature _Fuangfa Unob_

Co-Advisor's Signature _Nipaka Sukpirom_

ACKNOWLEDGEMENTS

CONTENTS

LIST OF TABLES

Table   page

LIST OF FIGURES

LIST OF SCHEMES

LIST OF SYMBOLS AND ABBREVIATIONS

AEPE	2-(3-(2-Aminoethylthio)propylthio)ethanamine
ATRP	Atom transfer radical polymerization
BET	Brunauer, Emmett, Teller
°C	Degree Celsius
CVAAS	Cold vapor atomic absorption spectroscopy
FAAS	Flame atomic absorption spectrometry
FT-IR	Fourier transforms infrared spectroscopy
GPC	Gel permeation chromatography
HCL	Hallow cathode lamp
MPs	Magnetic particles
MPs-Ini	Initiator-grafted magnetic particles
MPs-PS	Polystyrene-coated magnetic particles
MPs-PS-AEPE	Polystyrene-coated magnetic particles modified with 2-(3-(2-Aminoethylthio)propylthio)ethanamine
M_s	Saturation magnetization
NMR	Nuclear magnetic resonance spectroscopy
OSET	Outer-sphere electron-transfer
PMDETA	*N,N,N,N′,N′*-pentamethyldiethylanetriamine
SEM	Scanning electron microscopy
TGA	Thermogravimetric analysis
XRD	X-ray diffraction spectrometry
s	Singlet (^{1}H-NMR spectrum)
t	Triplet (^{1}H-NMR spectrum)
θ	Theta

CHAPTER I

INTRODUCTION

1.1 Statement of the Problem

Various metals and their compounds have been involved in the production process and in the industrial activities in Thailand. Mercury is almost used in petroleum industry, electricity, paper production and as amalgam material for dental restoration. Silver is used in electronic, batteries and silver jewelry industry. These industries are important for the economy of the country, but they could also cause the environmental problems, such as the contamination of these heavy metal ions in water which is one of the serious environmental problems. The heavy metals, especially mercury, in water resource are harmful to human life even at low concentration. Furthermore, several metals such as silver and gold are considered as precious metal of high economic value. Therefore, the extraction of mercury ions and the recovery of silver ions from wastewater are necessary.

There are several methods for extraction and recovery of heavy metals from wastewater such as chemical precipitation, coagulation, ion exchange, solvent extraction and extraction with various adsorbents such as clay [1], silica gel [2-3], activated carbon [4-5], resins [6-7] and magnetic particles [8-10]. Recently, the extraction with adsorbents is widely used to recover heavy metal ions from wastewater. Among the widely studied adsorbents, magnetic particles have drawn a lot of interest due to their high surface area, high temperature resistance, ion exchange mechanism and good dispersion in both aqueous and organic solvents. The hydroxyl groups on the magnetic particles surface could be used to extract the metal ions via ion

exchange mechanism [11-12]. However, the disadvantages of the magnetic particles when used as adsorbent to extract heavy metal ions are the low stability in acidic solution and low selectivity toward the metal ions. To overcome these disadvantages, the surface of magnetic particles is coated with polymer and subsequently modified with chelating ligand to increase the stability in acid and the selectivity for soft heavy metals e.g. Hg and Ag.

In this thesis, synthesized magnetic particles were coated with polystyrene via atom transfer radical polymerization (ATRP) and modified with 2-(3-(2-amino ethythio)propylthio)ethanamine (AEPE) to improve the extraction efficiency and selectivity toward mercury and silver ions due to the presence of both sulfur and nitrogen donor atoms in its structure that can extract mercury(II) and silver(I) ions via coordination.

1.2   Objectives of this thesis

The objectives of this research are listed below.

(1)   To synthesize and characterize a new adsorbent, the polystyrene-coated magnetic particles modified with 2-(3-(2-aminoethylthio)propylthio)ethanamine,

(2)   To study the effect of extraction parameters in order to obtain the suitable condition in Hg(II) and Ag(II) extraction,

(3)   To apply the synthesized adsorbent to extract mercuric(II) and silver(I) ions in real water sample.

1.3   Scope of this thesis

$CoFe_2O_4$ magnetic particles are synthesized via co-precipitation. The initiator is synthesized and grafted on magnetic particles surface. Then, the polymerization of polystyrene on the surface of magnetic particles is performed via atom transfer radical polymerization. Finally, the chelating ligand (AEPE) is synthesized and functionalized on the polymer coating of the particles.

The ligand is characterized by nuclear magnetic resonance spectrometer (NMR). The polystyrene-coated magnetic particles modified with AEPE are characterized by Fourier transform infrared spectroscopy (FT-IR), X-ray diffraction spectroscopy (XRD), scanning electron microscope (SEM), thermogravimetric analysis (TGA), and surface area analysis. Finally, the polystyrene-coated and AEPE-modified magnetic particles are used as adsorbent in the extraction of mercuric(II) and silver(I) ions in aqueous solution using batch method.

In metal ions extraction, effect of pH of metal ions solution, extraction time, ionic strength, coexisting ions, adsorbent dose, eluent and elution time are studied for both metal ions. The adsorption isotherm and adsorption kinetics are investigated. Moreover, the adsorbent was applied to extract mercuric(II) and silver(I) ions in real water sample. The concentrations of mercury and silver ions in solution are determined by cold vapor atomic absorption spectrometer (CVAAS) and flame atomic absorption spectrometer (FAAS), respectively.

1.4   The benefits of this research

To obtain a novel adsorbent derived from magnetic particles that could be used as efficient adsorbent in the extraction of mercury(II) and the recovery of silver(I) ions in aqueous solution and real wastewater samples.

CHAPTER II

THEORY AND LITERATURE REVIEW

2.1 Magnetic material

The mixed-metal oxides of formula MFe_2O_4 (M: divalent metals) with cubic spinel structure are magnetic materials which have been extensively used in various applications in the past decades [13]. The magnetic structure is composed of two magnetic sublattice (called A and B) separated by oxygen atoms as shown in Figure 2.1. The magnetic moments of A and B sublattices are not equal resulting in a net magnetic moment. The oxygen atoms are close packed in a cubic arrangement and the smaller cations fill in the gaps. The gaps are classified in two types which are tetrahedral sites and octahedral sites, A and B, respectively. The spins on the A sublattices are antiparallel to those on the B sublattices resulting in the very difference of magnetic moment between the two crystal sites. The particular swap between cations on the A and B sublattices lead to an inverse spinel structure. By the A and B sublattices exchange interaction, the net magnetic moment depends on the B-site [13].
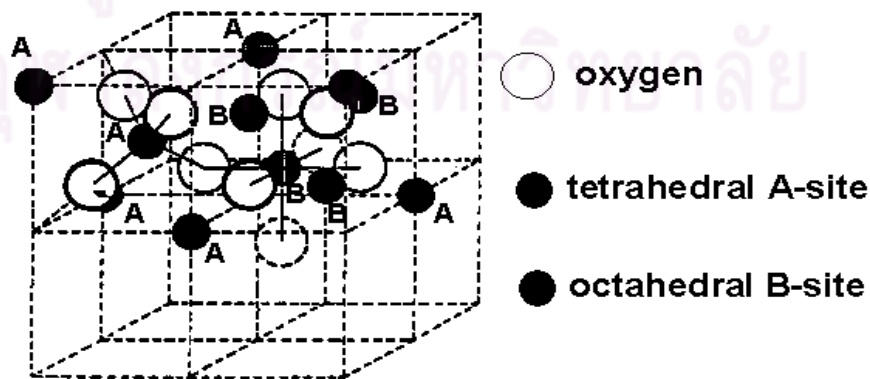
Figure 2.1 The two magnetic sublattices A and B of spinel magnetic material [13].

Magnetite (Fe_3O_4) is a well known magnetic material. Furthermore, it is considered as ferromagnetic until Néel provided the theoretical framework for understanding ferromagnetism in the 1940's [13]. The details of magnetic materials are described below.

2.1.1 Spinel structure of magnetic material

Spinel is the main structure of mixed-metal oxides, which has the general chemical composition of AB_2O_4. Normally, A is a divalent atom of radius between 80 and 110 pm, such as Mg, Fe, Mn, Zn, and Cu and B is a trivalent atom of radius between 75 and 90 pm, such as Ti, Fe, Al, and Co. The structure consists of a cubic closed-packed array of 32 oxide ions, which form 64 tetrahedral holes and 32 octahedral holes in one unit cell that contains eight formula units (($AB_2O_4)_8$) [14]. There are two types of sub-cells commonly described for the spinel structure. Figure 2.2a and 2.2b show occupied tetrahedral site and occupied octahedral site in spinel sub-cell, respectively. Structure 2.2a shows the filling of 2 tetrahedral sites within 1/8 of the unit cell and structure 2.2b shows a filled octahedral site. Spinel structure can be devided into two types: normal and inverse spinel. In a normal spinel structure of formula AB_2O_4 with A atoms in the tetrahedral sites and B atoms in the octahedral sites, all the trivalent cations are located in half the octahedral sites, while all the divalent cations occupy 1/8 of the tetrahedral sites. In contrast, the inverse spinel is an alternative arrangement where half of the trivalent cations swap with the divalent cations so that the divalent cations occupy octahedral sites. Therefore, the inverse spinels have half of B atoms in the tetrahedral sites and both A and half of B atoms in the octahedral sites. The formula of an inverse spinel is $B(AB)O_4$.
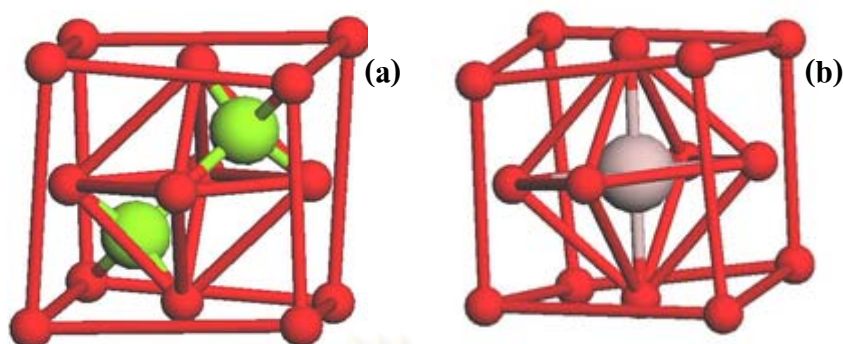
Figure 2.2 Occupied tetrahedral sites in spinel sub-cell A (a) and occupied octahedral site in spinel sub-cell B (b) [15].

2.1.2 Magnetite (Fe_3O_4)

The magnetite (Fe_3O_4) or ferrous ferrite is an inverse spinel magnetic material. The chemical IUPAC name is iron(II,III) oxide and the common chemical name is ferrous-ferric oxide. The formula of magnetite may also be written as $FeO \cdot Fe_2O_3$, which is one part wüstite (FeO) and one part hematite (Fe_2O_3). Cations are arranged with one Fe^{3+} per tetrahedral hole, and Fe^{2+} and the remaining Fe^{3+} randomly distributed in the octahedral holes. Therefore, half of the smaller cations (Fe^{3+}) place in the smaller tetrahedral sites while the larger Fe^{2+} cations in the larger octahedral sites [16]. The inverse structure of magnetite was first suggested with the fast electron hopping-continuous exchange of electrons between Fe^{2+} and Fe^{3+} in the octahedral positions [16]. It has been proposed recently that the magnetite structure should instead be described with $Fe^{2.5+}$ in the octahedral site at the ambient conditions to make the electron delocalization more obvious [17]. Figure 2.3 shows the inverse spinel structure of magnetite.
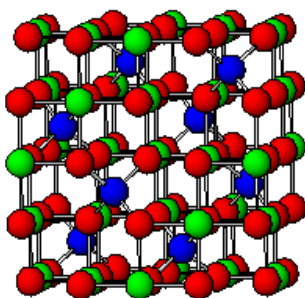
Figure 2.3 Inverse spinel structure of magnetite [15]. Red atoms represent oxygen, blue and green represent iron in different colors for tetrahedral and octahedral sites.

2.1.3 Cobalt ferrite

The cobalt ferrite ($CoFe_2O_4$) has an inverse spinel crystal structure. As mentioned previously, the normal crystal structure of spinel consists of the A^{2+} atoms occupying all of the tetrahedral coordination sites and the B^{3+} atoms occupying all of the octahedral sites [15]. In the case of an inverse spinel of $CoFe_2O_4$, the Co cations occupy a half of the octahedral coordination sites and Fe^{3+} cations occupy the other half of the octahedral coordination sites as well as all of the tetrahedral coordination sites. $CoFe_2O_4$ is a well-known hard magnetic material with high coercivity, great physical and chemical stability and moderate magnetization [18]. The crystal structure of $CoFe_2O_4$ is shown in Figure 2.4.
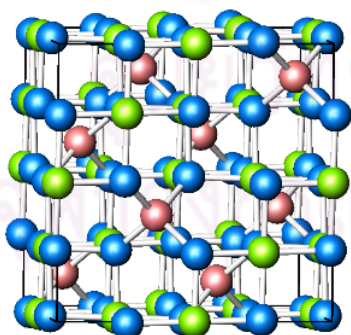
Figure 2.4 Inverse spinel structure of cobalt ferrite [15]. Green atoms are Co, pink atoms are Fe, and blue atoms are O.

Among various ferrites, $CoFe_2O_4$ is of particular interest because of its remarkable properties like high anisotropy constant ($2.65 \times 10^6 - 5.1 \times 10^6$ erg cm^{-3}) [19, 20], reasonable saturation magnetization ($M_s = 80$ emug^{-1}) [21], high

electromagnetic performance [22], excellent chemical stability, mechanical hardness, and high cubic magnetocrystalline anisotropy [23]. Different preparation techniques have been developed to produce $CoFe_2O_4$ particles, such as combustion reaction [24], microemulsion [25, 26], hydrothermal [27], thermal decomposition [28], polyol-process [29], and co-precipitation method [30, 31]. The co-precipitation technique is one of the most convenient and versatile methods [32].

2.1.4 Properties and advantages of magnetic particles

The use of magnetic particles offers a fast and efficient mean of separation the particles from the supernatant. The separation can be realized in a few minutes using commonly available lab magnets or external magnetic field. The special properties and advantages of the magnetic particles are listed below [33].

- They can be easily dispersed after attraction to a magnetic field.
- The particles are compatible with both aqueous and organic solutions.
- They have uniform surface area for coatings.
- They provide high capacity of functional groups after functionalization.

Regarding their properties and advantages, magnetic particles are used in various applications. Magnetic particles are commonly used as the primary material in jewelry worn for the controversial alternative medicine practice of magnet therapy [34]. Furthermore, magnetic particles can be applied as adsorbents or used as solid support to prepare the selective functionalized adsorbents. On the other hand, magnetic particles have some drawback such as the easy dissolution in acidic solution. In this study, this problem was solved by coating polystyrene on the magnetic particles surface via atom transfer radical polymerization (ATRP).

2.2   Atom transfer radical polymerization [35, 36]

Atom transfer radical polymerization (ATRP) is a controlled/"living" polymerization system. ATRP is based on a reversible transfer of halogen atom between a low concentration of growing radicals and a dormant species. Reactivation of the dormant species allows the polymer chains to grow and deactivate again. The overall reaction of ATRP is shown in Figure 2.5. The radical formation occurs when transition metal catalyst activates the organic initiator or dormant species by abstracting the halide at the chain end. The control of the polymerization afforded by ATRP is a result of the formation of radicals that can grow, but are reversibly deactivated to form dormant species. Reactivation of the dormant species allows the polymer chains to grow again, only to be deactivated later. Under appropriate conditions, the contribution of termination is small. This process results in a polymer chain that slowly but steadily grows and has a well-defined end group which usually is an alkyl halide. The initiator is generally a simple and commercially available alkyl halide. The catalyst is a transition metal that is complexed by one or more ligands. The catalyst does not need to be used in a one-to-one ratio with the initiator but can be used in a much smaller amount. The deactivator can be formed in situ, or for better control, a small amount (relative to the catalyst) can be added. Additionally, the catalyst is tolerant of water and trace amounts of oxygen. By ATRP, polymers with controlled molar masses and small polydispersities can be obtained. ATRP is capable of polymerizing wide variety of monomers and is tolerant of trace impurities, thus ATRP is readily applicable to industrial processes.

$$k_{act}$$

R-X $\;+\;$ M$_t^n$-Y/Ligand $\;\rightleftharpoons\;$ R$\cdot$ $\;+\;$ X-M$_t^{n+1}$-Y/Ligand

$$k_{deact}$$

organic initiator $\qquad$ metal catalyst $\qquad\qquad$ k$_p$ $\qquad\qquad\qquad$ termination

monomer
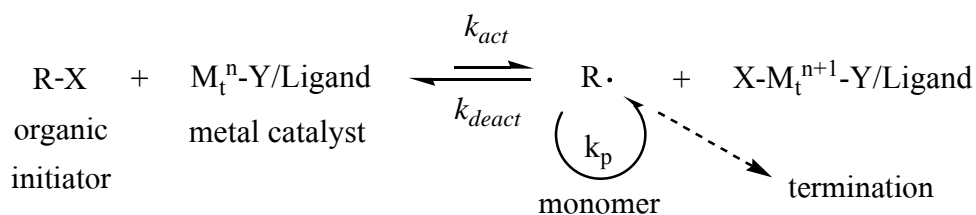
R-X $=$ dormant species

R$\cdot$ $=$ active species

k$_{act}$ $=$ rate constant of forward activation reaction

k$_{deact}$ $=$ rate constant of reverse deactivation reaction

k$_p$ $=$ rate constant of propagation in ATRP

Figure 2.5 The overall reaction of atom transfer radical polymerization (ATRP) [36].

2.3 Components of atom transfer radical polymerization [36]

As a multicomponent system, ATRP is composed of monomer, initiator with a transferable halogen atom and catalyst which is a complex of a transition metal species with a suitable ligand. For the success of ATRP, the other factors such as solvent and temperature must be used suitably in the reaction.

2.3.1 Monomers

A variety of monomers have been polymerized by ATRP such as styrene, acrylate, acrylamide, acrylonitrile and their derivatives containing substituents that can stabilize the propagating radicals [37, 38]. Even under the same condition, each monomer has its own unique atom transfer equilibrium constant for its active and dormant species. In the absence of side reactions other than radical polymerization, the equilibrium constant ($K_{eq} = k_{act}/k_{deact}$) determines the polymerization rate. ATRP occurs

slowly if the equilibrium constant is low. In contrast, the too high equilibrium constant will lead to the large extent of termination because of high radical concentration. Each monomer possesses its own intrinsic radical polymerization rate. Therefore, for each monomer, the radicals should have suitable concentration and the rate of radical deactivation should be adjusted to maintain polymerization control. For each monomer, the initiator and catalyst used should not cause the too fast deactivation reaction. Various monomers have been successfully polymerized using ATRP.

2.3.1.1 Styrene

ATRP of styrene and its derivatives has been commonly performed by using copper-mediated catalyst system [39]. One of the most extensively used system is the polymerization of styrene conducted at $110^{\circ}C$ with $CuBr(dNbpy)_2$ (dNbpy = 4,4'-di(5-nonyl)-2,2'-bipyridine) as catalyst and alkyl bromide as initiator. The reaction temperature can be decreased to 80-90°C to produce well-defined polystyrene by using more efficient catalyst such as CuBr/PMDETA (PMDETA = *N,N,N,N',N'*-pentamethyldiethylanetriamine) [40]. However, to maintain a sufficient large propagation rate and to increase the solubility of catalyst, the higher reaction temperature is applied in ATRP of styrene. The reaction can be carried out in bulk or using solution. The solvent that can dissolve monomer, initiator and metal complex catalyst is required. Therefore, the semi non-polar solvents are recommended for ATRP of styrenes.

2.3.1.2 Acrylates

The ATRP of acrylates has been commonly performed by the use of copper or ruthenium based catalyst systems [39, 41]. Copper appears to be more

efficient than other transition metals. The ATRP of acrylate produces the well-defined polyacrylates with low polydispersities in a short time due to the fast deactivation of the growing radicals by cupric halides.

The derivatives of acrylate with different side chains have been polymerized using ATRP (Figure 2.6). For example, the well-defined functional polymers were obtained by ATRP of 2-hydroxyethyl acrylate, glycidyl acrylate and *tert*-butyl acrylate.
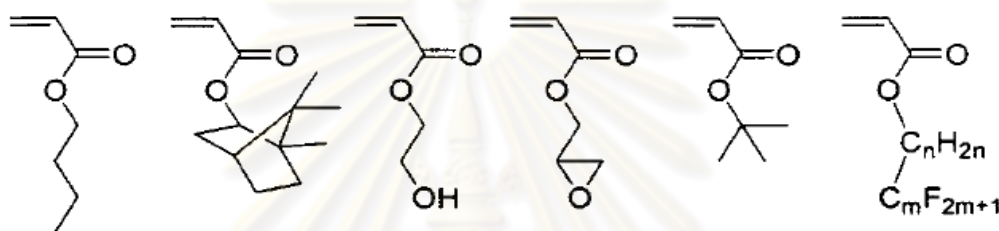
Figure 2.6 Various acrylate monomers that can be polymerized by ATRP [36].

2.3.1.3 Methacrylates

The ATRP of methyl methacrylate (MMA) can be performed by the use of various catalysts such as copper, ruthenium, nickel and palladium complexes [41-44]. Most polymerization reactions of MMA were carried out in solution at 70-80°C [36]. Solvents are necessary for the solubilization of the forming poly(methyl methacrylate) (PMMA), which has a glass transition temperature, $T_g > 100°C$. In addition, the polymerization solution helps to maintain the low concentration of growing radicals. Under comparable condition, the copper-mediated catalyst displays a significantly higher equilibrium constant in ATRP of MMA when compared to styrene. As a result, a higher dilution and a lower catalyst concentration should be used for the ATRP of MMA.

Moreover, the use of copper-mediated catalyst will give the sufficiently large rate constant of initiation (high atom transfer equilibrium constant) when use sulfonyl chlorides and 2-halopropionitrile as initiators [42, 45]. It should be noted that these initiators are active to copper-mediated catalyst and lead to excessive termination or other side reactions [46]. Figure 2.7 illustrates examples of the methacrylate monomers that can be polymerized by ATRP.
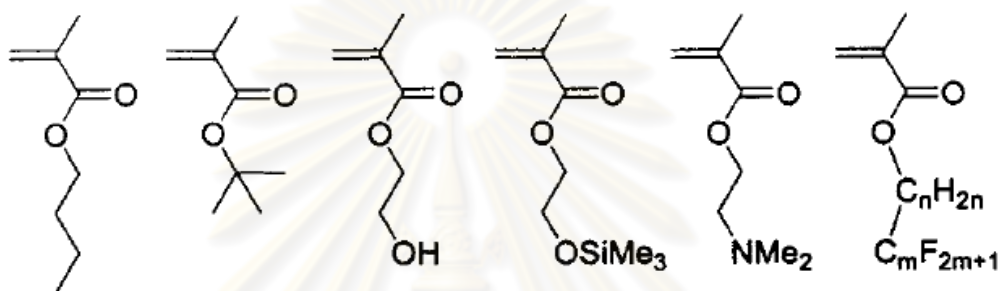
Figure 2.7 Various methacrylate monomers that can be polymerized by ATRP [36].

2.3.1.4 Acrylonitrile

The ATRP of acrylonitrile has been successfully performed only when copper-mediated catalyst is used [47, 48]. The solvents are required for the reaction because the polyacrylonitrile is not soluble in its monomer. The successful polymerizations have been carried out in ethylene carbonate using $CuBr(bpy)_2$ (bpy = bipyridine) complex as catalyst and 2-bromopropionitrile as initiator at the temperature range from 44 to 64 °C.

For this research, styrene was chosen to be polymerized and coated on the magnetic particles surface due to the high rigid structure, strength and good resistance to concentrated acid [49, 50].

2.3.2 Initiators

The main role of initiator is to determine the number of the growing polymer chains. If the initiation is fast and the transfer and the termination is negligible, then the number of growing chain is equal to the initiator concentration. In ATRP, alkyl halides (R–X) are commonly used as the initiator. The rate of ATRP is almost first order in respect to the concentration of alkyl halides. To obtain the narrow molecular weight distribution polymers, the halide groups (X) must migrate rapidly and selectively between the growing chain and the transition metal complex catalyst. The polymer molecular weight is well controlled when the alkyl bromide or alkyl chloride is used as initiator due to their good living group properties. Alkyl iodide works well for acrylate polymerization using copper-mediated catalysts [51]. Alkyl fluoride is not a suitable initiator because the C–F bond is too strong to undergo homolytic cleavage to generate radicals. Some functional groups acting as pseudo-halogen, such as thiocyanate and thiocarbamate, have been used successfully in the ATRP of acrylates and styrenes [51, 52].

The initiation should be fast and quantitative with a good initiator. In general, alkyl halide with the activating substituents on α-carbon such as aryl, carbonyl, or allyl group, can be used potentially as initiator in ATRP. The initiator with a weak R–X bond, such as N–X, S–X or O–X, can also be used [36]. When the initiating moiety is attached to macromolecular species, the macro initiators are formed and can be used to synthesize the block or graft copolymers.

However, not only the homolytic cleavage of the initiator, but also the heterolytic cleavage occurs depending mostly on the initiator structure and the choice of transition metal catalyst. For example, the side reactions are observed due to the oxidation of radical to carbocation leading to heterolytic cleavage [53]. Various types

of halogenated compound are efficient initiator and are discussed in detail in the following topics.

2.3.2.1 Halogenated alkanes

The halogenated alkanes are commonly used as initiator in ATRP. Tri-or tetrachloromethane are typically used as initiator in ATRP of MMA using the ruthenium-based catalyst. In contrast, di-or monochloromethane were not able to polymerize MMA under the same condition [54].

Tetrachloromethane has also been employed in other catalytic systems for ATRP of MMA including copper-mediated catalyst [39]. Furthermore, it has been used as a functional initiator in the ATRP of styrene at 130 $^\circ$C using CuCl(bpy)$_3$ as catalyst. In homogeneous system, tetrachloromethane is sometime less efficient due to a potential outer-sphere electron-transfer reaction (OSET) and the reduction of the radicals to anions. This problem can be solved by adding the catalyst slowly to the initiating system to improve the efficiency of initiation. Moreover, bromotrichloromethane initiated the ATRP of MMA successfully using ruthenium-based catalyst [55].

2.3.2.2 Benzylic halides

Benzyl-substituented halides are the useful initiators for the ATRP of styrene and its derivatives due to their structural resemblance. These initiators fail the ATRP of some more reactive monomers such as MMA. For example, the inefficient initiation was observed when used CuCl(dNbpy)$_2$ as catalyst and 1-phenylethylene chloride as initiator for ATRP of MMA [32]. To improve the initiation efficiency for ATRP of MMA, the use of primary and secondary benzylic halide is possible by

employing the halogen exchange concept [56]. Figure 2.8 illustrates some examples of halogenated alkanes and benzylic halides used as initiator in ATRP.
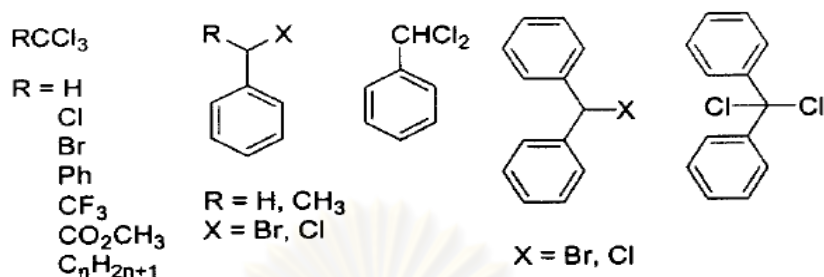
Figure 2.8 Some halogenated alkanes and benzylic halides used in ATRP [36].

2.3.2.3 Sulfonyl halides

Sulfonyl chlorides yield a much faster rate of initiation than monomer propagation [57], with the apparent rate constants of about four (for styrene and mathacrylate) and three (for acrylates) orders of magnitude higher than those of propagation. As a result, the well-controlled ATRP of a large number of monomers can be achieved in copper-mediated catalyst system [57, 58]. Furthermore, the end-functional polymers can be prepared by the use of sulfonyl chlorides containing aromatic ring as initiator [59]. The phenyl group substituent on sulfonyl halides has only a small effect on the rate constant of initiation because the sulfonyl radical and phenyl group are not related through conjugation [36].

A unique feature of the sulfonyl halides as initiators is that although the radicals are easily generated, they only dimerize slowly to form disulfone and slowly disproportionate [60]. Therefore, the sulfonyl halides can react with the monomers and initiate the ATRP efficiently.

In this research, the halogenated alkane synthesized from 3-aminopropyltriethoxysilane and ethyl-2-bromopropionate was used as initiator for the ATRP of styrene.

2.3.3 Catalysts

The catalyst is the most important component of the ATRP because it concerns the atom transfer equilibrium and the dynamics of the atom exchange between the dormant and active species. There are several necessary conditions for the efficient transition metal catalyst [36]. First, the metal center must have at least two oxidation states. Second, the metal center should have good affinity toward halogen atoms. Third, the coordination sphere around the metal should be expandable to selectively accommodate halogen atoms. Fourth, the ligand should complex strongly with the metal. Various types of transition metal complexes have been employed as catalyst in ATRP. To generate the growing radicals, the metal center should undergo an electron transfer reaction with the abstraction of a halogen and expansion of coordination sphere. In addition, to differentiate ATRP from the conventional redox-initiated polymerization and induce a controlled process, the oxidized transition metal should rapidly deactivate the propagating polymer chains to form the dormant species. The application of the different transition metal complexes is discussed in detail below.

2.3.3.1 Ruthenium

The Ruthenium complex was first reported for using as catalyst in the ATRP of MMA by Sawamato et al. in 1995 [61]. The polymerization was carried out by using tetrachloromethane as initiator and $RuCl_2$ complexed by three equivalents of PPh_3 as catalyst in toluene at 60 $^\circ$C.

The more reactive ruthenium-based catalysts have been reported by employing carbon-centered ligands such as 4-isopropyltoluene (*p*-cymene) [27], indenyl (Ind) [62] and cyclopentadienyl (Cp) [63]. A halogen-free Ru(II) hydride

complex such as $RuH_2(PPh_3)_4$ is more reactive than $RuCl_2(PPh_3)_4$ and can be used as catalyst for ATRP at or above room temperature [64]. Some Ruthenium-based catalysts are illustrated in Figure 2.9.
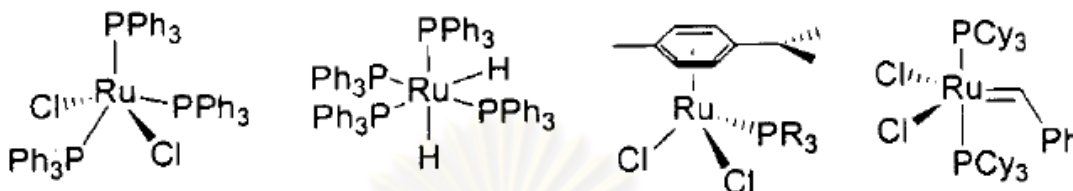
Figure 2.9 Ruthenium complexes used as ATRP catalysts [36].

2.3.3.2 Nickel

Most of nickel complexes are used as catalyst for the ATRP of MMA. However, they have relatively low efficiency [65]. More reactive catalyst of $Ni[(CH_2NMe_2)_2C_6H_3]Br$ named as Ni(NCN)Br was used, but it initially failed to promote the ATRP of styrene due to its instability at high temperature [66]. By lowering the reaction temperature, Ni(NCN)Br was successfully applied to the ATRP of MMA.

The nickel halides complexed by the phosphorus ligands such as $NiBr_2(PPh_3)_2$ have also been used for the ATRP of MMA, however, it is not stable or soluble in organic solvents. Decomposition of the metal complex catalyst was observed after prolonged use at high temperature and the rate of polymerization decreased with time. Other nickel complex catalysts have also been employed. $NiBr_2(N\cdot nBu_3)_2$ is more thermally stable and soluble than $NiBr_2(PPh_3)_2$ and leads to the controlled ATRP of both methacrylate and acrylate [67]. Figure 2.10 illustrates the example of nickel complexes used as ATRP catalysts.
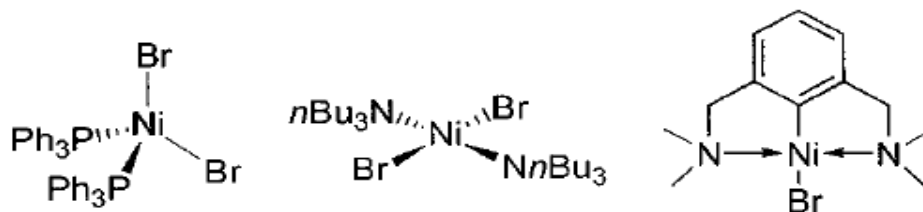
Figure 2.10 Nickel complexes used as ATRP catalysts [36].

2.3.3.3 Copper

The copper-mediated catalysts have been successfully employed in ATRP of styrene, acrylate and acrylonitrile [37, 38, 68]. The cuprus halide complexed by three molecules of bipyridine was the first copper-based catalyst used in ATRP [69].

Various polydentate ligands have been used for copper-mediated catalyst. The use of both linear [40] and branched [69] polydentate aliphatic amines as ligand greatly reduced the cost of catalyst and increased dramatically the rate of the ATRP. Copper(I) prefers a tetrahedral or square planar configuration which can be achieved in the cationic complexes using tetradentate ligands or two bidentate ligands. Tridentate ligands presumably form neutral complexes.

For the ATRP process, the copper complexes are widely used as catalyst due to the versatility and low cost. The examples of copper complexes are illustrated in Figure 2.11.
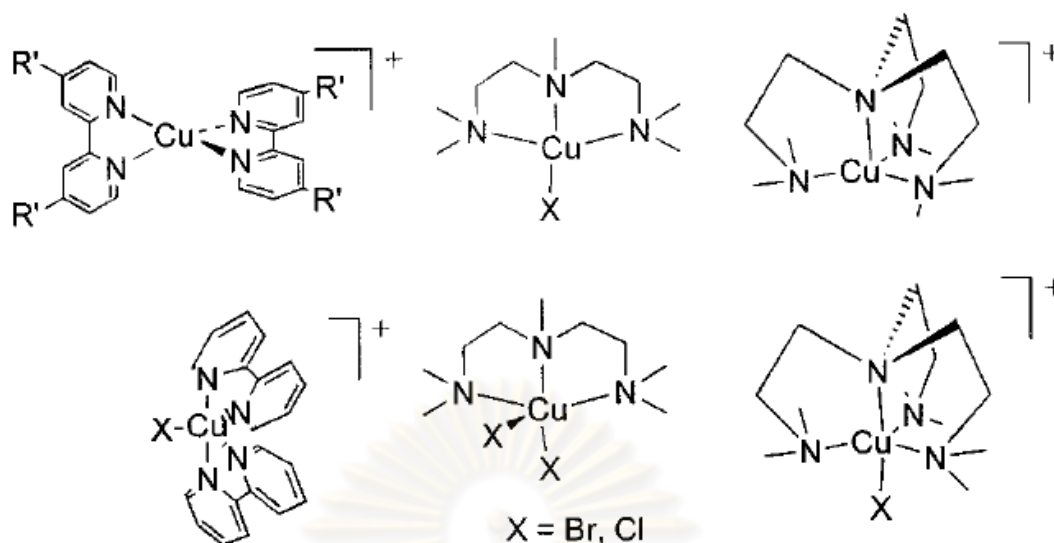
Figure 2.11 Copper complexes used as ATRP catalysts [36].

2.3.4 Ligands

The main role of the ligands in ATRP is to increase the solubility of the transition metal salt in the organic media and to adjust the redox potential of the metal center to the appropriate reactivity and dynamics for the atom transfer [70]. Nitrogen and phosphorus ligands are commonly used in ATRP.

2.3.4.1 Nitrogen ligands

Nitrogen ligands work particularly well for copper-mediated ATRP catalyst. In contrast, phosphorus ligands are less effective due to inappropriate electronic effects. Although monodentate phosphorus ligands are suitable for most of transition metal salts, phosphorus ligands do not promote the controlled copper-mediated ATRP. In contrast, the polydentate nitrogen ligands have been successfully used [70]. The electronic and steric effects of nitrogen ligands are important. The

reduced catalytic activity or efficiency is observed when there is excessive steric hindrance around the metal center or the ligands has strongly electron-withdrawing substituents. The activity of the catalyst containing nitrogen ligands in ATRP decreases with the decrease of the number of coordinating sites: N4 > N3 > N2 ≥ N1, respectively. The examples of some nitrogen ligands used in copper-mediated ATRP are shown in Figure 2.12.
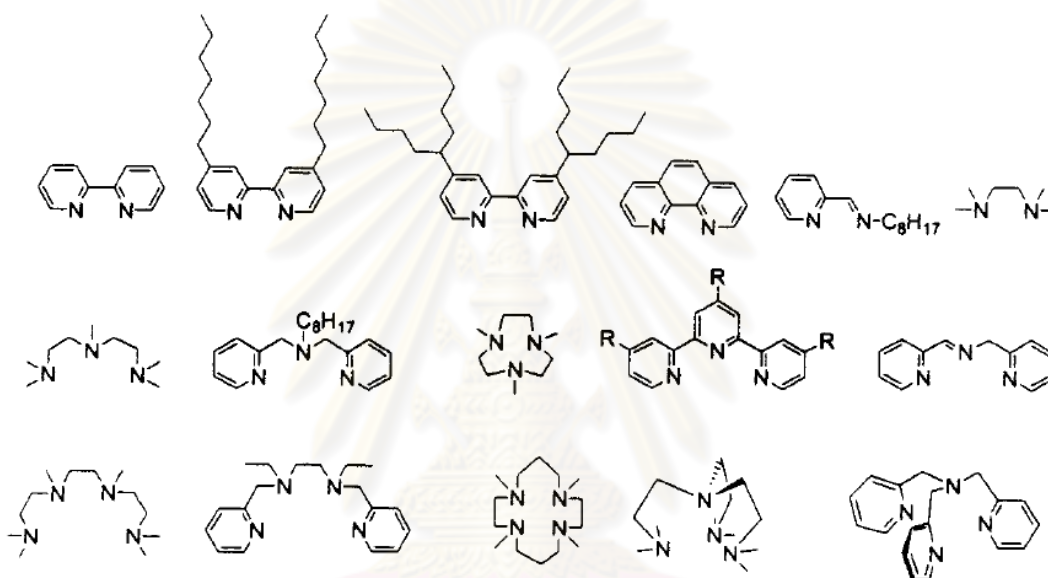
Figure 2.12 Example of nitrogen ligands used in copper-mediated ATRP [36].

2.3.4.2 Phosphorus ligands

Phosphorus ligands are used to form complexes with transition metals, including ruthenium [41], nickel [67] and palladium [44] with exception for copper. The ligand PPh_3 is the most commonly used ligand and has been successfully applied to coordinate all aforementioned transition metals. However, copper complexes and nitrogen ligands are more widely used when compared to other transition metals and phosphorus ligand.

In this research, copper (I) bromide and PMDETA nitrogen ligand (CuBr/PMDETA) were employed as catalyst due to the good compatibility and efficiency with styrene monomer.

2.3.5 Chain end functional polymers

One of the advantages of ATRP is the preservation of the end functional groups throughout the polymerization. If the termination and transfer are absent in ATRP, every polymer chains should contain halogen atoms at its headgroup. The halogen atoms can be replaced through the reactions resulting in the end functional polymer.

The terminal halogens on polymer can also be replaced by nucleophilic substitution, free-radical chemistry or electrophilic addition [36]. The first example of a chemical transformation of the halogen end groups involved bromo- and chloro-terminated polystyrene as shown in Figure 2.13 [71]. The nucleophilic substitution reaction with triethylsilyl azide yielded azide terminal polymer that was further reduced by lithium aluminium hydride to the primary amino-functionalized chain end polystyrene.
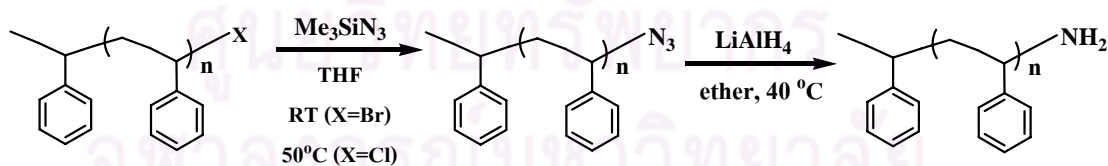
Figure 2.13 Synthesis reaction of end-functional polystyrene [71].

In this research, a chain end functional polystyrene was synthesized by nucleophilic substitution reaction with 2-(3-(2-aminoethylthio)propylthio)ethanamine (AEPE). The obtained functionalized material was used in the extraction of heavy metals.

2.4 Heavy metals in the environment

Heavy metals in the environment may come from their natural resource and from human activities, especially industrial activities. The contamination of heavy metals in water resource is a serious problem because they are toxic even in low concentration and harmful to plant, animal and human [72]. Furthermore, certain heavy metals are precious metals of high economic value. The best well-known precious metals are gold and silver. These metals are regarded as industrial commodities. Therefore, the extraction of toxic metals or recovery of precious metals from wastewater before releasing to the environment is necessary. In Thailand, the residual concentration of heavy metals in released water has to be in the acceptable value limited by the Pollution Control Department, PCD. The maximum acceptable concentration of heavy metals in drinking water and industrial wastewater are summarized in Table 2.1.

Table 2.1 The maximum acceptable concentration of heavy metal ions in drinking water and industrial wastewater [73]

Heavy metals	Maximum acceptable concentration (mg L^{-1})	
	Drinking water	**Industrial wastewater**
Arsenic	0.05	0.25
Cadmium	0.01	0.03
Copper	1.00	2.00
Chromium	0.05	0.75
Lead	0.05	0.20
Mercury	0.002	0.005
Silver	0.05	5.00

2.5   Information of metals

2.5.1 Mercury

Mercury is a chemical element with the symbol "Hg" and atomic number of 80. Mercury is one of six chemical elements that are in liquid form at or near room temperature and pressure. Mercury is the only metal that is in liquid form at standard temperature and pressure conditions. With a melting point of -38.83 °C and boiling point of 356.73 °C, mercury has one of the widest temperature ranges of its liquid state of any metal. Mercury is found in deposits throughout the world mostly as cinnabar (mercuric sulfide), which is the source of the red pigment, and elemental mercury is mostly obtained by reduction of cinnabar. Cinnabar is highly toxic when taken by ingestion or inhalation of the dust, and mercury poisoning can also be the result from the exposure to soluble forms (such as mercuric chloride or methyl mercury), inhalation of mercury vapor, or eating some contaminated food [74]. The forms or species of soluble inorganic mercury depend on the pH of solution. Figure 2.14 shows species of mercury at different pH of aqueous solution.

Mercury is used in thermometers, barometers, manometers, float valves and as amalgam material for dental restoration. Moreover, it is used in a number of applications in engineering, scientific research, electricity, industry, especially petrochemical industry.

The toxic effects of mercury depend on its chemical form and the route of exposure. Methyl mercury is the most toxic. It affects the immune system, alters genetic and enzyme systems, and damages the nervous system. Methyl mercury is particularly damaging the developing embryos, which are five to ten times more sensitive than adults. Exposure to methyl mercury is usually by ingestion, and it is absorbed more readily and excreted more slowly than other forms of mercury.

Elemental mercury (Hg^0) is released from broken thermometers and causes excitability when vapors are inhaled over a long period of time. Elemental mercury is less toxic than methyl mercury and may be found in higher concentrations in environment such as in gold mine sites, where it has been used to extract gold. If large amount of elemental mercury is ingested, it is absorbed relatively slowly and may pass through the digestive system without causing damage. Ingestion of other common forms of mercury, such as the salt $HgCl_2$, which is likely found in the environment, damages the gastrointestinal tract and causes kidney failure [75]. The well known danger of mercury is the Minamata disease.
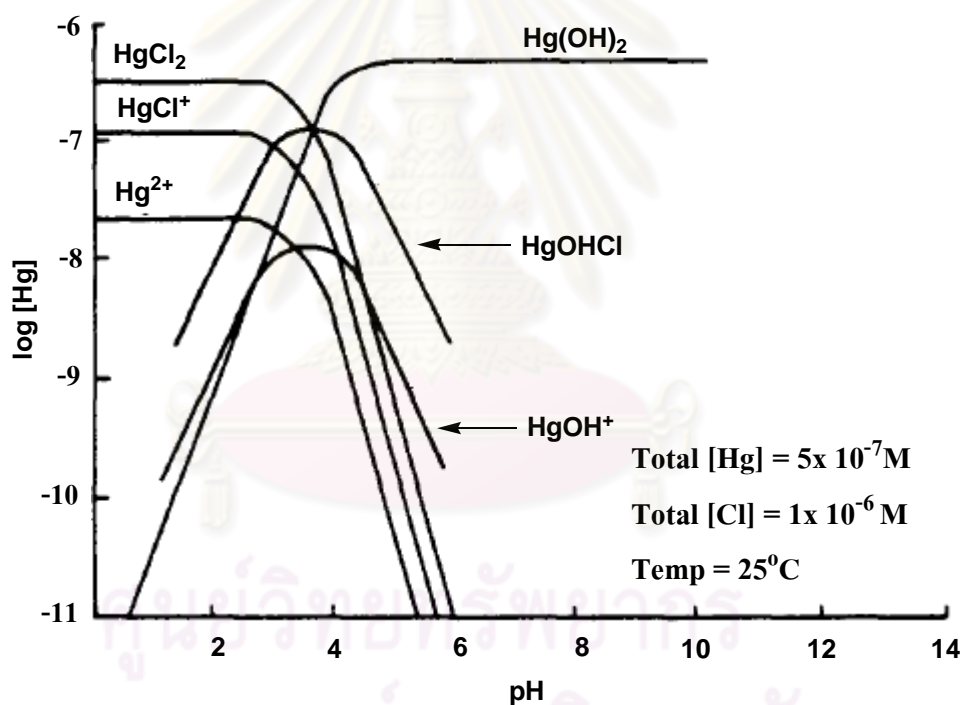
Figure 2.14 The diagram of mercury speciation as a function of aqueous solution pH [78].

2.5.1.1 Mercury in petroleum [77]

In petroleum industry, mercury is found in natural gas, condensates, crude oil, coal, tar sands and bitumens. Mercury compounds are found in various forms i.e. elemental, ionic and organometallic forms depending on the source. The elemental form is almost found in natural gas. In contrast, organomercury compounds are the predominant form of mercury in condensates and petroleum liquids.

The use of these products as fuels for the production, transportation and processing systems will result in the emission of the mercury to the environment. The mercury associated with petroleum and natural gas production and processing enters the environment primarily via drilling, combustion of fuels and release of refinery waste.

2.5.1.2 Source of mercury in environment [78]

Natural source

Mercury is found naturally in a free state or mixed in ores. It is also present in rocks. Generally, possible sources of mercury are degassing of the earth crust through emission and evaporation from the ocean.

Human activities

In the Gulf of Thailand, mercury is found in gas, condensate, coal and carbonaceous shale in or near the production reservoirs. One of the significant sources of mercury release is oil and gas operation. Nowadays, there is an increment of the number of platforms for oil and gas exploration and production in the Gulf, thereby leading to the increasing amount of mercury in the Gulf, which is immensely tied to the exploration, development, production and processing in oil and gas operation. The wastes

containing trace amount of mercury related to these activities are deemed as a source of mercury released to the environment. The other probable sources of mercury are hospitals, paint industries, fluorescence production and power plants.

2.5.2 Silver [79]

Silver is a chemical element with the chemical symbol "Ag" and atomic number of 47. It is a soft, white and lustrous transition metal and has the highest electrical conductivity of any element and the highest thermal conductivity of any metal, even higher than copper. Silver has oxidation number of 0, 1, 2 and 3. The Ag^0 and Ag^+ are the most common. Most silver is produced as a by-product of copper, gold, lead, and zinc refining.

Silver has long been valued as a precious metal, and it is used to produce jewelry, utensils, dental amalgam and currency coins. Nowadays, silver metal is used in electrical contacts and conductors, battery, mirrors and in catalysis of chemical reactions. Its compounds are employed in photographic film [80]. The silver waste that is released to the environment do not directly affect human health but it can cause allergic reactions of skin such as rashes, burning and swelling [81]. Furthermore, silver has been considered to be harmful to zooplankton, aquatic lives and mammals [80]. The forms or species of silver depend on inorganic ligand present in solutions and the pH of solution. Figure 2.15 shows species of silver at different pH of aqueous solution.
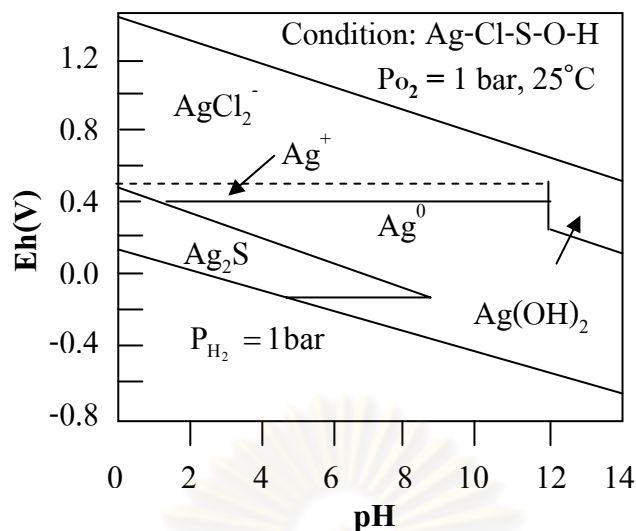
Figure 2.15 The diagram of silver speciation as a function of pH [79].

2.6 Chelation

The chelation mechanism occurs between the chelating ligand or electron donor atoms and the electron acceptor metals by coordination. The chelating ligand is a molecule that is capable of bonding to metal ion by donating a pair of electrons. Elements that act as electron donors are the more electronegative ones. Certain chelating ligands consist of electron donor atoms such as nitrogen, sulfur and oxygen and are summarized in Table 2.2

Table 2.2 Functional groups consisting of electron donor atoms

Electron donor atoms	Functional groups
nitrogen	amine, nitrile, imine
sulfur	thiol, thiocarbamate, thioether
oxygen	carboxylic, hydroxyl, carbonyl, phenolic

Pearson proposed that "hard acids bind strongly to hard bases and soft acids bind strongly to soft bases" [82]. These binding occur via ionic or covalent bond. In the case of borderline acids, which have intermediate characteristics, they possess affinity for both hard and soft bases. Table 2.3 shows the classification of hard-soft acids and hard-soft bases [82].

However, the binding ability between the metal ions in solution and the chelating ligands depends on various factors as following:

- Nature, charge and size of metal ions
- Nature of donor atoms present in ligand
- The pH of solution which may affect the extraction efficiency and the binding of metal ions by donor atoms

Table 2.3 The classification of hard-soft acids and hard-soft bases [82]

Acids	Bases
Hard	
H^+, Li^+, Na^+, K^+, Rb^+, Cs^+	NH_3, RNH_2, N_2H_4
Be^{2+}, $Be(CH_3)_2$, Mg^{2+}, Ca^{2+}, Sr^{2+}, Ba^{2+}	H_2O, OH^-, O^{2-}, ROH, RO^-, R_2O
Se^{3+}, La^{3+}, Ce^{3+}, Gd^{3+}, Lu^{3+}, Th^{3+}, U^{4+}, UO_2^{2+}, Pu^{4+}	
Ti^{4+}, Zr^{4+}, Hf^{4+}, VO^{2+}, Cr^{3+}, Cr^{6+}, MoO^{3+}, WO^{4+},	CH_3COO^-, CO_3^{2-}, NO_3^-, PO_4^{3-},
Mn^{2+}, Fe^{3+}, Co^{3+}	SO_4^{2-}, ClO_4^-
BF_3, BCl_3, $B(OR)_3$, Al^{3+}, $Al(CH_3)_3$, $AlCl_3$, AlH_3,	F^-, Cl^-
Ga^{3+}, In^{3+}	
CO_2, RCO^+, NC^+, Si^{4+}, Sn^{4+}, CH_3Sn^{3+}, $(CH_3)_2Sn^{2+}$	
N^{3+}, RPO_2^+, $ROPO_2^+$, As^{3+}	
SO_3, RSO_2^+, $ROSO_2^+$	
Cl^{3+}, Cl^{7+}, I^{5+}, I^{7+}	
HX (hydrogen-bonding molecules)	

Table 2.3 The classification of hard-soft acids and hard-soft bases (continued)

Acids	Bases
Borderline	
Fe^{2+}, Co^{2+}, Ni^{2+}, Cu^{2+}, Zn^{2+}	$C_6H_5NH_2$, C_5H_5N, N_3^-, N_2
Rh^{3+}, Ir^{3+}, Ru^{3+}, Os^{2+}	NO_2^-, SO_3^{2-}
$B(CH_3)_3$, GaH_3	Br^-
R_3C^+, $C_6H_5^+$, Sn^{2+}, Pb^{2+}	
NO^+, Sb^{3+}, Bi^{3+}	
SO_2	
Soft	
$Co(CN)_5^{3-}$, Pd^{2+}, Pt^{2+}, Pt^{4+}	H^-
Cu^+, Ag^+, Au^{3+}, Cd^{2+}, Hg^+, Hg^{2+}, CH_3Hg^+	R^-, C_2H_4, C_6H_6, CN^-, RNC, CO
BH_3, $Ca(CH_3)_3$, $GaCl_3$, $GaBr_3$, GaI_3, Tl^+, $Tl(CH_3)_3$	
CH_2, carbenes	SCN^-, R_3P, $(RO)_3P$, R_3As
π-acceptors: trinitrobenzene, chloroanil, etc.	R_2S, RSH, RS^-, $S_2O_3^{2-}$
HO^+, RO^+, RS^+, RSe^+, Te^{4+}, RTe^+	I^-
Br_2, Br^+, I_2, I^+, ICN,	
O, Cl, Br, I, N, RO, RO_2	
M^0 (metal atoms) and bulk metals	

2.7   Adsorption

Adsorption is the transferring process of substance from a fluid phase to a solid phase or the accumulation of atoms or molecules on the surface of a solid phase. This process creates a film of the adsorbate (the molecules or atoms being accumulated) on the adsorbent surface. It is a removal process where certain substances are bound to an adsorbent particle surface by either chemical or physical attraction [83]. The adsorption process is generally classified as physisorption and chemisorption. The amount of substance adsorbed depends on a number of factors including the degree of attraction, the surface area exposed to mobile substance, the concentration of the substance, and the pH and temperature of the liquid [84].

2.7.1 Physisorption

The physisorption or physical adsorption is referred to when the attraction between adsorbates and adsorbents are van der Waals force, generating from London dispersion force or the electrostatic force. Furthermore, the multilayer adsorption of adsorbates on the adsorbent surface can occur, when the concentration of adsorbates increases. The reaction of this adsorption is called outer-sphere surface reaction or non-specific reaction, which the analytes adsorb independently on the adsorbent surface and the adsorption is a reversible process. The reversibility of the reaction depends upon the attraction force of target ions or molecules with adsorbent, concentration of analytes and temperature. Figure 2.16 shows the outer-sphere surface reaction.

2.7.2 Chemisorption

The interaction between adsorbate and adsorbent in chemisorption or chemical adsorption is the chemical or covalent bond, which is stronger than van der Waals force in physisorption. The mechanism may occur when the surface of adsorbents has active sites specific to the target ions or molecules, resulting in irreversible reaction. The adsorption of analytes occurs in the monolayer regime on adsorbent surface. The chemical adsorption is also called inner-sphere surface reaction (Figure 2.16).
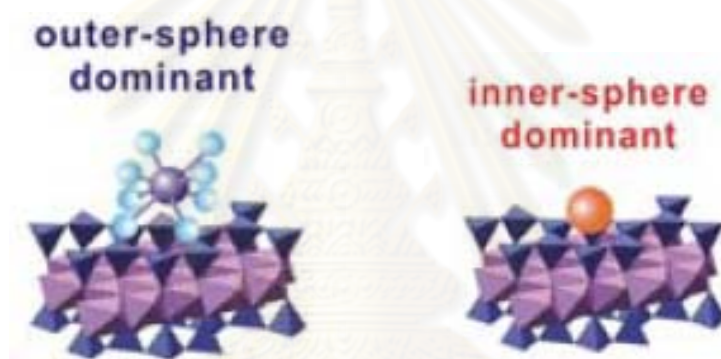
Figure 2.16 The outer-sphere (a) and inner-sphere (b) surface reaction [85].

The differences between physisorption and chemisorption are summarized in the Table 2.4.

Table 2.4 The differences between physisorption and chemisorption [86]

Parameters	Physisorption	Chemisorption
Enthalpy of adsorption	low (20 - 40 kJ mole^{-1})	high (200 - 400 kJ/mole^{-1})
Adsorption temperature	low	high
Forces of attraction	van der Waals forces	chemical bond
Types of process	reversible	irreversible
Layer of adsorption	mono and multilayer	monolayer

2.7.3 Rate of mass transfer

The adsorption occurs when the analytes in liquid or gas phase are transferred to adsorbent surface. The mass transfer is divided into three main steps as follows: (i) bulk transport, (ii) film transport and (iii) intraparticle transport. Figure 2.17 shows the steps of mass transfer. The step that controls the rate of mass transfer at adsorption equilibrium is the slowest step of adsorption mechanism.
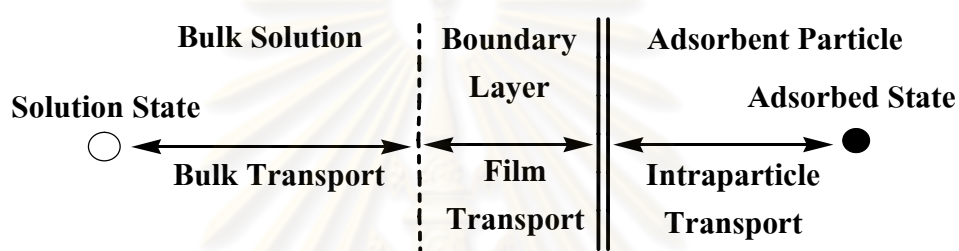
Figure 2.17 The steps of adsorption on the adsorbent surface [87].

(i) Bulk transport

In this step, the analytes move from the bulk solution to the surface of the boundary layer. It is a very fast process.

(ii) Film transport

The analytes transport from the boundary layer to the surface of the adsorbents, which is called film diffusion or external diffusion. Film transport may occur slowly and can be considered as the adsorption rate control step.

(iii) Intraparticle transport

The final step is one of the steps that can be the rate limiting step of the adsorption. The analytes transfer from the adsorbent surface to the internal pores of the adsorbent and react with the active sites. This step is called the internal diffusion.

2.7.4   Adsorption isotherms

The adsorption process that refers to the partition of analytes between aqueous phase and adsorbent (solid phase) at equilibrium at constant temperature is called adsorption isotherm. Moreover, the adsorption equilibrium can be described by using adsorption isotherm models which are the relations between the amount of adsorbate on adsorbent and the concentration of analytes in solution at equilibrium. Langmuir and Freundlich isotherm models are widely used to describe the adsorption equilibrium [88, 89].

2.7.4.1   Langmuir adsorption isotherm

The Langmuir isotherm model of adsorption is based on the following assumptions : (i) adsorption energy is constant over all sites and independent to the extent of a homogeneous surface, (ii) the adsorption takes place at specific sites of the adsorbents and no further adsorption occur at that sites, (iii) there is no interaction between adsorbates, (iv) each site can accommodate only one molecule or atom of adsorbate, and (v) the adsorption phenomena is the monolayer coverage on adsorbents surface and could be reversible or irreversible process. The general form of the Langmuir isotherm is shown in equation 2.1.

The equation 2.1 is further converted into the linear equation as shown in equation 2.2,

$$q = \frac{q_m b C_e}{1 + b C_e} \qquad (2.1)$$

$$\frac{C_e}{q} = \frac{1}{bq_m} + \frac{C_e}{q_m} \qquad (2.2)$$

where C_e = equilibrium concentration of the analyte in aqueous

solution (mg L^{-1} or mol L^{-1})

q = adsorption capacity of adsorbent (mg g^{-1} or mol g^{-1})

q_m = maximum adsorption capacity of adsorbent (mg g^{-1} or mol g^{-1})

b = Langmuir constant related to the affinity of binding sites

(L mg^{-1} or L mol^{-1})

The experimental data (q and C_e) are plotted either as shown in Figure 2.18 or in one of the two alternate linear relations as shown in Figure 2.19. The plot of $\frac{C_e}{q}$ against C_e yields a straight line with a slope of $\frac{1}{q_m}$ and intercept of $\frac{1}{bq_m}$ (Figure 2.19b).
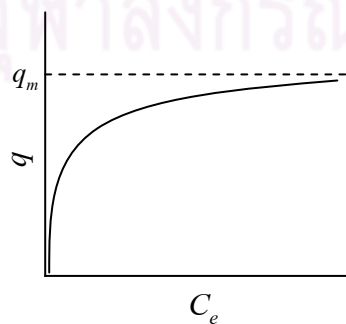
Figure 2.18

Form of Langmuir adsorption isotherm [90].

The plot of Langmuir isotherm will demonstrate whether the model is applicable and also will allow determination of the values of q_m and b. In many cases, a single model will not be satisfactory for a wide range of concentrations but will serve in narrow regions.

Figure 2.19 (a) Conventional linear form of Langmuir adsorption isotherm and (b) modified form of Langmuir adsorption isotherm emphasizing higher concentration data [90].

2.7.4.2 Freundlich adsorption isotherm

The Freundlich isotherm is used to describe multilayer adsorption of analytes on heterogeneous surface or surface with active sites of various affinities. The common form of the Freundlich model is presented in the equation 2.3. A plot of q versus C_e results in a curve of the form shown in Figure 2.20. The linear form of Freundlich isotherm is obtained by taking logarithm as shown in equation 2.4,

$$q = K_f C_e^{1/n} \tag{2.3}$$

$$\log q = \log K_f + \frac{1}{n} \log C_e \tag{2.4}$$

where K_f = Freundlich constant related to adsorption capacity

(mg g^{-1} or mol g^{-1})

n   =   the numerical value of Freundlich constant

A linear plot of log q versus log C_e gives a slope of $\dfrac{1}{n}$ and intercept of log K_f as presented in Fugure 2.21. The equation 2.3 is common and simple and has been used to fit experimental data quite often. The Freundlich isotherm plot is usually constructed on log-log scale (Figure 2.21) to facilitate the determination of the model validity and the values of K_f and n.
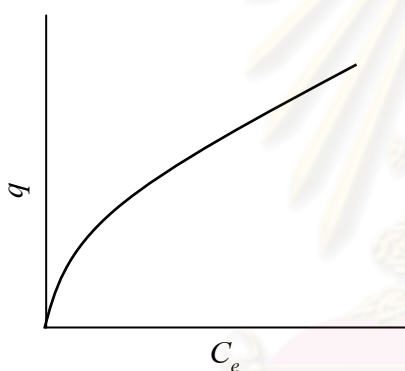
Figure 2.20 Form of Freundlich adsorption isotherm [90].
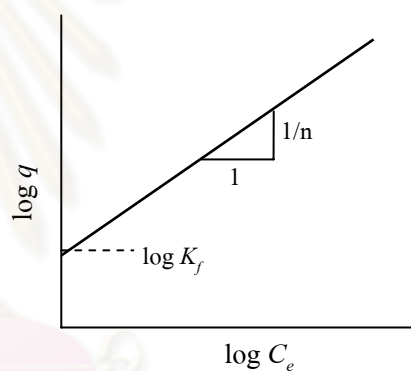
Figure 2.21 Linear form of Freundlich adsorption isotherm [90].

2.8 Characterization of adsorbent

The characterization of adsorbent (MPs-PS-AEPE) is necessary to confirm the success of the synthesis of adsorbent. Several characterization techniques such as FT-IR, XRD, TGA, SEM and BET are used. The principles of these techniques are described below.

2.8.1   Fourier transforms infrared spectroscopy (FT-IR)

The FT-IR spectroscopy is a technique that provides distinct identification and information about the structure of samples either organic or inorganic in term of functional groups or chemical bonds. It can be applied to the analysis of solids, liquids, and gasses. Most FT-IR spectrometers work in the mid-infrared region from 4000 cm^{-1} to 400 cm^{-1} and offer high sensitivity and accuracy as well as improve data collection speed compared to dispersive instruments because the whole spectra is measured at the same time and hence multiple scanning of the sample is possible [91].

The basic principle of IR-spectroscopy is based on the measurement of the molecular bond vibration when compounds are excited by radiation of a suitable frequency. FT-IR spectrum is recorded in term of the correlation between the percentage transmittance and the wavenumbers, which is the direct proportion to the frequency of the absorbed radiation responsible for the molecular vibration or the absorption process. FT-IR is a beneficial instrument to detect functional groups in a sample but it can not be used to clarify the complete structure of an unknown molecule. KBr pellet is commonly used in the analysis of solid sample. Solid samples are grounded and milled with potassium bromide (KBr) to obtain a homogeneous powder. This powder is compressed into a thin pellet and then analyzed [92].

In this research, FT-IR was used to determine the chemical bond or functional groups on the MPs surface before and after coating with polystyrene and modification with chelating ligand AEPE.

2.8.2 X-ray diffraction (XRD)

X-ray diffraction is one of the important non-destructive techniques used for the determination of crystalline structure and phase identification. The information about unit cell dimensions of solid and crystallographic structure of natural and manufactured solid materials can be obtained. It is an efficient analytical technique used to identify and characterize unknown crystalline and powder solid sample [93]. X-rays are generated by a cathode ray tube, filtered to produce monochromatic radiation, collimated to concentrate and directed toward the finely ground sample. Monochromatic X-rays are used to determine the interplanar spacing of the materials or samples. Samples are analyzed as powder with grains in random orientation to ensure that all crystallographic directions are sampled by the beam. The scattered intensity can be measured as a function of scattering angle 2θ. The different phase present in the sample are efficiently determined by XRD technique. The XRD pattern is plotted between the peak position (2θ angle) and the intensity of the diffracted beam. The positions and intensities of peaks act as a distinctive "fingerprint" which provides the information of samples. The Joint Committee on Powder Diffraction Standards (JCPSD) database is used as reference to identify the crystalline materials.

The main components of XRD instrument are an X-ray tube, a sample holder and a detector. Figure 2.22 shows a monochromatic beam of X-rays incident on the surface of atomic arrays at angle θ. The interaction of X-rays with a sample creates secondary "diffracted" beam of X-rays related to interplanar spacing in the crystalline powder according to an equation called "Bragg's Law" (equation 2.5) [93],

$$n\lambda = 2d\sin\theta \qquad \text{"Bragg's Law"} \qquad (2.5)$$

where   n = an integer number

λ = wavelength of the X-rays

d = the interplanar spacing generating the diffraction

θ = the diffraction angle
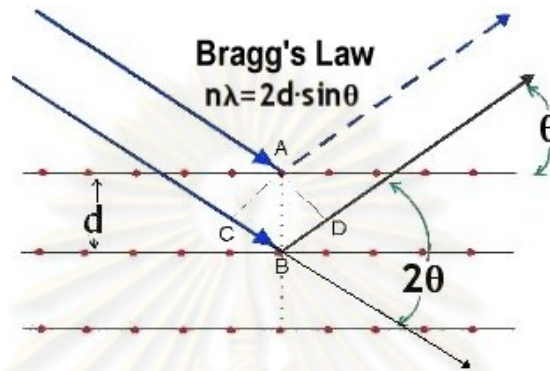
Figure 2.22 Diffraction of X-rays by regular planes of crystals [94].

Generally, an integer number is equal to 1, therefore, the Bragg's Law can be written as shown in equation 2.6.

$$\lambda = 2d\sin\theta \qquad\qquad (2.6)$$

In this research, XRD technique was used to characterize the main structure of MPs whether it was changed after surface modification.

2.8.3 Thermogravimetric analysis (TGA)

Thermogravimetry is a thermal analysis technique that measures the weight loss or weight change of materials as a function of temperature against percentage weight. The measurement can be carried out in air or nitrogen atmosphere. During the measurement, the decrease of sample weight is observed due to the loss of volatile components and moisture. This technique is usually used to determine the

thermal stability and the composition of both inorganic and organic material, especially polymer [95].

The TGA provides both qualitative and quantitative information. The qualitative analysis is done by comparing the onset temperature, which is the temperature of the weight loss, of the modified material to that of the unmodified material. The difference in onset temperature and percentage weight loss indicates the different in material composition. The quantitative analysis is done by measuring the weight loss when a known molecular weight component is vaporized from the sample [96]. In the characterization of polymers and composite materials, TGA commonly provides the information about degradation temperature, residual solvent levels and the amount of inorganic (noncombustible) filler in polymer or composite material compositions.

In this research, TGA technique was used to investigate the thermal stability of the synthesized materials and to confirm the difference in the chemical composition of the material.

2.8.4 Scanning electron microscopy (SEM)

SEM uses a focused beam of high-energy electrons to generate a variety of signals at the surface of solid samples. The signals derived from electron-sample interactions reveal information about external morphology, sample shape and orientation of materials making up the sample. In most applications, a 2-dimensional image is generated and collected over a selected area of the sample surface [97].

In SEM, a fine electron probe scans in a raster across the sample surface that has to be conductive, stable in vacuum as well as not temperature-sensitive. Hence sample preparation is necessary depending on the nature of the

sample. The magnification of the sample images depends on the area scanned in the raster pattern relative to the fixed size of the display.

The incident electrons are scattered both elastically (high energy) and inelastically (lower energy) by the sample. The inelastic scattering leads to the excitement of the electrons in the sample atoms that can leave the sample as secondary electrons. The full SEM image is formed by measuring the signal of secondary electrons. SEM offers high resolution analysis and inspection. It gives information about the relief surfaces of a solid, its size, electrical properties and is widely used in flaw detection of microelectronic devices [98].

In this research, SEM was used to exhibit the outer surface, size and shape of bare MPs, MPs-Ini, MPs-PS and MPs-PS-AEPE.

2.8.5 Nitrogen adsorption-desorption technique [99]

The nitrogen adsorption-desorption technique is employed to identify the physical properties of porous material such as surface area, pore volume, pore diameter and pore-size distribution. The BET method (Brunauer, Emmett, Teller method) is used for the determination of total surface area which is correlated to the amount of gas adsorbed on the material at a fixed temperature as a function of pressure. Pore volume and pore diameter are commonly derived from gas sorption data. Pore size distribution is measured by the use of nitrogen adsorption-desorption isotherm at liquid nitrogen temperature and relative pressures (P/P_0) ranging from 0.05-0.1.

The nitrogen desorption is sometimes used to determine the pore size distribution, but the results are not entirely reliable probably due to the surface tension of nitrogen film. The nitrogen desorption tends to be unreliable for very large pore of over 60 nm in diameter where adsorption occurs at near atmospheric pressures.

In this study, this technique was used to analyze the specific surface area of MPs, MPs-Ini, MPs-PS and MPs-PS-AEPE.

2.9   Determination of metal concentration

The atomic absorption spectroscopy is commonly used to determine the metals concentration in aqueous solution. The flame atomic absorption spectroscopy (FAAS) is used for metals determination. In the case of mercury, the cold vapor atomic absorption spectroscopy (CVAAS) is used.

2.9.1   Cold vapor atomic absorption spectrometry [100]

The cold vapor atomic absorption spectrometry (CVAAS) is the most widely used technique for mercury determination because of its high sensitivity, simplicity, robustness, and relative freedom from interferences. It is a flameless atomization technique and atomic vapor is generated at room temperature. Excellent detection limits can be achieved with the modern instruments. Organic mercury compounds should be oxidized to inorganic mercury before determination. Then, the inorganic mercury in a liquid sample is reduced normally with tin (II) chloride ($SnCl_2$) or sodium borohydride ($NaBH_4$) to elemental mercury (Hg^0) as shown in equation 2.7.

$$Hg^{2+}(aq) \; + \; Sn^{2+}(aq) \quad \rightarrow \quad Hg(l) \; + \; Sn^{4+}(aq) \qquad\qquad (2.7)$$
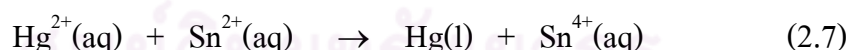
With an inert gas, the mercury vapor is purged out of the solution and transported to an absorption cell of the atomic absorption spectrometer. Light is then transmitted along the axis of the quartz tube from hallow cathode mercury lamp and the absorption at 253.7 nm is measured. A typical absorption cell for mercury determination with CVAAS is made of quartz tube of 25 cm length and 0.5 cm in inner diameter. This method provides sensitivities of approximately four orders of magnitude better than flame atomic absorption spectrometry (FAAS). Considering the acceptable

concentration of mercury in drinking water (2 µg L^{-1}), the cold vapor technique is the only approved method for determining mercury at this level. The common instrumental diagram of CVAAS is shown in Figure 2.23.
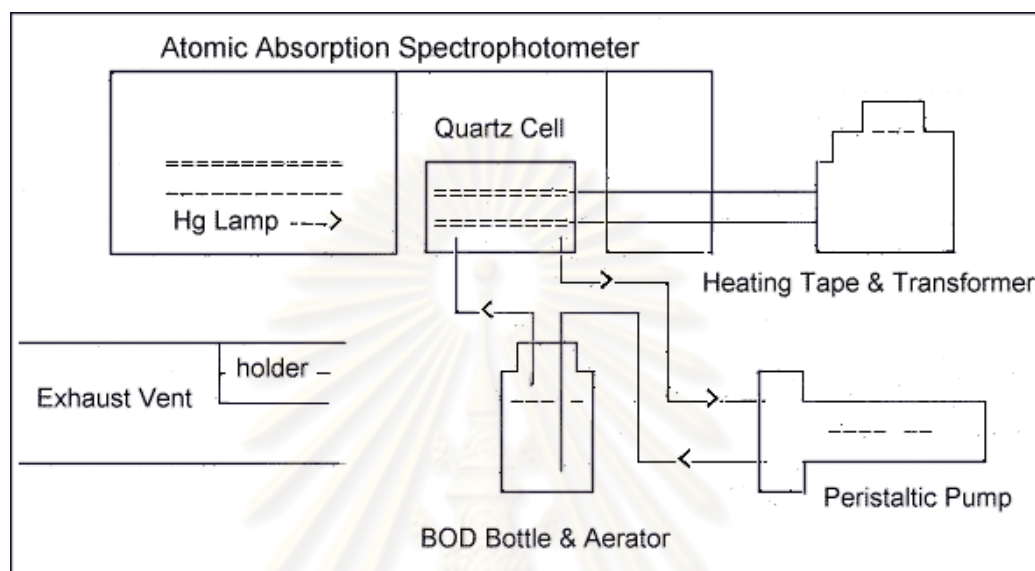
Figure 2.23 Block diagram of cold vapor atomic absorption spectrometer [101].

2.9.2 Flame atomic absorption spectrometry [102]

Flame atomic absorption spectrometry (FAAS) is one of the techniques used to analyze various metals in aqueous sample. This technique offers many advantages, for example, rapid, low cost operation, high precision, and specificity. Therefore, it is regularly used for determination of metals concentration in the mg L^{-1} level. However, it has some drawback such as poor sensitivity. The basic principle of FAAS is the absorption of element specific radiation by free atoms in the ground state. The free atoms in the gas phase are generated by flame. Due to the absorption of specific quanta, the amount of atoms in an excited state increases and hence leads to a decrease of the atoms in ground state. The value of the absorbed light corresponds to

the initial concentration of atoms in the ground state and therefore correlates as well to the concentration of the element. The common instrumental diagram is shown in Figure 2.24.
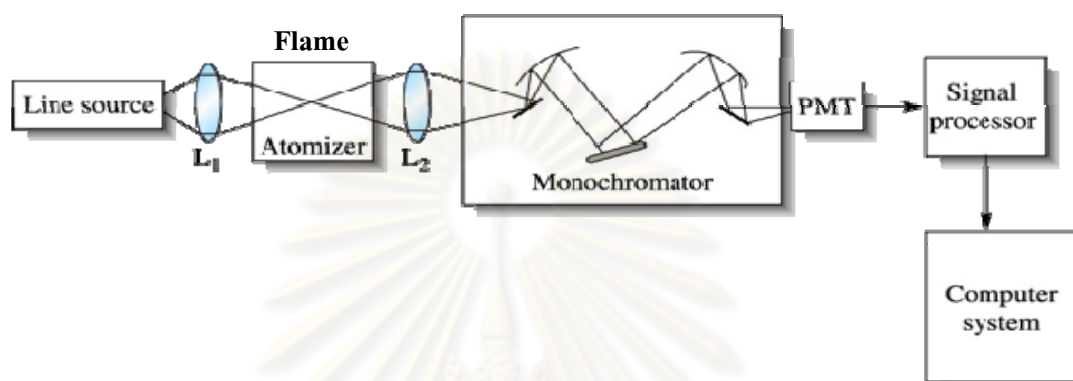
Figure 2.24 Block diagram of general atomic absorption spectrometer [103].

Atomic absorption spectrometry is commonly used for quantitative analysis and only one element can be measured at a time by conventional instrument. Based on the measurement of absorbed radiation, a quantitative determination of the amount of analyte in the sample is possible with the Lambert-Beer's law as shown in equation 2.8 [98],

$$A_{abs} = -\log T = \log\left(\frac{I_o}{I}\right) \tag{2.8}$$

where A_{abs} = absorbed radiation (absorbance) of the analyte

T = light transmission (transmittance) of the analyte

I_0 = incident intensity without absorption

I = transmitted intensity of light which has passed through the atomizer

2.10   Literature review

The extraction of heavy metals could be performed using various materials as adsorbents. One problem of metals extraction from solution is the difficulty in adsorbent separation from the solution. Recently, magnetic particles have drawn a lot of interest due to their high surface area, high temperature resistance, ion exchange mechanism and high capacity of functional groups after functionalization. Many researches present the use of magnetic particles as adsorbent that could be separated easily from the solution by external magnetic field. There are many types of magnetic particles with the formula of MFe_2O_4 (M = Mn, Mg, Ni, Co, Cu, Fe) [104]. Different preparation techniques have been developed to synthesize magnetic particles. Liu *et al.* (2000) [25] synthesized the magnetic nanoparticles $MgFe_2O_4$ and $CoFe_2O_4$ via microemulsion process and studied the magnetic anisotropy of these particles. The average size of $MgFe_2O_4$ and $CoFe_2O_4$ nanoparticles was in the range of 2 to 45 nm and 2 to 35 nm, respectively when characterized by TEM technique. Furthermore, the results showed that magnetic anisotropy of $CoFe_2O_4$ nanoparticles was higher than that of $MgFe_2O_4$ nanoparticles.

During 2007 to 2009, many researches focused on the magnetic particles synthesis by various methods as following: Maaz *et al.* (2007) [18] prepared magnetic nanoparticles of cobalt ferrite by chemical co-precipitation. XRD and TEM results confirmed the formation of single-phase cobalt ferrite nanoparticles in the range of 15-48 nm depending on the annealing temperature and time. The size of particles increased with the increase of annealing temperature and time. Xiao *et al.* (2007) [24] synthesized cobalt ferrite nanoparticles via combustion method. The size and magnetic anisotropy of particles increased with the increase of annealing temperature. The average size was in the range of 22.7 to 43.1 nm when characterized by TEM technique. The saturation magnetization increased from 38.30 emu g^{-1} at 600 °C to

63.26 emu g^{-1} at 800 °C. Carp *et al.* (2007) [28] produced $CoFe_2O_4$ particles with the average size in the range of 3.8 to 5.7 nm and the surface area of 60 to 67 m^2 g^{-1} through thermal decomposition method. The maximal magnetization of the obtained particles was 42.55 emu g^{-1}.

In 2008, Arelaro *et al.* [104] synthesized Fe_3O_4, $CoFe_2O_4$ and $MnFe_2O_4$ via the high-temperature solution phase reaction. The synthesis was successful and the narrow size distribution about 4.50 ± 0.15 nm was observed. The order of magnetic anisotropy was $CoFe_2O_4 > MnFe_2O_4 > Fe_3O_4$. Xiantao *et al.* [105] synthesized the magnetite (Fe_3O_4) via chemical co-precipitation and thermal decomposition and combined the use of sodium oleate ($C_{18}H_{33}Na$) as surfactant that could prevent the agglomerization of particles. The size distribution around 6.36 nm was observed by TEM and DLS techniques. Liu *et al.* [27] synthesized $CoFe_2O_4$ nanoparticles by hydrothermal treatment method. From TEM characterization, the results reveal that the product consisted of both nanoplatelets and nanoparticles. The width and length of $CoFe_2O_4$ nanoplatelets was in the range of 7 to 30 nm and 8 to 48 nm, respectively. The size of $CoFe_2O_4$ nanoparticles was in the range of 2 to 8 nm. Wang *et al.* [29] synthesized $MnFe_2O_4$ and $CoFe_2O_4$ nanoparticles via polyol-process and studied their magnetic property. From TEM characterization, the average diameter of $MnFe_2O_4$ nanoparticles was about 7.4 nm and the size of $CoFe_2O_4$ nanoparticles was in the range of 4 to 6 nm. The saturation magnetization of $MnFe_2O_4$ and $CoFe_2O_4$ nanoparticles were 29.77 emu g^{-1} and 27.14 emu g^{-1}, respectively.

In 2009, Ayyappan *et al.* [106] synthesized cobalt ferrite nanopaticles via chemical co-precipitation by varying the solvent dielectric constant using different ethanol-water ratio. XRD results confirmed the cubic spinel phase of particles. From TEM characterization, the average particle size increased from 10 ± 1 to 16 ± 1 nm as the dielectric constant of solvent increased from 47 to 80. Zi *et al.* [107] synthesized $CoFe_2O_4$ nanoparticles by chemical co-precipitation. XRD results confirmed the spinel single phase of particles. SEM and TEM images showed that the particles were

spherical with diameters in the range of 20-30 nm. Cendeno-Mattei *et al.* [108] synthesized $CoFe_2O_4$ particles in nano-size via co-precipitation. XRD and FT-IR results confirmed the formation of the ferrite structure. The average crystalline size of particles was around 24 nm.

These researches demonstrated that the synthesis of cobalt ferrite and other ferrites could be done by different method. Among these methods, the chemical co-precipitation is widely used due to the convenience, ease and versatility. Cobalt ferrite particles have drawn a lot of interest due to the higher magnetization and magnetic anisotropy compared to other ferrites. In this work, cobalt ferrite magnetic particles were synthesized by chemical co-precipitation of cobalt ions and ferric ions.

The magnetic particles were applied as adsorbent by the coating or functionalization with ligands for adsorption of heavy metals from aqueous solution as following: Chang *et al.* (2005) [109] prepared the monodisperse chitosan-bound Fe_3O_4 nanoparticles as a novel adsorbent for the removal of Cu^{2+} ions. The analyses of TEM and XRD indicated that the adsorbents were monodisperse with a mean diameter of 13.5 nm and the amount of chitosan bound on Fe_3O_4 nanoparticles was estimated to be about 4.92 %w/w. The maximum adsorption capacity was 21.5 mg g^{-1} and the adsorption isotherm followed Langmuir model. Huang *et al.* (2008) [110] prepared a new adsorbent of silica-coated magnetic nanoparticles modified with 3-mercapto propyltrimethoxysilane for extraction of Cd, Cu, Hg, and Pb from biological and environmental samples. The maximum adsorption capacity of Cd, Cu, Hg, and Pb were 45.2, 56.8, 83.8 and 70.4 mg g^{-1}, respectively. Kraus *et al.* (2009) [111] synthesized cobalt ferrite nanoparticles modified with 3-mercaptopropyltrimethoxy silane for the extraction and recovery of Au(III) from aqueous solutions. The adsorption behavior followed Langmuir isotherm and the maximum adsorption capacity was 120.5 mg g^{-1}. However, the magnetic particles have some drawback such as the low stability in acidic solution. In this work, the surface of magnetic particles was coated with polymer via ATRP to increase acid resistance of the particle. The

special characteristic of the polymer obtained from ATRP is the preservation of the end halogen atoms throughout the polymerization leading to the end functional polymer.

In the past decade, there are many researches concerning the polymer synthesis using ATRP method. Zhang et al. (2002) [112] synthesized the copolymer of polystyrene and poly(2,5-*bis*[(4-methoxyphenyl)oxycarbonyl]styrene). GPC, ^{1}H-NMR and DCS techniques were used to confirm the success of the synthesis. The obtained polymer was diblock copolymer with low polydispersity. The average molecular weight of diblock copolymer was about 9,300 g mol^{-1}. Next, Iddon *et al.* (2004) [113] polymerized sodium 4-styrenesulfonate via ATRP using sodium 4-bromomethyl benzoate and water-methanol mixture as initiator and solvent, respectively. Copper(I) chloride complexed with *2,2′*-bipyridine was used as catalyst. The polymerization was successful with high polydispersities (M_w/M_n = 1.61), confirmed by ^{13}C-NMR and GPC measurement. Li *et al.* (2006) [114] synthesized the core-shell block copolymer of poly(*t*-butyl acrylate-*co*-acrylic acid)-*b*-poly(*N*-isopropyl acrylamide) by ATRP. From ^{1}H-NMR and TEM characterization, poly(*t*-butyl acrylate) was a core part while poly(acrylic acid) and poly(*N*-isopropylacrylamide) were the shell of the copolymer obtained. Moreover, from the thermo and pH responsive study, it was observed that the copolymer was stable at pH 5.8 and 25˚C. Gao *et al.* (2007) [115] synthesized and characterized the syndiotactic polystyrene-*graft*-poly(glycidyl methacrylate) copolymer by ATRP using 2-bromo-2-methylpropanoyl bromide modified syndiotactic polystyrene as macroinitiator and copper bromide combined with *2,2*-bipyridine as catalyst in anisole. The obtained polymer was characterized by using FTIR and NMR technique to confirm the success of the synthesis.

From the researches mentioned above, it has been shown that various polymers can be synthesized successfully via ATRP method with their suitable conditions. For the preparation of solid support/polymer composite, it can be performed by various methods such as γ-irradiation [116], emulsion polymerization

[117-118], embedding method [119] and atom transfer radical polymerization [120-125]. In addition, many researchers polymerized monomers via ATRP method on solid supports in the form of core-shell structure.

Chen *et al.* (2006) [120] synthesized poly(*N,N'*-dimethylacrylamide) and poly-(ethylene glycol)-coated Merrifield resin in the form of core/shell structure via ATRP employing the Cu(I)Br/PMDETA catalyst system. FT-IR spectroscopy and optical microscopy were used to characterize and confirm the success of the synthesis. The particle sizes of polymer composite were larger after polymerization. In the following year, Lei and Bi (2007) [121] synthesized poly(*tert*-butyl acrylate)-coated silica gel of core/shell structure via ATRP using Cu(I)Br/PMDETA as catalyst . The initiator was synthesized by the reaction between 3-aminopropyltriethoxysilane and 2-bromo propyonyl bromide. The average particles size of polymer composite increased from 250 to 300 nm after polymerization. Zhou *et al.* (2007) [122] synthesized the poly(ethylene glycol)methacrylate-*b*-methyl methacrylate-coated Fe_3O_4 nanoparticles via ATRP. The initiator was synthesized by the reaction between 3-aminopropyl triethoxysilane and 3-chloropropionic acid. Cu(I)Br complexed with *2,2'*-bipyridine was used as catalyst. Zhang *et al.* (2007) [123] synthesized the poly(*N*-isopropyl acrylamide)-coated silica nonoparticles via ATRP employing Cu(I)Cl/*2,2'*-bipyridine as catalyst. The initiator was synthesized by the reaction between 3-aminopropyl triethoxysilane and α-bromoisobutyryl bromide. The resulting polymer composite particles were characterized by using FT-IR, XPS and TEM. The results showed that these particles owned both core/shell structure and thermoresponsiveness with the lower critical solution temperature (LCST) of 32°C. Moreover, in 2008 [124], Lei *et al.* synthesized poly(sodium 4-styrenesulfonate)-coated Fe_3O_4/SiO_2 particles via ATRP using Cu(I)Br/*2,2'*-bipyridine as catalyst. The initiator was synthesized by the reaction between 3-aminopropyltriethoxysilane and 2-bromopropyonyl bromide. These resulted polymer composites were characterized by using XRD, TEM, FT-IR, TGA and XPS to confirm the success of the synthesis. The detection of sulfur and sodium

signals from XPS analysis indicated that sodium 4-styrenesulfonate was polymerized onto the Fe_3O_4/SiO_2 particles surface. In addition, the polymerization of styrene on the surface of magnetic particles via ATRP has been also reported, Sun *et al.* (2007) [125] synthesized polystyrene-coated Fe_3O_4 nanoparticles in core/shell structure via ATRP using 2-bromo-2-methyl-*N*-(3-(triethoxysilyl)propyl)propanamide and Cu(I)Br/ PMDETA as initiator and catalyst, respectively. These polymer composite particles had an exceptionally good dispersity in organic solvents. The average particles size of polymer composite increased from 10 to 40 nm after polymerization. The researches mentioned above demonstrated that some monomer can be successfully polymerized via ATRP on various solid supports in the form of core/shell structure. In our study, the polystyrene-coated magnetic particles were prepared by ATRP of styrene on particles surface using the initiator that was synthesized from the reaction between 3-aminopropyltriethoxsilane and ethyl-2-bromopropionate. Cu(I)Br complexed with PMDETA was used as catalyst. To increase the affinity toward metal ions, the coated polymer was functionalized with a chelating agent.

Many papers presented the functionalization of halogen chain-end polymer to another functional groups chain-end polymer. Garamszegi *et al.* (2003) [126] synthesized bromo-functional polystyrene via ATRP. The bromine end-groups were reacted with thiourea to give an isothiouronium salt. Then, this salt was treated with sodium hydroxide to obtain thiol groups. The conversion of the bromine end-groups into thiol groups was confirmed by ^{1}H NMR. The gel permeation chromatography (GPC) showed that polydispersity and the molecular weight remain unchanged after end-thiol functionalization. Posma *et al.* (2006) [127] synthesized polystyrene via ATRP. The obtained polystyrene containing bromo groups at chain end was reacted with sodium azide (NaN_3) to convert bromo-functional polystyrene to the corresponding azido-functional polystyrene by nucleophilic substitution. Thereafter, the azido-functional polystyrene was reduced by lithium aluminium hydride $(LiAlH_4)$ to yield the amine-functional polystyrene.

In addition, the functionalization of halogen chain-end polymer on solid support has been also reported. Wang *et al.* (2009) [128] synthesized bromo-functional polystyrene-coated silica nanoparticles via ATRP. The terminal bromides of polystyrene-coated silica nanoparticles were then substituted with azido groups. These azido-terminated polystyrene on the nanoparticle surface were reacted with various alkyne-terminated functional end groups. FT-IR and ^{1}H-NMR characterization indicated quantitative transformation of the chain ends of polystyrene on silica nanoparticles into the desired functional groups. Bayramoglu *et al.* (2009) [129] synthesized poly(glycidyl methacrylate) via ATRP on poly(vinyl benzyl chloride) beads that contained chlorine groups on surface and acted personally as initiator. The epoxy groups of the poly(glycidylmethacrylate) were reacted afterward with hydrazine to obtain the hydrazine-functionalized copolymer beads. Moreover, these functionalized copolymer beads were applied as adsorbent for the invertase. The maximum adsorption capacity of invertase onto copolymer beads was 86.67 mg g^{-1} at pH 4.0. The researches shown above indicated that the halogen end-groups of ATRP polymers can be further functionalized with functional groups and the final product can be applied as adsorbent to adsorb the interested analytes. In this work, to increase the affinity toward metal ions, the ligand 2-(3-(2-aminoethylthio)propylthio) ethanamine (AEPE) was functionalized on the polystyrene-coated magnetic particles to improve the efficiency and selectivity in Hg(II) and Ag(I) ions extraction due to the presence of sulfur and nitrogen donor atoms.

CHAPTER III

EXPERIMENTALS

3.1   Instruments

The instruments used for measurements and characterization in this thesis are shown in Table 3.1.

Table 3.1 List of instruments

Instruments	Manufacture : Model	Purpose
1. Nuclear magnetic resonance spectrometer (NMR)	Varian : Mercury Plus 400	Identification of ligand structure
2. X-ray diffractometer (XRD)	Rigaku : D/MAX-2200	Identification of adsorbents crystallinity
3. Fourier transforms infrared spectrometer (FT-IR)	Nicolet : Impact 410	Functional group identification
4. Thermo gravimetric analyzer (TGA)	Perkin Elmer: Pyris1	Thermal stability of the materials
5. Surface area analyzer	BEL Japan, BELSORP-mini	Surface area determination
6. Flame atomic absorption spectrometer (FAAS)	Perkin-Elmer : AAnalyst 100	Determination of Ag(I) concentration
7. Cold vapor atomic absorption spectrometer (CVAAS)	Perkin-Elmer : AAnalyst 100 coupled with FIAS 400 system	Determination of Hg(II) concentration

Table 3.1 List of instruments (continued)

Instruments	Manufacture : Model	Purpose
9. Scanning electron microscope (SEM)	JOEL JSM-5410 LV	Surface analysis of adsorbent
10. pH meter	Hanna instruments : pH 211	pH measurement
11. Centrifuge	Sanyo : Centaur 2	Separation of adsorbents from solution
12. Stirrer	Gem: MS 101	Agitation of solution in extraction experiments
13. Rotary evaporator	Eyela : N-1000	Removal of solvent from ligand

3.2   Chemicals

All chemicals used in this research are listed in Table 3.2.

Table 3.2 List of chemicals

Chemicals	Suppliers / Grade
Ferric chloride	Fisher Chemicals / AR
Cobalt nitrate hexahydrate	Fisher Chemicals / AR
Sodium nitrate	Fluka / purum p.a. > 99%
Sodium sulfate anhydrous	Fisher Chemicals / AR
Potassium nitrate	BDH / AR
Magnesium (II) nitrate hexahydrate	Merck / GR for analysis
Calcium nitrate tetrahydrate	Riedel-de Haen[®] / Assay 98% (GC)
Nickel (II) nitrate hexahydrate	Merck / for analysis

Table 3.2 List of chemicals (continued)

Chemicals	Suppliers / Grade
Cadmium (II) nitrate tetrahydrate	CARLO ERBA / for synthesis
Lead (II) nitrate	M&B Laboratory Chemicals / Assay $\geq 99\%$
Sodium hydroxide	Merck / for synthesis
Potassium hydroxide	Merck / ACS
Nitric acid	Merck / for analysis
Sodium acetate anhydrous	CARLO / for analysis
Silver standard solution (1000 ppm)	Merck
Mercury standard solution (1000 ppm)	BDH / spectrosol
Dichloromethane	Fisher / AR
Acetonitrile	Merck / isocratic grade for LC
Ethanol	Merck / for synthesis
Methanol	Merck / for synthesis
1,3-dibromopropane	Merck / for synthesis
Pentamethyldiethylenetriamine	Merck / for synthesis
Copper (I) bromide	BDH / Laboratory reagents
Cysteamine hydrochloride	Fluka / purum $\geq 97\%$
Calcium hydride	Fluka / Assay $\geq 95\%$
Dimethylformamide	Fluka / puriss. p.a., Reagent. ACS
Styrene monomer	Fluka / for synthesis Assay $\geq 99\%$
3-aminopropyltriethoxysilane	Fluka / purum $\geq 98\%$ (GC)
Ethyl-2-bromopropionate	Aldrich / 99% (GC)
Chloroform D1	Merck / 99.8% for NMR spectroscopy
Tin (II) chloride dihydrate	Scharlau / ACS
Sodium metal	RDH

Table 3.2 List of chemicals (continued)

Chemicals	Suppliers / Grade
Hydrochloric acid	Merck / for analysis
Potassium bromide	Merck / for IR spectroscopy
Sodium borohydride	Merck
Potassium persulfate	Merck/ for analysis
Potassium permanganate	Suksapan
Hydroxylammonium chloride	Merck/ for analysis

3.3 Experimental procedures

3.3.1 Preparation of chemicals and reagents

De-ionized (DI) water and 0.05 M CH_3COONa buffer solution were used to prepare all reagents.

Mercury solutions

Mercury standard solution (1000 mg L^{-1}) was used to prepare the mercury solutions of desired concentrations by dilution with 0.05 M CH_3COONa solution.

Silver solutions

Silver standard solution (1000 mg L^{-1}) was used to prepare the silver solutions of desired concentrations by dilution with 0.05 M CH_3COONa solution.

Nitric acid solutions

Nitric acid solutions (1 and 5% v/v) were prepared by dilution of the concentrated nitric acid solution with DI water and used for pH adjustment and dilution of metal solutions for atomic absorption spectroscopic analysis.

Potassium hydroxide solutions

Potassium hydroxide solutions (1 and 5% w/v) were prepared by dissolving the appropriate amount of KOH in DI water and used for pH adjustment.

Sodium acetate solution

Sodium acetate solution (0.05 M) was prepared by dissolving the appropriate amount of CH_3COONa in DI water and used in the preparation of metal solutions.

Acid carrier

Hydrochloric acid solution (3% v/v) was prepared by dilution of the concentrated hydrochloric acid solution with DI water and used in mercury analysis by CVAAS.

Tin (II) chloride solution

Tin (II) chloride solution was prepared by dissolving 80 g of $SnCl_2$ in 200 mL of concentrated HCl. Then, the volume was adjusted to 1000 mL using DI water and used as reducing agent for mercury analysis by CVAAS.

Sodium borohydride solution

Sodium borohydride solution (0.5% w/v) was prepared by dissolving 5 g of $NaBH_4$ in 1000 mL of 0.05% NaOH solution. Then, it was used as reducing agent for mercury analysis by CVAAS in the desorption experiment.

Potassium permanganate solution

Potassium permanganate solution (5% w/v) was prepared by dissolving 5 g of $KMnO_4$ in 100 mL of DI water. It was used in wastewater digestion for Hg(II) determination.

Potassium persulfate solution

Potassium persulfate solution (5% w/v) was prepared by dissolving 5 g of $K_2S_2O_8$ in 100 mL of DI water. It was used in wastewater digestion for Hg(II) determination.

Sodium chloride-hydroxylammonium hydrochloride solution

NaCl (6 g) and $NH_2OH \cdot HCl$ (6 g) were dissolved in 50 mL of DI water. It was used to reduce the excess permanganate in wastewater digestion method for Hg(II) determination.

Co-existing ions solutions

The solutions containing alkali and alkali earth metal ions (Na^+, K^+, Mg^{2+} and Ca^{2+}) of 0.1 and 1.0 M and heavy metal ions (Ni^{2+}, Cd^{2+}, Pb^{2+}) of 0.15, 0.5, 1.5 and 5.0 mM were prepared by dissolving the appropriate amount of $NaNO_3$, KNO_3, $Mg(NO_3)_2 \cdot 6H_2O$, $Ca(NO_3)_2 \cdot 4H_2O$, $Ni(NO_3)_2 \cdot 6H_2O$, $Cd(NO_3)_2 \cdot 4H_2O$ and $Pb(NO_3)_2$ in DI water. The solutions containing NO_3^-, SO_4^{2-} and Cl^- anions of 0.1 and 1.0 M were prepared by dissolving the appropriate amount of $NaNO_3$, Na_2SO_4 and NaCl in DI water. These solutions were used in the study of the co-existing ions effect.

Ninhydrin solution

Ninhydrin solution was prepared by dissolving 500 mg of ninhydrin in 10 mL of ethanol. The yellow solution appeared after complete dissolving. This solution was used to confirm the presence of free terminal amine groups of AEPE on the surface of adsorbent and the success of AEPE modification.

3.3.2 Synthesis of cobalt ferrite magnetic particles (CoFe₂O₄)

The cobalt ferrite magnetic particles (CoFe$_2$O$_4$) were synthesized via chemical co-precipitation and used as solid support for preparation of adsorbent. The synthesis reaction is shown in scheme 3.1.

$$Co^{2+} + 2Fe^{3+} + 8OH^- \rightarrow Co(OH)_2 + 2Fe(OH)_3$$

$$nCo(OH)_2 + 2nFe(OH)_3 \rightarrow [Fe^{3+} + (OH)_2Co^{2+} + (OH)_2Fe^{3+}]_n$$

$$[Fe^{3+} + (OH)_2Co^{2+} + (OH)_2Fe^{3+}]_n \rightarrow nCoFe_2O_4 + nH_2O$$
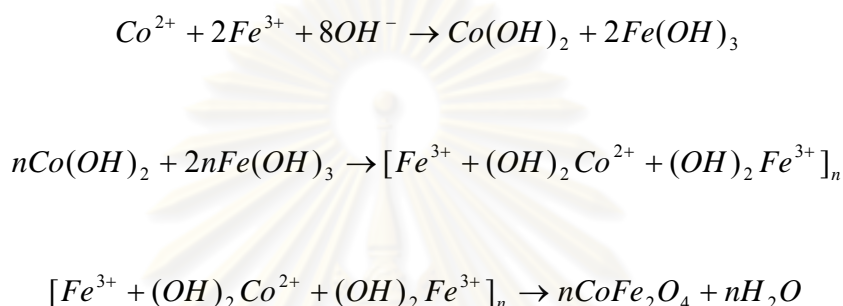
Scheme 3.1 Steps of the synthesis of cobalt ferrite magnetic particles (CoFe$_2$O$_4$) [130].

In the first step, 3.52 g of ferric chloride (FeCl$_3$) and 3.16 g of cobalt nitrate hexahydrate (Co(NO$_3$)$_2$.6H$_2$O) were dissolved in 250 mL of DI water. This solution was stirred, followed by adding 29 mL of 6 M NaOH quickly at room temperature [111, 131]. The color of solution changed from red-orange to black and the black precipitates were formed. In the second step, the black precipitates were separated by centrifuge machine, washed with DI water for four times and dried in the oven overnight. In the last step, the precipitates were grided in a motar and calcined at 500 $^\circ$C for 6 hours and then grided again to obtain fine particles.

3.3.3 Initiator modification of magnetic particles

In this work, the initiator was synthesized by the reaction between 3-aminopropyltriethoxysilane and ethyl-2-bromopropionate. Then the obtained initiator was modified on the surface of magnetic particle (MPs). These two reactions are shown in scheme 3.2.
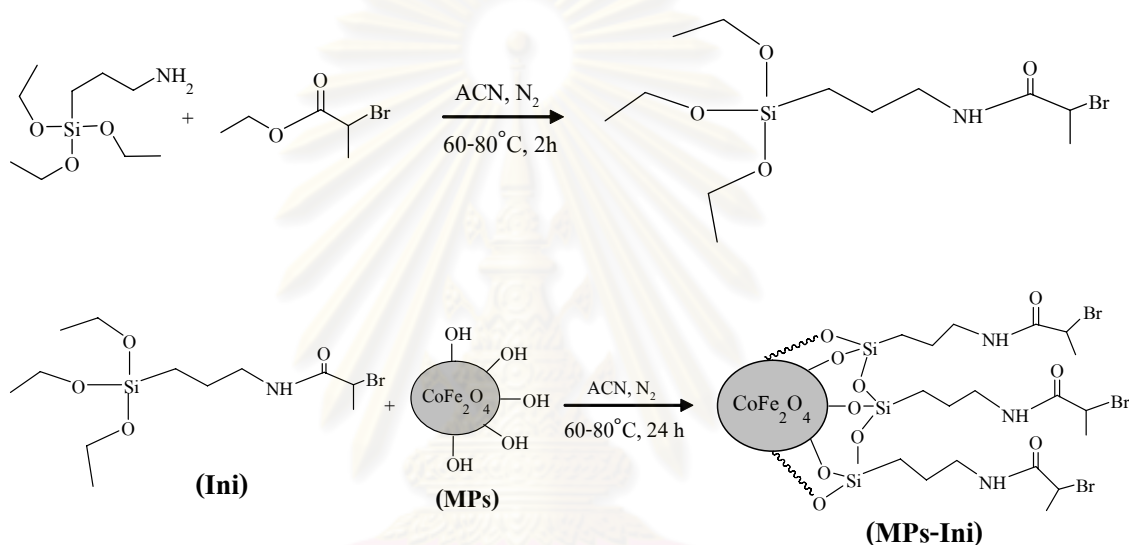
Scheme 3.2 Synthesis of initiator and modification of magnetic particles with the initiator.

The initiator was synthesized as the following method. In the first step, 1.52 mL of 3-aminopropyltriethoxysilane, 0.96 mL of ethyl-2-bromopropionate and 40 mL of dried acetonitrile were added into the two-necked round bottom flask. The solution was stirred for 2 hours at 60 $^{\circ}$C under nitrogen atmosphere. In the second step, 1.0 g of MPs was added into the solution and finally, the mixture was stirred for 24 hours at the same condition [125]. The particles were washed with ethanol (3×30 mL) and dichloromethane (3×30 mL) and dried at room temperature under vacuum.

3.3.4 Coating of polystyrene on magnetic particles

The polystyrene coating was synthesized on the surface of magnetic particles via atom transfer radical polymerization (ATRP). The synthesis reaction is shown in scheme 3.3.

Scheme 3.3 Atom transfer radical polymerization of styrene on the surface of magnetic particles.

In the first step, 57.6 mg (0.4 mmol) of Cu(I)Br, 0.084 mL (0.4 mmol) of PMDETA and 2.0 mL of DMF were added into the flask and the mixture was stirred under nitrogen atmosphere until the blue color appeared. Then 4 mL of styrene monomer and 1.0 g of initiator-coated magnetic particles (MPs-Ini) were added. The flask was degassed with nitrogen gas for one hour. Next, the mixture was stirred at $110^{\circ}C$ for 16 hours under nitrogen atmosphere. Finally, after the polymerization was completed, the polymerization solution was transferred to cold methanol [125]. The final product particles (MPs-PS) were washed with methanol (3×30 mL) and dried at room temperature under vacuum.

3.3.4.1 Effect of initiator dose on polymer coating

The appropriate amount of the initiator for the polymer coating was studied by varying the initiator amount in the range of 3.2 – 8.0 mmol g^{-1} MPs. Then, these initiator-modified MPs (MPs-Ini) were used in the polymerization of styrene monomer via ATRP. To investigate whether the polymer was well coated on magnetic particles surface, the leaching amount of Co or Fe from the coated particles was determined and compared to that of uncoated particles. If the particles are well coated with the polymer, the particles would not be dissolved in strong acid solution. The polystyrene-coated particles (MPs-PS) were stirred in 0.1 M HNO_3 for 90 minutes. Finally, the mixture was filtered to separate MPs-PS from solution. FAAS analysis was performed to determine the concentration of Co and Fe dissolved in solution. Furthermore, the TGA analysis was employed to determine the amount of initiator grafted on MPs surface. The Co and Fe leaching results after FAAS determination and the results from TGA analysis were used in the consideration of the appropriate amount of initiator.

3.3.5 Synthesis of chelating ligand AEPE

The chelating ligand 2-(3-(2-aminoethylthio)propylthio)ethanamine (AEPE) was synthesized and used for the modification of magnetic particles. The synthesis reaction is shown in scheme 3.4.
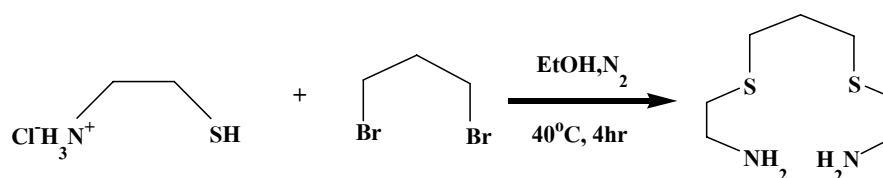
Scheme 3.4 Synthesis of 2-(3-(2-aminoethylthio)propylthio)ethanamine (AEPE).

Sodium metal (1 g, 42.9 mmol) was dissolved in 20 mL of ethanol and the solution was transferred into the flask that contained cysteamine hydrochloride (2.3 g, 20 mmol). The mixture was stirred for 15 minutes at 15 $^{\circ}$C before adding 1,3-dibromo propane (1.0 mL, 9.8 mmol) and then stirred for 4 hours at 40 $^{\circ}$C under nitrogen atmosphere. The ethanol was evaporated by rotary vacuum evaporator at 50 $^{\circ}$C. Sodium hydroxide solution (5 g in 15 mL DI water) was added to the residue and the mixture was kept in refrigerator overnight for phase separation of AEPE and aqueous solution. The AEPE ligand was then extracted by adding 10 mL of dichloromethane into the mixture. The obtained dichloromethane phase was washed with DI water (2×20 mL) and the moisture was removed by sodium sulfate anhydrous. Then, the dichloromethane phase was filtered and the solvent was removed by rotary vacuum evaporator at 40 $^{\circ}$C [132]. The yellow oil of AEPE was obtained after removing dichloromethane and characterized by ^{1}H-NMR and ^{13}C-NMR.

3.3.6 Modification of polystyrene-coated magnetic particles (MPs-PS) by AEPE

The polystyrene-coated magnetic particles (MPs-PS) were modified with ligand AEPE. The synthesis reaction is shown in scheme 3.5.
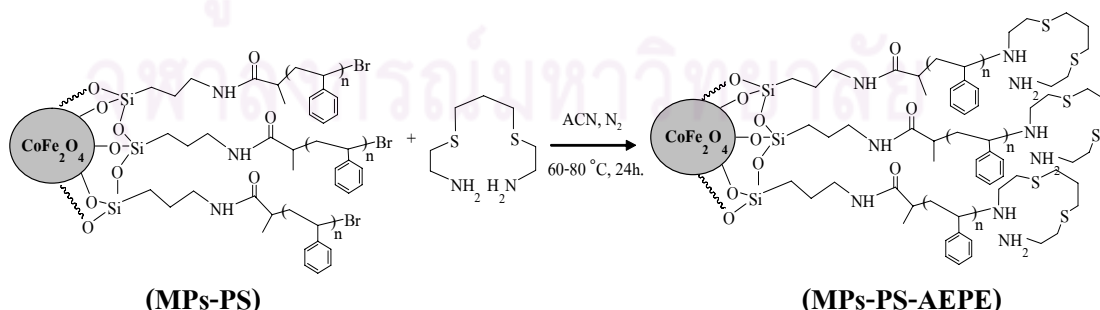
Scheme 3.5 Reaction of MPs-PS with ligand AEPE.

The MPs-PS (3 g) was dispersed in 100 mL of dried acetonitrile contained in round bottom flask and 1 g of AEPE was added. The mixture was stirred at 60 ^{o}C for 24 hours under nitrogen atmosphere. The final product (MPs-PS-AEPE) was separated by external magnetic field, washed with ethanol (3 × 50 mL) and dried at room temperature under vacuum. The overall synthesis pathway of MPs-PS-AEPE is shown in scheme 3.6.

The products were kept in desiccator. All the synthesized products obtained from each step were characterized by X-ray diffraction (XRD), Fourier transform infrared spectrometry (FT-IR), surface area analysis, scanning electron microscopy (SEM) and thermogravimetric analysis (TGA).
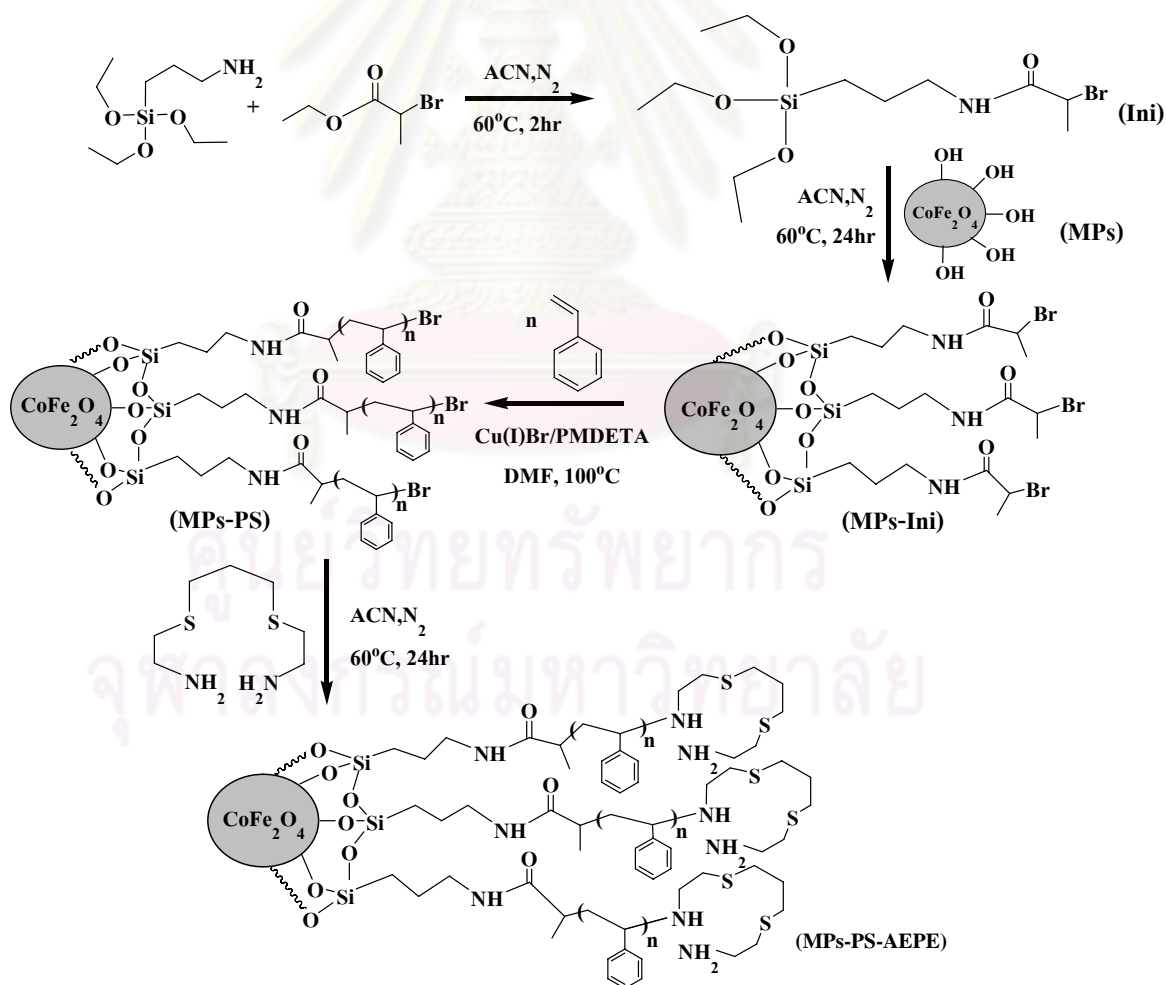
Scheme 3.6 Synthesis pathway of MPs-PS-AEPE.

3.4 Characterization

The materials were characterized to confirm the success of the synthesis of each step. The characterization techniques used are NMR, XRD, FT-IR, TGA, SEM and surface area analysis.

3.4.1 Characterization of chelating ligand

The ligand AEPE was dissolved in deuterated chloroform D1 ($CDCl_3$) and characterized by ^{1}H-NMR and ^{13}C-NMR. The chemical shifts were recorded and reported in part per million (ppm).

3.4.2 Characterization of modified magnetic particles

The modified and bare MPs were characterized by XRD, FT-IR, TGA, SEM and surface area analysis. The details of each characterization technique or operating instrument conditions are given as following.

X-ray diffractometer (XRD)

X-ray diffractometer was used for the characterization and the XRD pattern was recorded in the range of 25 to 65 two-theta (2θ). The d-spacing values were also determined.

Fourier transforms infrared spectrometer (FT-IR)

FT-IR was used for characterization of functional groups modified on the MPs surface using KBr pellet technique. Infrared spectra were recorded from 400-4000 cm^{-1} in transmittance mode.

Thermogravimetric analysis (TGA)

Thermogravimetric analysis is an analytical technique used to investigate the thermal stability of the materials. The weight loss of materials as function of temperature was measured under nitrogen atmosphere from 50 to 900 ^{o}C at the heating rate of 10 ^{o}C min^{-1} to confirm the difference in the chemical composition of the material before and after the modification.

Surface area analysis

The BET model and N$_2$ adsorption-desorption isotherms were used to determine the specific area of the modified and bare MPs.

Scanning electron microscopy (SEM)

SEM was used to exhibit the outer surface, size and shape of the bare MPs, MPs-Ini, MPs-PS and MPs-PS-AEPE.

3.5   Ninhydrin test

Ninhydrin test is the well-known method for qualitative analysis of amino acid group. In this work, ninhydrin test was used to detect terminal primary amine groups of chelating ligand AEPE modified on adsorbent. A small amount of adsorbents (MPs-PS-AEPE) was transferred into a glass test tube and 1 mL of ninhydrin solution was added. The mixture was heated to 100 ^{o}C. The color of solution will change from yellow to purple or dark blue when terminal primary amine groups are present. The color of solution remains yellow when there is no terminal primary amine group on the surface of adsorbent.

3.6   Adsorption study

The batch method was used for adsorption study in this research. The adsorption of Hg(II) and Ag(I) ions in aqueous solutions by MPs-PS-AEPE was studied. Adsorbent (0.005 g) was added to 5 mL of metal ions solutions. The pH and ionic strength of solutions were controlled by using 0.05 M CH_3COONa. The mixture was stirred at a specific time before the adsorbents were separated by external magnetic field or centrifugation. Atomic absorption spectrometer was used to determine the residual concentrations of metal in solution. The operating parameters are shown in Table 3.3. The values of the initial pH and the pH at equilibrium were measured before and after extraction.

The effect of pH of metal solution, extraction time, ionic strength, co-existing ions, initial concentration, adsorbent dose were studied. All adsorption experiments were performed in triplicates.

Table 3.3 AAS operating conditions for measurement of metals concentrations in aqueous solutions

Operating condition	Hg	Ag
Wavelength (nm)	253.7	328.1
Slit width	0.70	0.70
Lamp type	HCL[a]	HCL[a]
Lamp current (mA)	8	15
C_2H_2 flow rate (min^{-1})	-	3
Air flow rate (min^{-1})	100[b]	10
Working range (mg L^{-1})	0.05-0.3	0.5-3.0

The concentrations of mercury and silver were determined by CVAAS and FAAS, respectively.

[a] Hallow Cathode Lamp

[b] Argon flow rate

3.6.1 Effect of pH of metal ion solutions

The effect of pH on extraction efficiency was studied by varying the pH in the range of 1.0-8.0. The initial concentrations of Hg(II) and Ag(I) ions were 30 and 50 mg L^{-1}, respectively. The pH and ionic strength were controlled by 0.05 M CH_3COONa buffer solution. The pH of solutions was adjusted to the desired value using KOH (1 and 5% w/v) or HNO_3 (1 and 5% v/v). The experiments were performed by using 0.005 g of adsorbent in 5 mL of metal solutions. The mixture was stirred for an hour and then the adsorbent was separated by external magnetic force or centrifugation. The residual concentration of metal were determined by FAAS for Ag(I) solution and CVAAS for Hg(II) solution.

3.6.2 Effect of extraction time

The influence of extraction time on extraction efficiency was studied by using contact time from 5 to 180 minutes. The initial concentration of Hg(II) and Ag(I) ions were 30 and 50 mg L^{-1}, respectively. The experiments were performed by using 0.005 g of adsorbent in 5 mL of metals solution at pH 7 for Hg(II) or pH 5 for Ag(I). Furthermore, the pH and ionic strength were controlled by 0.05 M CH_3COONa buffer solution. The residual Hg(II) and Ag(I) ions concentrations were determined by CVAAS and FAAS, respectively.

3.6.3 Effect of ionic strength

The effect of ionic strength on extraction of Hg(II) and Ag(I) ions was investigated using $NaNO_3$ in the concentration range of 0.01-1.00 M. The experiments were performed by using 0.005 g of adsorbent in 5 mL of metals solution at pH 7 for Hg(II) or pH 5 for Ag(I). The mixture of adsorbent and metals solution was stirred for 60 minutes.

3.6.4 Effect of coexisting ions

The effect of coexisting ions on extraction efficiency was investigated using alkali, alkali earth metal ions (Na^+, K^+, Mg^{2+} and Ca^{2+}), heavy metal ions (Ni^{2+}, Cd^{2+} and Pb^{2+}) and NO_3^-, SO_4^{2-} and Cl^- anions as coexisting ions. The extraction of Hg(II) ions was performed using the concentration of alkali, alkali earth metal ions and anions of 0.1 and 1.0 M and heavy metal ions of 0.15 and 1.50 mM in Hg(II) solution (30 mg L^{-1}).

The extraction of Ag(I) ions was performed using the concentration of alkali, alkali earth metal ions and anions of 0.1 and 1.0 M and heavy metal ions of 0.5 and 5.0 mM in Ag(I) solution (50 mg L^{-1}).

3.6.5 Adsorption isotherm

In this experiment, the initial concentrations of Hg(II) and Ag(I) solution were varied in the range of 30-200 and 40-170 mg L^{-1} at fixed adsorbent amount. The experiments were performed using the optimum pH and extraction time. The temperature was controlled at 25±0.5 ^{o}C. The equilibrium concentrations were determined by CVAAS and FAAS for Hg(II) and Ag(I) ions, respectively.

3.6.6 Effect of adsorbent dose and adsorption kinetics

In this study, the adsorbent dose was varied in the range of 0.005-0.030 g for extraction of metal ions in 5 mL solution. The initial concentration of Hg(II) and Ag(I) solutions at pH 7 and 5 were 30 and 100 mg L^{-1}, respectively. The extraction time was varied from 5-180 minutes. The extraction efficiencies of each adsorbent dose were determined as the function of extraction time. Two models of adsorption kinetics plot (pseudo-first order and pseudo-first order) were adopted.

3.7 Desorption study

The elution of adsorbed Hg(II) or Ag(I) from used adsorbent (MPs-PS-AEPE) was investigated using batch method. Thiourea and HNO$_3$ were used as eluent in this study. Eluent (5 mL) was added to 0.005 g of used adsorbent. Then, the mixture was

stirred for one hour and adsorbent was separated from eluent. The concentrations of eluted Hg(II) and Ag(I) were determined by CAAAS and FAAS, respectively.

3.7.1 Type of eluent

Thiourea and nitric acid (HNO_3) were used as eluent. The HNO_3 concentration was varied in 1% and 5% v/v. The concentration of thiourea was varied in 0.1, 0.5 and 1.0 M, then mixed with 1% and 5% v/v HNO_3. The used adsorbent was obtained from the adsorption experiment using the initial concentration of 100 and 50 mg L^{-1} for Hg(II) and Ag(I), respectively. The used adsorbent containing Hg(II) or Ag(I) ions was stirred with 5 mL of various type and concentration of eluents for an hour. Then, the adsorbent was separated. The concentrations of Hg(II) and Ag(I) in eluent after desorption were determined by CAAAS and FAAS, respectively.

3.7.2 Effect of desorption time

The suitable eluent was selected from the results of experiment 3.7.1. In the study of Ag(I) desorption , the desorption time was investigated by using the time from 15-180 minutes. Then, the concentrations of Ag(I) in eluent were determined.

3.7.3 Reusability of the adsorbent

The repeated adsorption/desorption cycles were performed 6 and 10 cycles for extraction of Ag(I) and Hg(II), respectively. The suitable eluent and desorption time from the experiment 3.7.1 and 3.7.2 were used. Then, the Hg(II) and Ag(I) concentrations after both extraction and desorption were determined.

3.8   Application to real water sample

The wastewater samples used in this experiment were collected from the laboratory of Gem and Jewelry Institue of Thailand and a petrochemical industry plant. The extraction efficiency of Hg(II) and Ag(I) from real samples by MPs-PS-AEPE was investigated.

3.8.1 Wastewater from Gem and Jewelry Institute of Thailand

Before application in extraction experiments, the concentration of Ag(I) in wastewater from the laboratory of Gem and Jewelry Institue of Thailand was determined by FAAS. The pH was also measured. The pH value and concentration of Ag(I) in wastewater was about 1.7 and 4,600 mg L^{-1}, respectively.

The sample solution used in this experiment was prepared by dilution 3.30 mL of the wastewater to 100 mL with 0.05 M CH_3COONa to control pH value to pH 5.0. The concentration of Ag(I) ions in wastewater after dilution was 145 mg L^{-1}. The sample solution (5.0 mL) was extracted by using 0.005, 0.010, 0.020 or 0.030 g of MPs-PS-AEPE with the extraction time of 60 minutes. The residual concentration of Ag(I) was determined by FAAS. The experiment was performed in triplicate.

3.8.2 Wastewater from petrochemical industry plant

The wastewater containing mercury provided from the petrochemical industry plant (Rayong province) was filtered and preserved by treating with nitric acid. The pH of sample solution was measured. Then, the wastewater sample was digested using ASTM3223 standard method [133] to reduce the interference and to ensure that the mercury in sample was converted to the mercuric ions before the

extraction and determination of the mercury concentration by cold-vapor atomic absorption standard method [134]. Wastewater sample was digested with nitric acid, sulfuric acid, potassium persulfate and potassium permanganate solutions. After the digestion was completed, the excess permanganate was reduced with hydroxylamine. Thereafter, the obtained transparent aqueous solution was used to determine the initial mercury concentration in wastewater sample.

The raw wastewater (10.0 mL) was filtered and extracted by using 0.005 and 0.010 g of MPs-PS-AEPE with the extraction time of 60 minutes. After extraction, the sample was digested using standard method and the residual concentration of Hg(II) was determined by CVAAS. This experiment was performed in triplicate.

The steps of the digestion method adapted from ASTM3223 and cold-vapor atomic absorption standard method are described below.

Digestion method

1. Wastewater sample (10 mL) was transferred into the 250 mL flask.

2. The concentrated sulfuric acid (0.5 mL) and nitric acid (0.25 mL) was added under the continuous stirring.

3. Potassium permanganate solution (5% w/v) (1.0 mL) was added to the flask. The solution in the flask was stirred. If necessary, more volume of $KMnO_4$ could be added until the purple color persists.

4. Potassium persulfate solution (5% w/v) (5.0 mL) was added to the flask. The flask was heated in water bath at the digestion temperature of 95 $^{\circ}$C for 2 hours.

5. The flask was cooled and the sodium chloride-hydroxylammonium hydrochloride solution was added to reduce the excess permanganate until the solution was transparent. The concentration of mercury in the obtained solution was then determined.

CHAPTER IV

RESULTS AND DISCUSSION

4.1 Characterization

4.1.1 Characterization of chelating ligand AEPE

The chelating ligand AEPE was synthesized by the reaction between cysteamine hydrochloride and 1,3-dibromopropane via nucleophilic substitution reaction proposed by S.B. Choudhury [135]. The nucleophile was generated by ethoxide base that abstracted proton of -SH group and then reacted with 1,3-dibromo propane containing bromides as leaving groups. The synthesis of AEPE was carried out with the 2:1 mole ratio of cysteamine hydrochloride and 1,3-dibromopropane. The product was obtained as yellow oil. The synthesis of AEPE is shown in scheme 4.1.
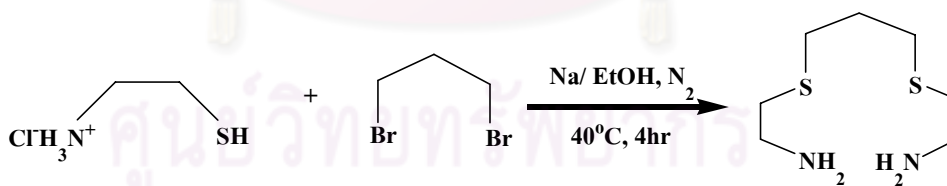
Scheme 4.1 The synthesis of 2-(3-(2-aminoethylthio)propylthio)ethanamine (AEPE).

The ^{1}H-NMR spectrum of AEPE was recorded in $CDCl_3$ (Figure 4.1). ^{1}H-NMR spectrum of aliphatic protons showed 3 multiplets due to the symmetrical structure of chelating ligand AEPE as follows : δ (ppm) 1.83 (2H, t, $CH_2C\underline{H}_2CH_2$, $J =$ 7.02 Hz), 2.59 (8H, t, $SC\underline{H}_2$, $J = 6.24$ Hz) and 2.84 (4H, t, $C\underline{H}_2NH_2$, $J = 6.24$ Hz).

The ^{13}C-NMR spectrum of AEPE was obtained with the chemical shifts as follows: δ (ppm) 29.4 (1C, *s*, CH$_2$CH$_2$CH$_2$), 30.5 (2C, *s*, SCH$_2$CH$_2$NH$_2$), 36.2 (2C, *s*, CH$_2$CH$_2$CH$_2$S), and 41.0 (2C, *s*, NH$_2$CH$_2$CH$_2$). The ^{13}C-NMR spectrum of AEPE is shown in Figure 4.2. These results indicate that AEPE was successfully synthesized.
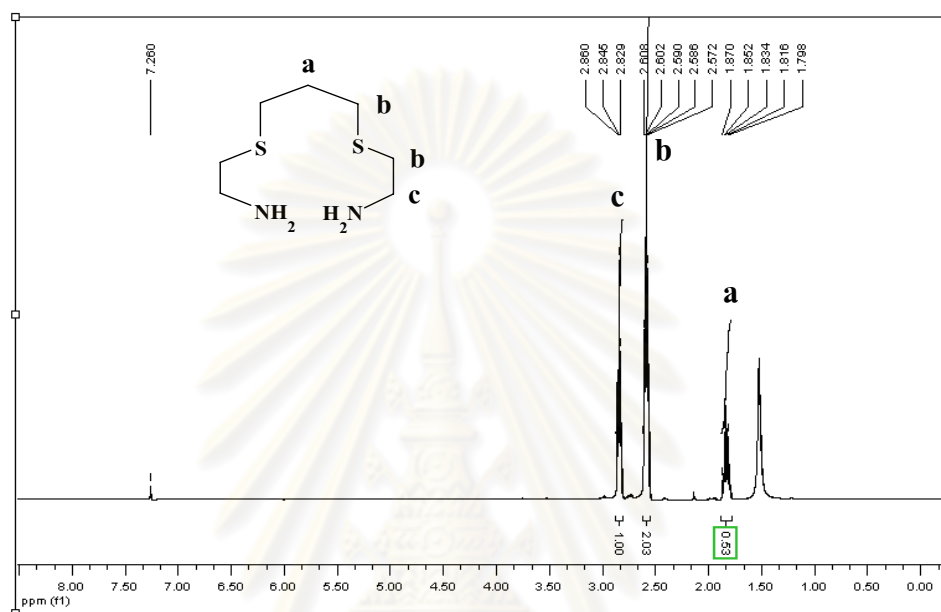
Figure 4.1 The ^{1}H-NMR spectrum of AEPE in CDCl$_3$.
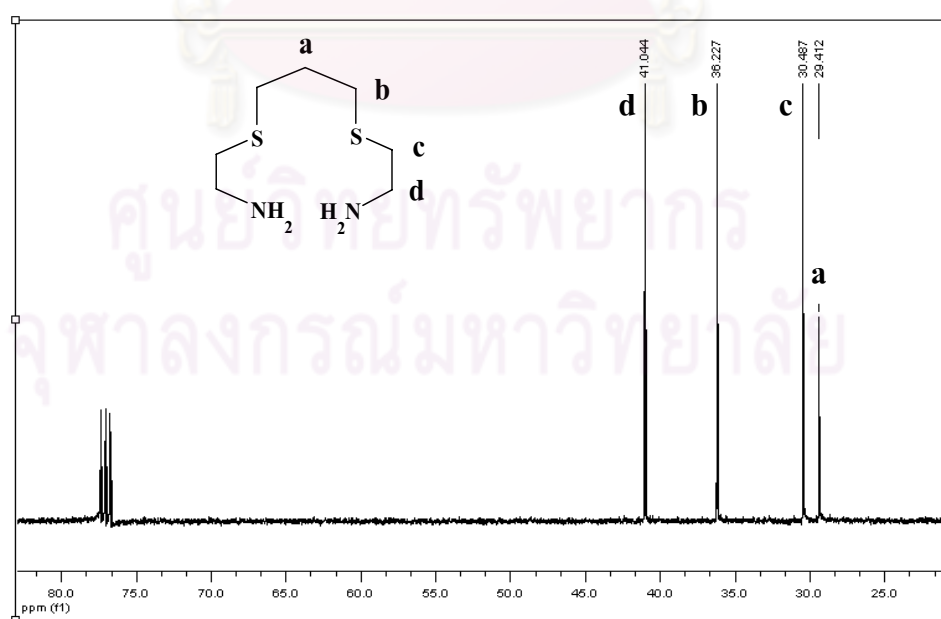
Figure 4.2 The ^{13}C-NMR spectrum of AEPE in CDCl$_3$.

4.1.2 Synthesis and characterization of polystyrene-coated magnetic particles modified with 2-(3-(2-aminoethylthio)propyl thio)ethanamine (MPs-PS-AEPE)

The synthesis pathway of MPs-PS-AEPE is shown in scheme 4.2.
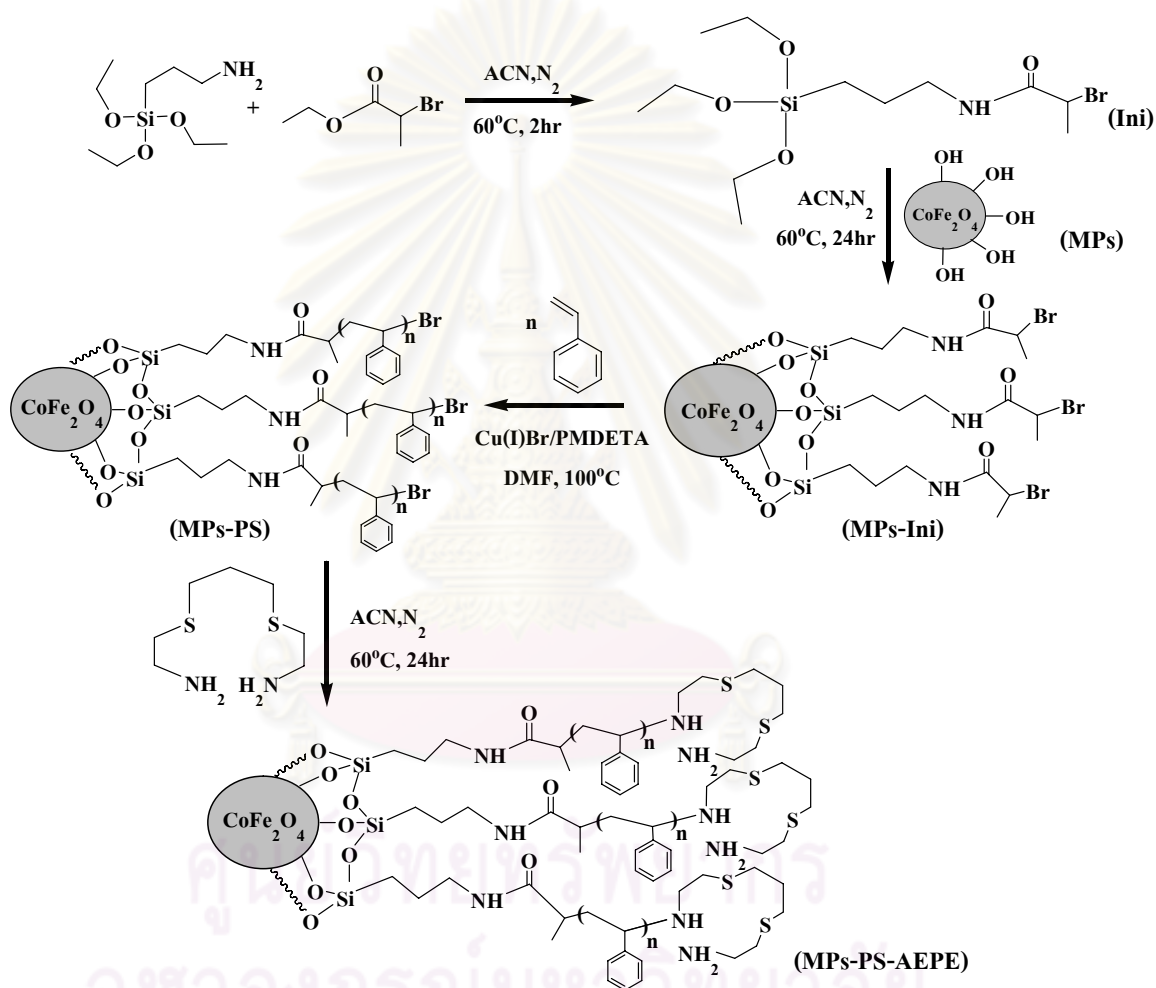
Scheme 4.2 The synthesis pathway of MPs-PS-AEPE.

The synthesis of MPs-PS-AEPE started with the synthesis of magnetic particles (MPs) by chemical co-precipitation between Co^{2+} and Fe^{3+}. In the second step, the synthesis of initiator (Ini) was performed by reaction between 3-aminopropyl triethoxysilane and ethyl-2-bromopropionate, followed by silanization of silane groups

of initiator onto the surface of MPs. The reaction occurred between ethoxy groups of initiator and hydroxyl groups on MPs surface yielding MPs-Ini as a product and ethanol as a by-product. In the next step, the styrene monomer was polymerized on the surface via atom transfer radical polymerization (ATRP) to give the product MPs-PS, which had polystyrene coating on the surface with bromide leaving groups at the chain end of polystyrene. In the final step, the polystyrene shell was modified with the chelating ligand AEPE through nucleophilic substitution reaction and the final product MPs-PS-AEPE was obtained.

4.1.2.1 Effect of initiator dose

In the synthesis of MPs-PS-AEPE, the effect of the initiator amount used to graft on the surface of magnetic particles (MPs) was investigated by varying the amount of synthesized initiator in the range of $3.2 - 8.0$ mmol g^{-1} MPs prior to the polymerization of styrene monomer.

The thermal stability of MPs-Ini prepared from each initiator amount was investigated. The results from thermo gravimetric analysis (TGA) are shown in Figure 4.3. The decomposition of the initiator grafted on the surface of magnetic particles (MPs) was observed in the temperature range of $250\text{-}550^{\circ}\text{C}$. This temperature onset was not present in bare magnetic particles' TGA profile. The TGA curve of MPs-Ini shows the average weight loss of 3.30, 4.54, 5.01 and 4.25 % when used the initiator amount of 3.2, 4.8, 6.4 and 8.0 mmol g^{-1} MPs, respectively. This weight loss corresponds to the loss of initiator molecules grafted on MPs surface. Furthermore, the slight weight loss above 500°C of MPs-Ini confirms that the siloxy groups of the synthesized initiator were present and the initiator was grafted on the MPs surface [14]. The results of the initiator amount grafted on MPs surface in each added initiator amount are shown in Table 4.2. The results indicate that an increase of initiator amount

above 4.8 mmol g^{-1} MPs would not result in a higher amount of initiator on MPs. Therefore, the initiator dose of 6.4 mmol g^{-1} MPs was chosen to prepare the MPs-PS-AEPE due to the least % leaching and the appropriate amount grafted on MPs surface.
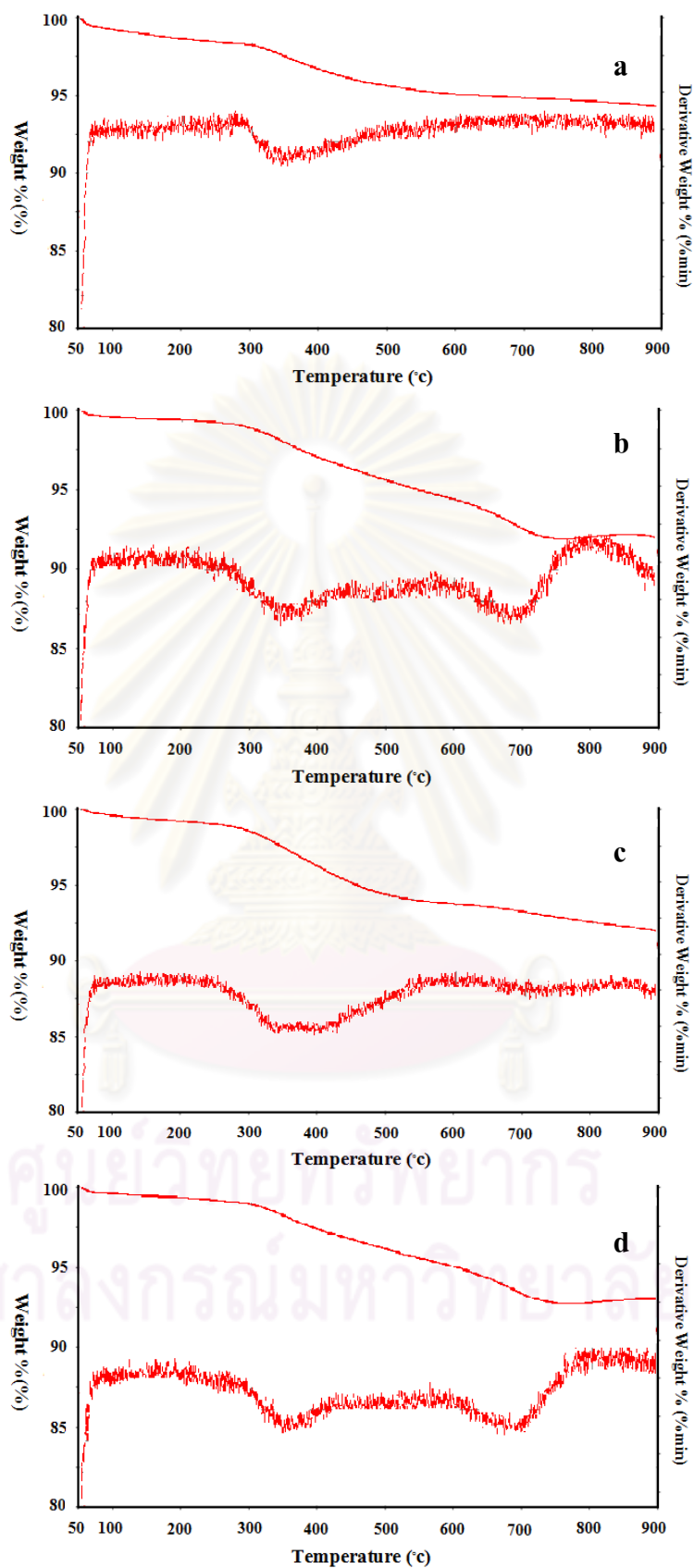
Figure 4.3 TGA curves of MPs-Ini prepared by using initiator amount of (a) 3.2, (b) 4.8, (c) 6.4 and (d) 8.0 mmol g^{-1} MPs.

Table 4.1 The amount of initiator grafted on MPs calculated from TGA of MPs-Ini using different initiator amount in the synthesis

Added initiator amount (mmol g^{-1} MPs)	Grafted initiator amount (mmol g^{-1} MPs)[a]
3.2	0.18 ± 0.01
4.8	0.25 ± 0.01
6.4	0.28 ± 0.02
8.0	0.23 ± 0.01

[a] Mean $\pm$ S.D. (n=3)

The obtained MPs-PS was tested for stability in acidic solution and the leaching amount of Co and Fe from the particles was determined. If the MPs surface is well coated by polystyrene, the extent of particles dissolution in acid solution will diminish, compared to the bare magnetic particles. The % leaching was calculated from the amount of the metal ions leached from MPs-PS in acidic solution using the equation 4.1.The results are shown in Table 4.1.

$$\% \text{ leaching} = \frac{\text{amount}_{leaching}}{\text{total amount}_{particles}} \times 100 \qquad (4.1)$$

amount $_{leaching}$ = amount of Co or Fe leached from particles (mg)

total amount $_{particles}$ = amount of Co or Fe in particles (mg)

Table 4.2 The results of % leaching of MPs-Ini and MPs-PS when varied the initiator amount

Amount of initiator (mmol g^{-1} MPs)	% Leaching*			
	MPs-Ini		MPs-PS	
	Co	Fe	Co	Fe
3.2	0.26±0.01	0.25	0.06	0.06±0.01
4.8	0.20	0.21	0.04	0.04
6.4	0.18	0.21±0.01	0.03	0.03±0.01
8.0	0.22	0.23±0.01	0.04	0.04±0.01

* Mean ± S.D. (n=3)

The % Co and Fe leaching of MPs were 2.25 ± 0.16 and 2.56 ± 0.08 %, respectively.

The high % leaching of Co and Fe was observed when the bare magnetic particles (MPs) were in the strong acidic solution. When MPs was grafted with the initiator, the percentage leaching decreased because the grafted initiator layer prevented the direct contact between MPs and acid. Therefore, the particles dissolution was less likely to occur. Moreover, the percentage leaching decreased more significantly when MPs was coated with polystyrene. The results can infer that the MPs-PS was successfully prepared in each initiator dose. From the leaching results of MPs-Ini prepared by using various initiator doses, a slight decrease of percentage leaching was observed with an increase of initiator dose from 3.2 to 6.4 mmol g^{-1} MPs. On the other hand, a slight increase of % leaching was observed when used 8.0 mmol of initiator per gram of MPs. The use of a high concentration of initiator may lead to the condensation of siloxy groups of initiator molecules resulting in a lower amount of the free initiator to be grafted on MPs surface. The trends of % leaching of Co and Fe from MPs-PS and MPs-Ini are in the same direction. From the *ANOVA* statistic calculation, in each initiator dose, the % leaching of Co and Fe from MPs, MPs-Ini and

MPs-PS are different significantly at the 95% confidence limit. Thus, the initiator grafting and polystyrene coating on MPs surface improved the stability of the particles in acidic solution. When increased the initiator amount from 3.2 to 8.0 mmol g^{-1} MPs, the Co^{2+} and Fe^{3+} % leaching values of both MPs-Ini and MPs-PS are different significantly at the 95% confidence limit. The increase in the initiator amount resulted in a better coating of polymer on MPs surface and hence improved the stability of the particles in acidic solution. The initiator doses of 3.2 and 4.8 mmol g^{-1} MPs are not suitable due to the relatively high % leaching. When compared the amount of initiator of 6.4 to 8.0 mmol g^{-1} MPs, the calculation from *t-Test* statistics showed that the values of % leaching of Co and Fe from MPs-PS are not different. Therefore, the initiator dose of 6.4 mmol g^{-1} MPs was chosen to prepare the MPs-PS-AEPE afterwards due to the least % leaching.

4.1.2.2 X-ray diffraction spectrometry

X-ray diffraction spectrometry was used to characterize the structure of the modified magnetic particles compared to the bare magnetic particles. The results are shown in Table 4.3 and Figure 4.4.

Table 4.3 The d-spacing and 2-theta values of modified magnetic particles compared to bare magnetic particles

Phase	$d_{220}(A°)/2\theta$	$d_{311}(A°)/2\theta$	$d_{400}(A°)/2\theta$	$d_{422}(A°)/2\theta$	$d_{511}(A°)/2\theta$	$d_{440}(A°)/2\theta$
MPs	2.94/30.34	2.52/35.58	2.08/43.40	1.71/53.64	1.61/57.34	1.48/62.95
MPs-Ini	2.96/30.20	2.52/35.60	2.09/43.20	1.71/53.60	1.61/57.10	1.48/62.66
MPs-PS	2.96/30.10	2.52/35.50	2.09/43.35	1.71/53.56	1.61/57.11	1.48/62.75
MPs-PS-AEPE	2.96/30.20	2.53/35.48	2.09/43.25	1.71/53.56	1.61/57.16	1.48/62.77
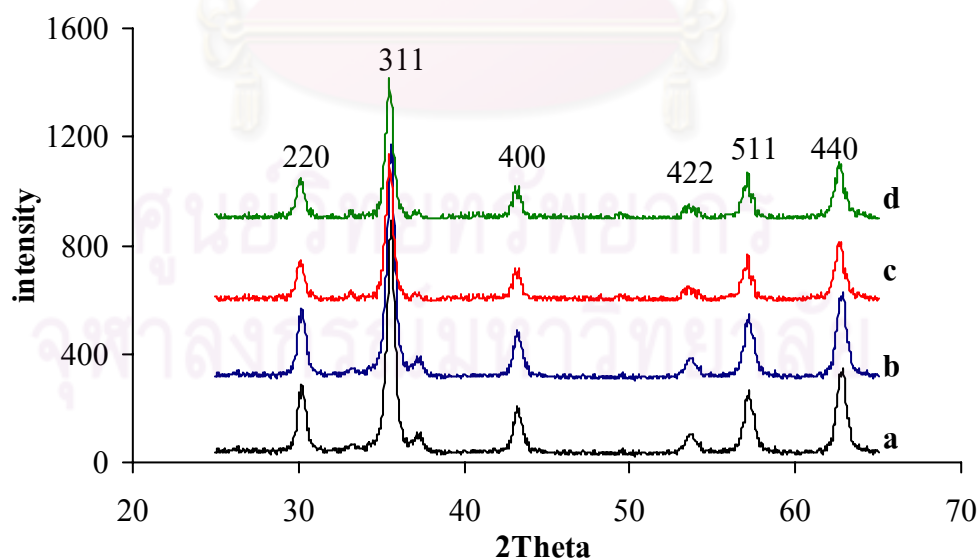
Figure 4.4 XRD patterns of (a) MPs, (b) MPs-Ini, (c) MPs-PS and (d) MPs-PS-AEPE.

The XRD pattern of MPs (Figure 4.3a) shows the characteristic peaks at around 30.3°, 35.6°, 43.4°, 53.6°, 57.3° and 62.9° 2θ, which are well indexed to the reflection of the crystal plane of spinel structure and correspond to the miller indices of (220), (311), (400), (422), (511) and (440), respectively [136, 137]. Moreover, the XRD patterns of MPs-Ini, MPs-PS and MPs-PS-AEPE (Figure 4.3b-d) show the same characteristic peaks as those of MPs. These patterns of all diffraction peaks match well to those of JCPDS card 22-1806 for $CoFe_2O_4$. It indicates that the main structure of MPs did not change after coating with polystyrene and modification with AEPE. These results also reveal that the modification occurred only on the surface of MPs. The XRD reflections show the characteristics of cubic spinel structure resulted from the formation of oxyhydroxide phase as an intermediate in the process which was converted to spinel under controlled conditions [136]. The interplanar reflections of oxyhydroxide phase and spinel phase are closely related.

4.1.2.3 Fourier transforms infrared spectroscopy

The functional groups and surface chemical compositions of the magnetic particles (MPs), MPs-Ini, MPs-PS and MPs-PS-AEPE were investigated by FT-IR technique. The FT-IR spectra of MPs, MPs-Ini, MPs-PS and MPs-PS-AEPE are shown in Figure 4.5. The FT-IR bands of the bare magnetic particles and the new bands after coating with polystyrene and modification with chelating ligand AEPE are interpreted as follow.
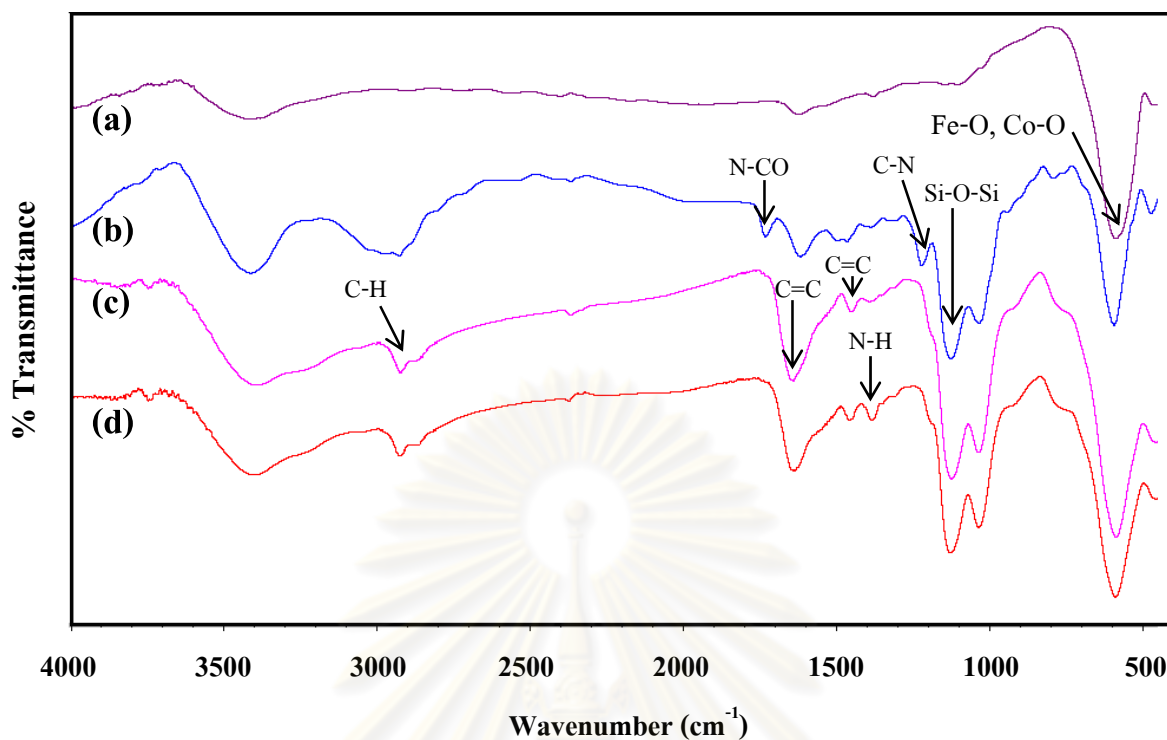
Figure 4.5 FT-IR spectra of (a) MPs, (b) MPs-Ini, (c) MPs-PS and (d) MPs-PS-AEPE.

Figure 4.5(a) shows the FT-IR spectrum of bare magnetic particles. The characteristic peak at 587 cm^{-1} corresponds to the Fe-O and Co-O vibrations at tetrahedral site related to magnetite phase [121, 138-140]. After initiator modification (Fig 4.5(b)), the characteristic peaks of the Si-O-Si stretching vibration are present at 1035 cm^{-1} and 1127 cm^{-1}. The small peak at 1226 cm^{-1} corresponds to C-N bond stretching and the peaks at 1614 cm^{-1} and 1742 cm^{-1} correspond to amide bond (N-CO) stretching. When the particles were coated with polystyrene (Fig 4.5(c)), the signal of aliphatic C-H bond stretching appears at 2929 cm^{-1} and the C=C bond stretching of the conjugated ring does at 1642 cm^{-1} and 1458 cm^{-1}. A new small peak for N-H bond bending is observed at 1378 cm^{-1} after surface modification with AEPE (Fig 4.5(d)). These results are sufficient to infer that the adsorbent MPs-PS-AEPE was successfully prepared.

4.1.2.4 Thermogravimetric analysis

The thermal stability of the modified magnetic particles was investigated to confirm the presence of modified components by following the decomposition of organic contents and the structural degradation of metal oxide. The results from thermogravimetric analysis (TGA) are shown in Figure 4.6. All TGA curves show the weight loss at the temperature below $200^{o}C$ due to the vaporization of moisture and organic solvent used for synthesis. The decomposition of the organic compounds modified on the surface of magnetic particles (MPs) was observed in the temperature range of $175\text{-}550^{o}C$ as shown in Figure 4.6b-d. The TGA curve of MPs-Ini (Figure 4.6b) shows the weight loss of 6.60% at the temperature range of $250\text{-}500^{o}C$. This weight loss corresponds to the loss of initiator molecules grafted on MPs surface in the first step. Furthermore, the slight weight loss above $500^{o}C$ of MPs-Ini confirms that the siloxy groups of the synthesized initiator were present and the initiator was grafted on the MPs surface [141].

The TGA curve of MPs-PS (Figure 4.6c) shows the weight loss of 12.80% at the temperature range of $350\text{-}550^{o}C$. The similar result was found in the previous research of Sun *et al.* [125] when Fe_3O_4 particles were coated with polystyrene. This weight loss corresponds to the loss of polystyrene coated on MPs surface. An increase in weight loss of 0.95% in the temperature range of $175\text{-}300^{o}C$ was observed when MPs-PS was modified with AEPE ligand (Figure 4.6d). The TGA curve of MPs-PS-AEPE shows the weight loss of 13.75 % in the temperature range of $175\text{-}550^{o}C$ due to the presence of AEPE and polystyrene molecules [141]. The increasing trend of weight loss from the materials indicates that the surface was successfully modified by different molecules.
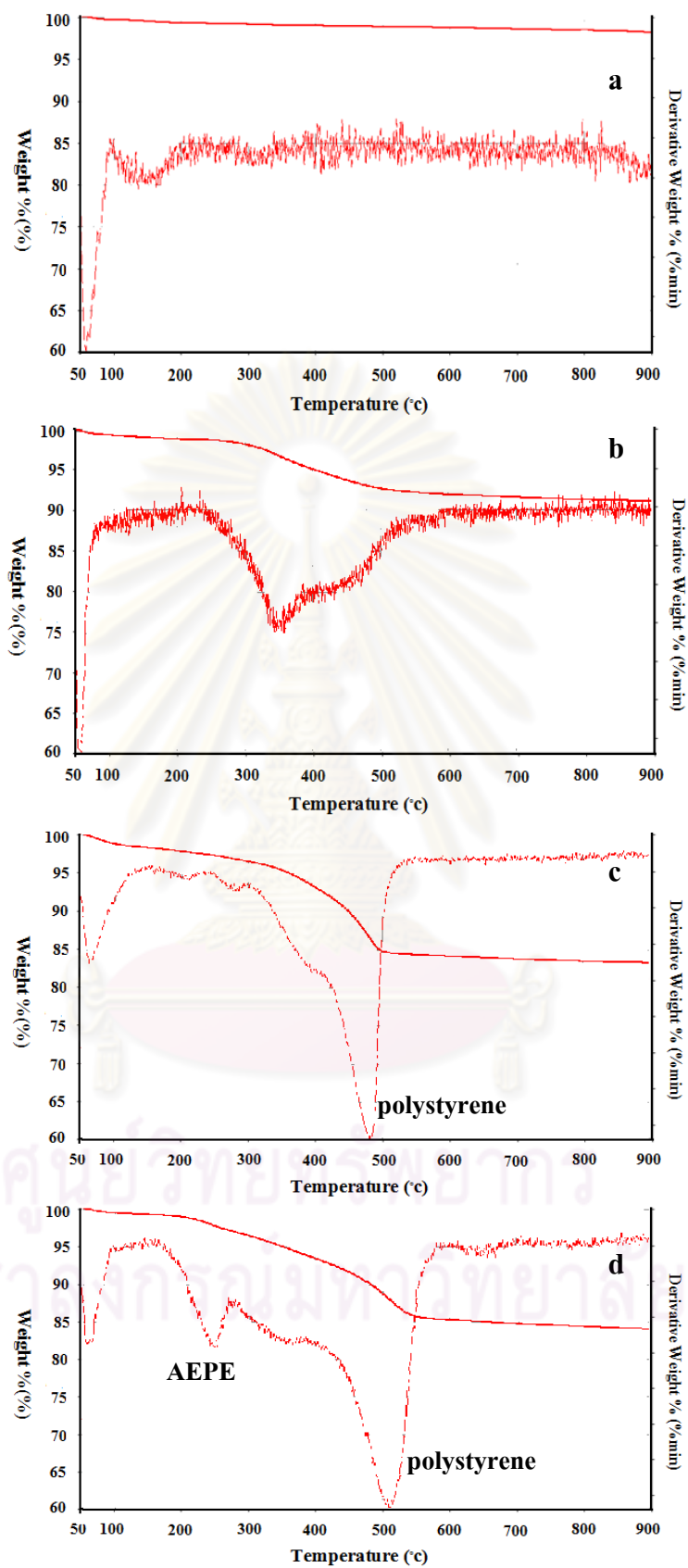
Figure 4.6 TGA curves of (a) MPs, (b) MPs-Ini, (c) MPs-PS and (d) MPs-PS-AEPE.

4.1.2.5 Surface area analysis

The surface area of MPs, MPs-Ini, MPs-PS and MPs-PS-AEPE were determined by surface area analyzer using BET model. The results are shown in Table 4.4. The results show a significant decrease in surface area of MPs-Ini compared to MPs due to the grafting of initiator molecules on MPs surface. Moreover, MPs-PS and MPs-PS-AEPE show the very low surface area compared to MPs and MPs-Ini because of the non porous polystyrene coating on the agglomerates of MPs. Thus, these results indicate that the polystyrene was coated on the surface after initiator grafting.

Table 4.4 The results of surface area analysis

Phase	Surface area $(m^2 g^{-1})$*	Total pore volume $(\times 10^{-3} cm^3 g^{-1})$ *
MPs	47.54 ± 4.30	217.87 ± 4.44
MPs-Ini	23.69 ± 1.90	78.61 ± 5.62
MPs-PS	1.02 ± 0.28	4.81 ± 1.03
MPs-PS-AEPE	0.71 ± 0.21	4.63 ± 0.91

* Mean ± S.D. (n=3)

4.1.2.6 Scanning electron microscopy

Scanning electron microscope (SEM) was used to exhibit the change of surface of materials after polystyrene-coating and AEPE-modification. The SEM images are shown in Figure 4.7.
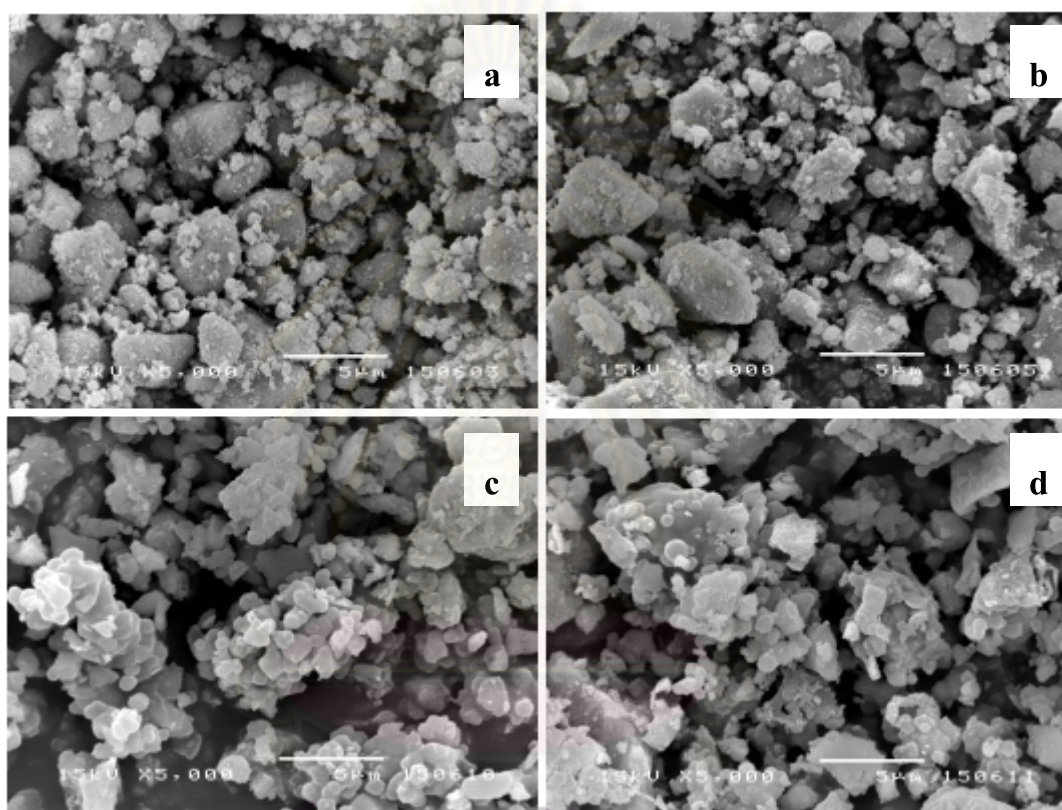
Figure 4.7 SEM images of (a) MPs, (b) MPs-Ini, (c) MPs-PS and (d) MPs-PS-AEPE.

From SEM images, the outer surface of MPs was changed after polystyrene coating and AEPE modification. The outer surface of agglomerate particles appears to be smoother as a result of polymer coating. This confirms that the polystyrene was coated on MPs surface.

4.1.2.7 Ninhydrin test

Ninhydrin method was used to detect terminal primary amine groups of the chelating ligand AEPE on the surface of adsorbent. The color of ninhydrin solution changes from yellow to purple if the free primary amine groups are present in solution. The color of ninhydrin solutions was yellow when tested with MPs, MPs-Ini and MPs-PS. These results agreed with their structure, which had no free terminal primary amine groups. However, when tested with MPs-PS-AEPE, the color of ninhydrin solution changed from yellow to purple as shown in Figure 4.8. The expected color change indicates that there were free terminal primary amine groups of AEPE on the adsorbents. The experimental results of ninhydrin test are shown in Table 4.5.
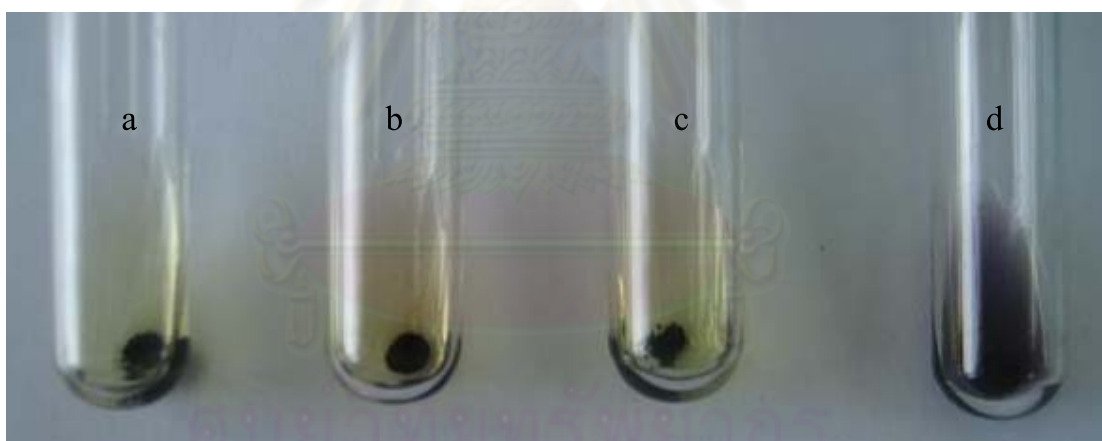
Figure 4.8 Ninhydrin test of (a) MPs, (b) MPs-Ini, (c) MPs-PS and (d) MPs-PS-AEPE.

Table 4.5 Ninhydrin test results

Phase	Color of solution
MPs	yellow
MPs-Ini	yellow
MPs-PS	yellow
MPs-PS-AEPE	purple

4.2 Adsorption study

The MPs-PS-AEPE was used as adsorbent in adsorption study of Hg(II) and Ag(I) ions in aqueous solutions using batch method. The effect of pH, extraction time, ionic strength, and coexisting ions were studied and the optimized condition for metal ions extraction was proposed. The adsorption isotherms and adsorption kinetics were also investigated. Moreover, types of eluent, elution time and adsorbent reusability were studied after adsorption experiment.

The metal ions extraction efficiency is presented in term of % extraction and adsorption capacity, calculated from the change of the metal concentration in solution using the equations 4.2 and 4.3, respectively,

$$\text{Extraction (\%)} = \frac{C_i - C_e}{C_i} \times 100 \tag{4.2}$$

$$\text{Adsorption capacity } (q) = \frac{(C_i - C_e)V}{m} \tag{4.3}$$

where q = adsorption capacity (mg g^{-1})

C_i = initial concentration of metal ions in aqueous solution (mg L^{-1})

C_e = equilibrium concentration of metal ions in aqueous solution (mg L^{-1})

V = volume of metal ions solution (L)

m = mass of adsorbent (g)

4.2.1 Effect of pH of metal ion solutions

The influence of solution pH on metal extraction depends on the nature of adsorbent (e.g. functional groups on adsorbent surface) and metal ions. The solution pH may have two effects on metal ions extraction in the following: (i) the form of chelating ligand would change due to the protonation or deprotonation of the donor site of chelating ligand and (ii) the metal ions are present in different species in solution e.g. hydrolyzed species, metal-hydroxide. Thus, the suitable pH value of solution must be higher than pK_a value of the donor site and lower than K_{sp} of the metal-hydroxide formation. The extraction of metal ions as a function of solution pH was investigated to obtain the suitable pH for extraction.

The initial pH of Hg(II) or Ag(I) solution was varied in the range of 1-8 using buffer solutions. The extraction of Hg(II) and Ag(I) in aqueous solution by MPs, MPs-PS and MPs-PS-AEPE are shown in Figures 4.9 and 4.10, respectively.
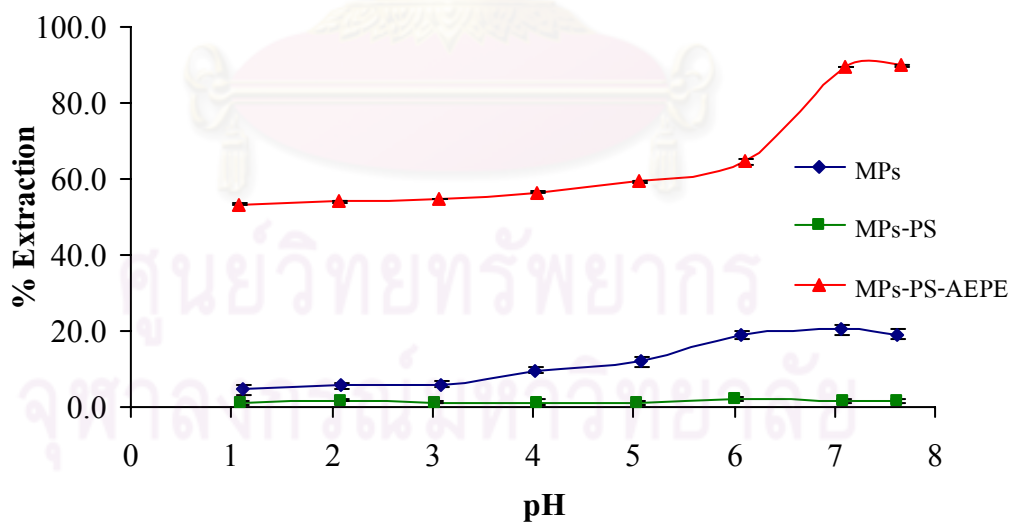
Figure 4.9 Effect of pH on extraction of Hg(II) ions (30 mg L^{-1}) by MPs, MPs-PS and MPs-PS-AEPE.
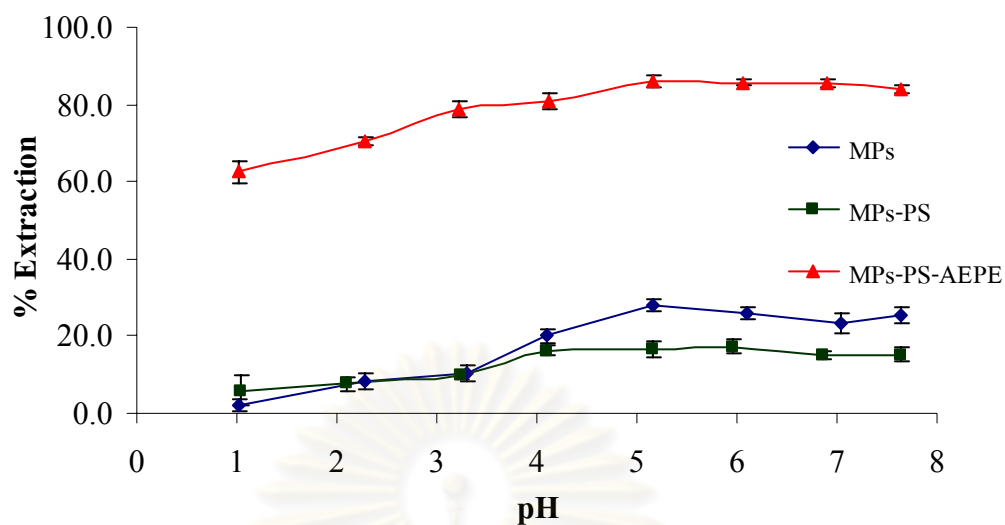
Figure 4.10 Effect of pH on extraction of Ag(I) ions (50 mg L^{-1}) by MPs, MPs-PS and MPs-PS-AEPE.
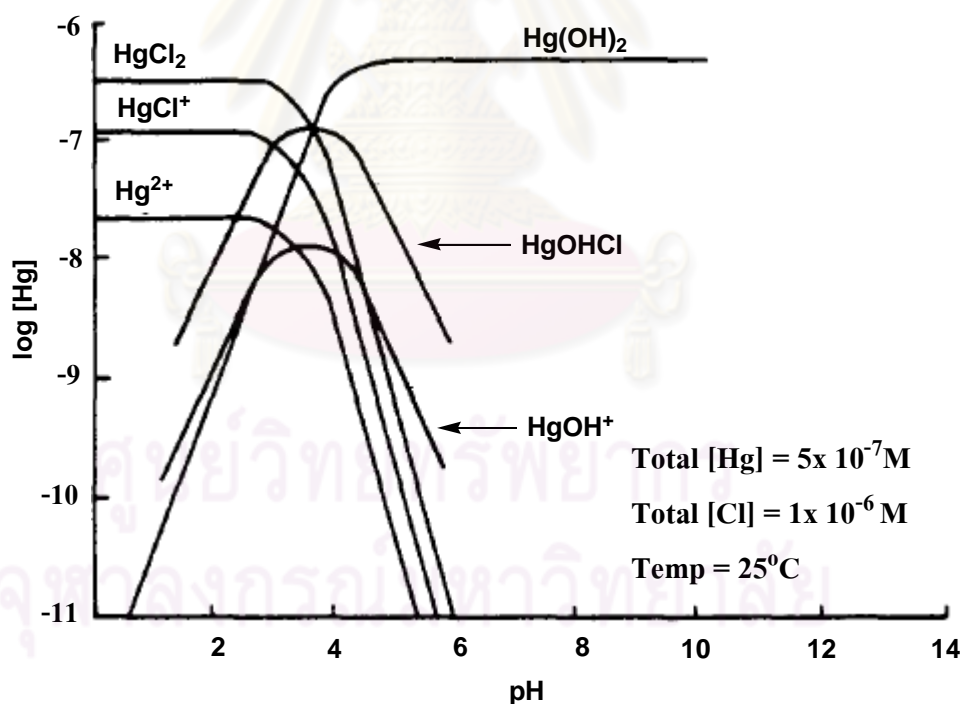
Figure 4.11 The diagram of mercury speciation as a function of pH [76].

The extraction efficiency of both metals by MPs-PS-AEPE was clearly greater than that observed when used MPs and MPs-PS. This result could be explained by the presence of sulfur and nitrogen donor atoms on the surface of MPs-PS-AEPE

which can form complex with Hg(II) and Ag(I) via coordination. According to Pearson rule, sulfur is a soft base that prefers to form complex with the soft acid i.e. Hg(II) and Ag(I) [142, 143]. It was found that the extraction efficiency of Hg(II) in aqueous solution by MPs were low ($\leq 20.3\%$) at all pH values. Considering the pH_{PZC} or the pH at the point of zero charge, that is the pH at which the net charge on surface is equal to zero (the extent of positive charge equal to that of negative charge), the pH_{PZC} of magnetic particles (MFe_2O_4, M: Fe, Co and Mn) was reported to be in the range of 6.50 - 6.78 [121, 144-146]. If the pH of aqueous solution is lower than pH_{PZC}, the surface of MPs can be protonated resulting in positively charged surface. On the other hand, if the solution pH is higher than pH_{PZC}, the surface of MPs can be deprotonated and becomes the negatively charged surface [144, 162]. Furthermore, the Hg(II) speciation diagram (Figure 4.10) obtained from literature [76, 147, 148] shows that Hg(II) species exist as Hg^{2+}, $HgOH^+$ and $Hg(OH)_2$ at pH lower than 6.0 and the dominant species of Hg(II) at the pH higher than 6.0 is $Hg(OH)_2$ only. Therefore, the low efficiency in Hg(II) extraction by MPs observed at pH lower than 6.0 can be explained by the electrostatic repulsion between positively charged surface and cationic species of Hg(II). At the pH higher than 6.0, the adsorption of neutral species ($Hg(OH)_2$) on the negatively charged surface may occur, the mechanism is still unknown, resulting in higher extraction efficiency.

In the case of MPs-PS-AEPE, the results show that the % extraction increased with increasing the pH of solution and the optimal pH for extraction was pH 7.0-8.0 with the % extraction of 89.51 - 89.83%. These results can be explained by the different affinity of sulfur and nitrogen donor atoms of AEPE toward different Hg(II) species. Regarding the mercury speciation (Figure 4.10) [76], the major species of Hg(II) are Hg^{2+} at pH less than 4.0. The mixture of Hg^{2+}, $Hg(OH)^+$ and $Hg(OH)_2$ may be found at pH 4-6, and $Hg(OH)_2$ is the dominant species at the pH higher than 6.0. The neutral molecules are softer acid than metal ions according to Pearson rule. Therefore, at the equilibrium pH of 7.0 - 8.0 the coordination of AEPE with $Hg(OH)_2$

occurred with higher affinity, compared to the coordination of AEPE with Hg(II) cationic species [142, 143]. On the other hand, in acidic solution, the amine groups of AEPE on MPs-PS-AEPE surface would be protonated, resulting in the lower binding affinity of the protonated AEPE with Hg(II) cationic species, compared to the binding affinity of the non-protonated AEPE with $Hg(OH)_2$. Hence, the low extraction efficiency of Hg(II) by MPs-PS-AEPE was observed at the equilibrium pH of 1.0 - 6.0.

In the case of Ag(I) extraction, Figure 4.10 shows the effect of pH on extraction of Ag(I) in aqueous solution by MPs, MPs-PS and MPs-PS-AEPE. The % extraction of Ag(I) by MPs and MPs-PS-AEPE increased with increasing the solution pH. The maximum values of % extraction were 25.92 and 85.88% for MPs and MPs-PS-AEPE, respectively. When the pH value was increased from pH 1 to 8, the surface of MPs became more negatively charged, while the silver species in the solution having pH value of 2.0 - 10.0 was Ag^+ cations [79]. Thus, the adsorption of Ag^+ on MPs surface via electrostatic interaction occurred favorably when the pH of solution increased. The extraction efficiency of Ag(I) by MPs-PS-AEPE increased with increasing pH due to the decrease of degree of ligand protonation, resulting in the better coordination between Ag^+ and AEPE on adsorbent surface. On the other hand, the lower extraction efficiency was observed at the lower pH (pH 1 - 3) for both MPs and MPs-PS-AEPE. These results could be explained by the protonation of MPs surface and AEPE molecules, resulting in the positively charged MPs surface and protonated AEPE that have low binding affinity toward Ag^+ cations.

It should be noted that the extraction efficiency of both Hg(II) and Ag(I) in aqueous solution by MPs-PS were very low ($\leq$ 2.05% for Hg(II) and $\leq$ 17.20% for Ag(I) extraction) at all pH values due to the loss of ion exchange ability as a result of polystyrene coating. However, the very low % extraction was observed, indicating that the MPs surface was not grafted with initiator or coated with polystyrene wholly.

By considering the leaching of Co^{2+} and Fe^{3+} from MPs-PS-AEPE, in strong acid solution (pH 1.0-4.0), very low % leaching was observed in the range of 0.005 -0.049% and 0.004 - 0.078% for Co^{2+} and Fe^{3+}, respectively. The high acidity of metals solution could erode the MPs-PS-AEPE surface where was not covered by the polymer resulting in the leaching of Co^{2+} and Fe^{3+}. In contrast, at higher pH (pH 5.0-8.0), there was no Co^{2+} and Fe^{3+} leaching. The leaching results at various solution pH is summarized in Table 4.6.

The suitable pH for extraction of Hg(II) and Ag(I) are pH 7.0 and pH 5.0, respectively due to the high extraction efficiency and no leaching of Co^{2+} and Fe^{3+} from adsorbent. These pH values were used in the extraction experiments for the study of the effect of other parameters afterwards.

Table 4.6 The leaching of Co^{2+} and Fe^{3+} from MPs-PS-AEPE in metal solution at various pH

pH values	% Co^{2+} leaching[a]		% Fe^{3+} leaching[a]	
	in Hg(II) extraction	in Ag(I) extraction	in Hg(II) extraction	in Ag(I) extraction
1.0	0.036 ± 0.003	0.049 ± 0.003	0.078 ± 0.013	0.073 ± 0.003
2.1	0.027 ± 0.006	0.041 ± 0.006	0.059 ± 0.010	0.042 ± 0.003
3.1	0.012 ± 0.003	0.027 ± 0.003	0.028 ± 0.013	0.031
4.1	0.006 ± 0.003	0.005 ± 0.003	0.004 ± 0.003	0.008 ± 0.002
5.1	n.d.	n.d.	n.d.	n.d.
6.1	n.d.	n.d.	n.d.	n.d.
7.0	n.d.	n.d.	n.d.	n.d.
7.6	n.d.	n.d.	n.d.	n.d.

[a] Mean ± S.D. (n=3)

n.d. = Non detectable, the detection limit of the determination of Co^{2+} and Fe^{3+} by FAAS were 3.5×10^{-3} and 35.7×10^{-3} mg L^{-1}, respectively.

4.2.2 Effect of extraction time

The adsorption mechanism of metal ions in aqueous solution on adsorbents can be described by the boundary model, which has three main steps as following: (i) bulk transport, (ii) film transport and (iii) intraparticle transport. The bulk transport is the transportation of metal ions from bulk solution to boundary film which occurs rapidly [89, 149]. The film transport is the transportation of metal ions from boundary film to the surface of adsorbents. The intraparticle transport is the metal ions transfering from the surface to the intraparticle active sites. The process of film and/or intraparticle transport is often the rate determining step of adsorption equilibrium. Thus, the kinetics of mass transport in adsorption mechanism is dependent to the time. In this experiment, the effect of extraction time was investigated to obtain the equilibrium time of the Hg(II) or Ag(I) adsorption using the extraction time in the range of 5-180 minutes at the pH values of 7.0 and 5.0 for Hg(II) and Ag(I) extraction, respectively. The initial concentration of Hg(II) and Ag(I) were 30 mg L^{-1} and 50 mg L^{-1}, respectively. The experiment was performed by increasing extraction time until the constant value of % extraction was observed. The results are shown in Figure 4.12.
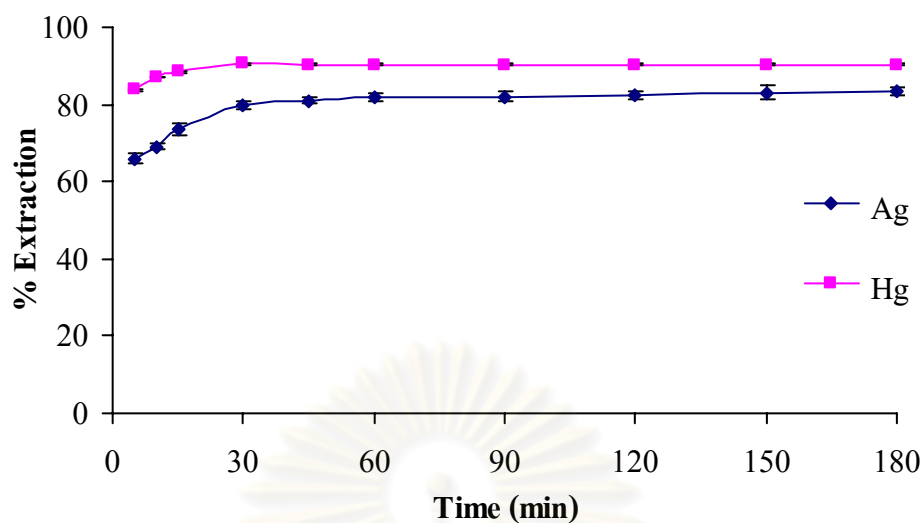
Figure 4.12 Effect of extraction time on extraction of Hg(II) and Ag(I) ions by MPs-PS-AEPE.

The extraction efficiency was enhanced when the extraction time was increased due to the longer contact time between metal ions and donor sites and the adsorption equilibrium was reached equilibrium after 30 minutes and 45 minutes in Hg(II) and Ag(I) extraction, respectively. Therefore, the extraction time of 60 minutes was chosen for extraction experiment of both metals to assure the adsorption equilibrium.

4.2.3 Effect of ionic strength

In general, the wastewater from factories and natural water, especially sea water, contain ions other than the interested metal ions in different concentration depending on the source. In the sea water, it has high concentration of Na^+ and Cl^- of about 0.46 M [150-152]. These ions may affect the extraction efficiency of the MPs-PS-AEPE. For this reason, the effect of ionic strength on extraction efficiency was investigated by using $NaNO_3$ in the range of 0.01-1.00 M, which represents the concentration of Na^+ in various source of water. The results are summarized in Table 4.7.

Table 4.7 Effect of ionic strength of aqueous solution on extraction of Hg(II) and Ag(I) ions by MPs-PS-AEPE

Concentration of $NaNO_3$ (M)	Times		Extraction efficiency (%)[a]	
	$NaNO_3$: Hg (II)	$NaNO_3$: Ag(I)	Hg (II)	Ag(I)
0.01	67	22	89.53 ± 0.13	80.03 ± 2.30
0.02	133	43	89.81 ± 0.16	80.24 ± 1.49
0.05	333	108	89.85 ± 0.12	79.82 ± 2.03
0.10	667	216	89.90 ± 0.63	80.17 ± 1.25
0.25	1667	539	90.16 ± 0.19	79.81 ± 0.25
0.50	3333	1078	89.99 ± 0.15	79.95 ± 1.01
0.75	5000	1617	90.34 ± 0.24	80.82 ± 1.34
1.00	6667	2156	90.53 ± 0.09	82.37 ± 1.75

[a] Mean ± S.D. (n=3)

The initial concentration of Hg(II) and Ag(I) were 0.15 and 0.47 mM, respectively.

The extraction efficiency was observed in the range of 79.81 – 82.37% for Ag(I) and 89.53 – 90.53% for Hg(II) when used the concentration of $NaNO_3$ 22 to 2156 times (0.01 - 1.00 M) higher than the concentration of Ag(I). The ionic strength seem to have a slight effect on the extraction efficiency of Hg(II) and Ag(I). These results reveal that the adsorption between MPs-PS-AEPE and metallic species ($Hg(OH)_2$ and Ag^+) occurred mainly via coordination of AEPE with metallic species. Moreover, the adsorbent can be used to extract mercury and silver ions from water containing high concentration of salt with the good extraction efficiency.

4.2.4 Effect of coexisting ions

The alkali, alkali earth and heavy metal ions can be commonly found in the natural water and wastewater. These ions may affect the extraction efficiency of Hg(II) and Ag(I) ions by adsorbents due to the competitive adsorption with the analyte metal ions. In the case of anions, they can form complex or precipitate with analyte metal ions. Therefore, the effect of coexisting ions such as cations (i.e. alkali, alkali earth and heavy metal ions) and anions was investigated to evaluate the selectivity of MPs-PS-AEPE toward Hg(II) and Ag(I) ions. The salts used in the experiments were nitrate salts of cations and sodium salts for anions in this study. The experiments were preformed under optimum extraction condition of each analyte metal.

4.2.4.1 Effect of alkali and alkali earth ions

The nitrate salt of alkali and alkali earth ions (Na^+, K^+, Mg^{2+} and Ca^{2+}) were added to both Hg(II) and Ag(I) solution with the concentrations of 0.1 and 1.0 M. The extraction efficiency of the analyte metal ions by MPs-PS-AEPE was determined (Table 4.8). It was found that there was no change in extraction efficiency of both Hg(II) and Ag(I) in the presence of 0.10 and 1.0 M of different alkali and alkali earth metal ions. The results show that the competitive adsorption between the analyte metal ions and the alkali and alkali earth coexisting ions is less likely to occur on the surface of MPs-PS-AEPE. The presence of these coexisting ions in a high concentration did not affect the extraction efficiency of the adsorbent for Ag(I) and Hg(II) ions. These results indicated that the main adsorption mechanism is the coordination between AEPE and analyte metal ions rather than the ion exchange between cationic metal species and charged surface of MPs-PS-AEPE. Moreover, the complex formation of analyte metal ions and AEPE could occur well according to the hard/soft-acid/base principle [132, 143, 153].

Table 4.8 Effect of cations on the extraction of Hg(II) and Ag(I) ions onto MPs-PS-AEPE

Salts	Concentration of salt (M)	Extraction efficiency (%)[a]	
		Hg(II)	Ag(I)
NaNO$_3$	0.1	88.28 ± 0.35	78.37 ± 1.64
	1.0	88.25 ± 0.14	79.47 ± 1.59
KNO$_3$	0.1	89.26 ± 0.28	80.03 ± 0.51
	1.0	88.14 ± 0.32	78.22 ± 1.50
Mg(NO$_3$)$_2$	0.1	89.03 ± 0.24	78.77 ± 1.28
	1.0	88.17 ± 0.37	78.54 ± 0.69
Ca(NO$_3$)$_2$	0.1	88.71 ± 0.31	80.32 ± 1.54
	1.0	88.14 ± 0.33	78.13 ± 0.91

[a] Mean ± S.D. (n=3)

The initial concentration of Hg(II) and Ag(I) ions were 0.15 and 0.47 mM, respectively.

4.2.4.2 Effect of anions

The effect of anions (i.e. NO_3^-, SO_4^{2-} and Cl^-) on the extraction of Hg(II) and Ag(I) was studied (Table 4.9). The sodium salts of these anions were added to Hg(II) or Ag(I) solutions with the concentrations of 0.1 and 1.0 M. It was found that an increase in NO_3^- and SO_4^{2-} concentration did not affect the extraction efficiency of analyte metal ions. On the other hand, the presence of Cl^- had a significant effect on the extraction efficiency of the two analyte metal ions due to the precipitation between Ag(I) and Cl^- resulting in AgCl precipitates and complex formation between Hg(II) and Cl^- as different Hg-Cl species according to the formation constants shown in Table 4.10. Furthermore, the dominant species of Hg(II) in solution are different depending on Cl^- concentration. Regarding the formation constants and the results in Table 4.9, a

hypothesis to rationalize is proposed. It is possible that ligand AEPE can reduce Hg(II) to Hg(I) ions which was confirmed by the precipitation with Cl⁻ as Hg_2Cl_2 [132]. Using the formation constants, the dominant species are $HgCl_2$, $HgCl_3^-$ and $HgCl_4^{2-}$ in 0.1 M NaCl with the distribution of 36%, 26% and 38%, respectively, while the major species found in 1.0 M NaCl is only $HgCl_4^{2-}$. Regarding the standard reduction potential of these Hg species, the standard reduction potential of Hg^{2+}, $HgCl_2$ and $HgCl_4^{2-}$ are 0.91, 0.63 and 0.54 V, respectively [154, 155]. Therefore, $HgCl_2$ could be reduced by chelating ligand AEPE more readily than $HgCl_4^{2-}$ resulting in both Hg_2Cl_2 precipitate and coordination of Hg(I) on surface and the greater extraction efficiency was observed in the 0.1 M NaCl solution, compared to the extraction in the 1.0 M NaCl solution [132]. These results reveal that the adsorption of Hg-Cl species onto MPs-PS-AEPE is less favorable than Hg^{2+}, $Hg(OH)^+$ and $Hg(OH)_2$ species present in solution containing $NaNO_3$ or no salt, resulting in a significant decrease of extraction efficiency of Hg(II) in this experiment.

Table 4.9 Effect of anions on the extraction of Hg(II) and Ag(I) ions onto MPs-PS-AEPE

Salts	Concentration of salt (M)	Extraction efficiency (%)[a]	
		Hg(II)	Ag(I)
$NaNO_3$	0.1	90.79 ± 0.38	78.56 ± 1.18
	1.0	90.35± 0.12	78.59 ± 1.32
Na_2SO_4	0.1	90.15 ± 0.19	77.22 ± 1.47
	1.0	89.96 ± 0.36	75.26 ± 0.81
NaCl	0.1	78.76 ± 0.88	-[b]
	1.0	22.87 ± 1.81	-[b]

[a] Mean ± S.D. (n=3)

[b] Ag ions precipitate as AgCl.

The initial concentration of Hg(II) and Ag(I) ions were 0.15 and 0.47 mM, respectively.

Table 4.10 Aqueous speciation reactions and formation constants of Hg(II) ions with different anions [154, 156]

Reaction	Log K
$Hg^{2+} + H_2O \leftrightarrow Hg(OH)^+ + H^+$	-2.70
$Hg^{2+} + 2H_2O \leftrightarrow Hg(OH)_2 + 2H^+$	-6.19
$Hg^{2+} + NO_3^- \leftrightarrow HgNO_3^+$	0.45
$Hg^{2+} + Cl^- \leftrightarrow HgCl^+$	6.67
$Hg^{2+} + 2Cl^- \leftrightarrow HgCl_2$	6.44
$Hg^{2+} + 3Cl^- \leftrightarrow HgCl_3^-$	0.87
$Hg^{2+} + 4Cl^- \leftrightarrow HgCl_4^{2-}$	1.15
$Hg^{2+} + Cl^- + H_2O \leftrightarrow HgClOH + H^+$	3.23
$Hg^{2+} + SO_4^{2-} \leftrightarrow HgSO_4$	1.39
$Hg^{2+} + SO_4^{2-} + 2H_2O \leftrightarrow Hg(OH)_2SO_4^{2-} + 2H^+$	-4.83

4.2.4.3 Effect of heavy metal ions

The effect of the presence of heavy metal ions other than Hg(II) and Ag(I) ions on extraction efficiency was studied (Table 4.11). The nitrate salts of Ni^{2+}, Cd^{2+} and Pb^{2+} were added to Hg(II) or Ag(I) solutions with the concentrations equal to and ten times higher than these of Hg(II) and Ag(I). It was observed that the extraction efficiency of Hg(II) and Ag(I) was affected by the presence of coexisting heavy metal ions at the two concentrations. A slight decrease of the extraction efficiency of Hg(II) was observed, while a significant decrease of the extraction efficiency of Ag(I) was observed in the presence of Pb^{2+}, Ni^{2+} and Cd^{2+} at the two concentrations. This decrease is due to the competitive adsorption between Ag(I) and interfering heavy metal ions on the surface of MPs-PS-AEPE via coordination. Nevertheless, the adsorption efficiency

for Hg(II) and Ag(I) were relatively high, indicating that the MPs-PS-AEPE has high selectivity toward Hg(II) and Ag(I) ions compared to Pb(II), Ni(II) and Cd(II).

Table 4.11 Effect of heavy metal ions on the extraction of Hg(II) and Ag(I) ions onto MPs-PS-AEPE

Salts	Hg(II)		Ag(I)	
	Concentration of salt (mM)	Extraction efficiency (%)[a]	Concentration of salt (mM)	Extraction efficiency (%)[a]
NaNO$_3$	0.1×10^3	90.93 ± 0.54	0.1×10^3	79.36 ± 0.74
Pb(NO$_3$)$_2$	0.15	87.84 ± 0.27	0.50	75.56 ± 0.99
	1.50	86.63 ± 0.48	5.00	72.37 ± 1.21
Ni(NO$_3$)$_2$	0.15	90.61 ± 0.26	0.50	72.85 ± 1.00
	1.50	90.44 ± 0.47	5.00	69.36 ± 0.28
Cd (NO$_3$)$_2$	0.15	89.81 ± 0.23	0.50	71.03 ± 0.55
	1.50	89.47 ± 0.23	5.00	69.55 ± 1.24

[a] Mean ± S.D. (n=3)

The initial concentration of Hg(II) and Ag(I) ions were 0.15 and 0.47 mM, respectively.

4.2.5 Adsorption isotherm

In this experiment, adsorption isotherm of analyte metal ions on MPs-PS-AEPE surface was investigated. The adsorption behavior of metal ions on adsorbent at equilibrium would reveal the adsorption mechanism. The distribution of metal ions between solution and adsorbent (liquid and solid phase) at adsorption equilibrium can be described by several adsorption isotherms [157]. Langmuir and Freundlich isotherm are two models commonly used in the study of adsorption behavior. Langmuir isotherm is based on the assumption that analytes are chemically adsorbed on the

adsorbent surface at a fixed number of well defined sites. Each site can hold on one analyte molecule with the monolayer coverage or monolayer adsorption, all sites are energetically equivalent (homogeneous surface) and there is no interaction between analyte molecules [88, 158, 159]. While, Freundlich isotherm is based on the assumption that the uptake of metal ions occur on a heterogeneous surface by monolayer adsorption [160] or multilayer adsorption [158, 161]. The experimental data were fitted to both adsorption isotherms. The Langmuir adsorption isotherm model is described by equation 4.4 [88],

$$\frac{C_e}{q} = \frac{C_e}{q_m} + \frac{1}{bq_m} \qquad (4.4)$$

where C_e = equilibrium concentration of the analyte metal ions in
aqueous solution (mg L^{-1} or mol L^{-1})

q = adsorption capacity of adsorbent (mg g^{-1} or mol g^{-1})

q_m = maximum adsorption capacity of adsorbent (mg g^{-1} or mol g^{-1})

b = Langmuir constant related to energy of adsorption
(L mg^{-1} or L mol^{-1})

The linearized Langmuir isotherm allows the calculation of adsorption capacity (q_m) and the Langmuir constant (b). From the linear plot, the value of q_m and b could be calculated from slope and intercept, respectively.

The linearized form of Freundlidh isotherm is shown in equation 4.5 [89],

$$\log q = \log K_f + \frac{1}{n} \log C_e \qquad (4.5)$$

where K_f = Freundlich constant related to adsorption capacity

                    ($mg\ g^{-1}$ or $mol\ g^{-1}$)

           n = the numerical value of Freundlich constant

From the linear Freundlich isotherm plot, the value of K_f and n could be calculated from intercept and slope, respectively.

The experiment was performed at $25.0 \pm 0.5^{\circ}C$ by adding the fixed weight of MPs-PS-AEPE to solutions containing different initial concentration of Hg(II) or Ag(I). The remained concentration of Hg(II) and Ag(I) ions in solutions were determined by CVAAS and FAAS, respectively. The adsorption capacities and the equilibrium concentration are shown in Figure 4.13. The adsorption capacity for Hg(II) ions increased rapidly, whereas, the adsorption capacity for Ag(I) ions increased slowly at low initial concentration. The experimental data was plotted using Langmuir and Freundlich equation. Linear regression was performed to confirm the applicability of both Langmuir and Freundlich isotherms. The Langmuir and Freundlich isotherm plots are shown in Figure 4.14 and 4.15, respectively. Then, the constant values of both isotherm models were calculated using linear equations obtained and the results are listed in Table 4.12 and 4.13.
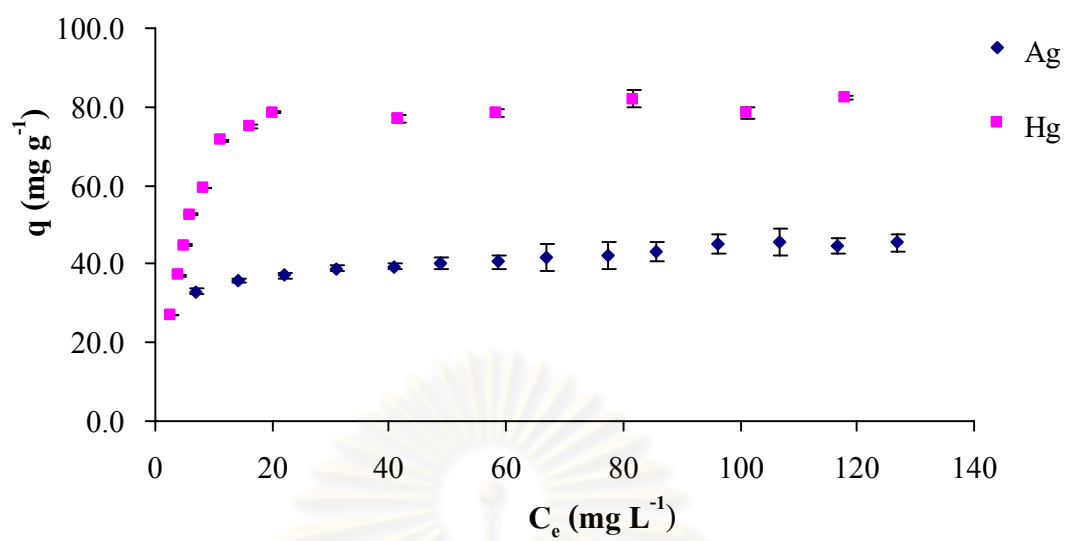
Figure 4.13 Adsorption isotherm of Hg(II) and Ag(I) at $25.0 \pm 0.5^{\circ}$C.

ศูนย์วิทยทรัพยากร

จุฬาลงกรณ์มหาวิทยาลัย
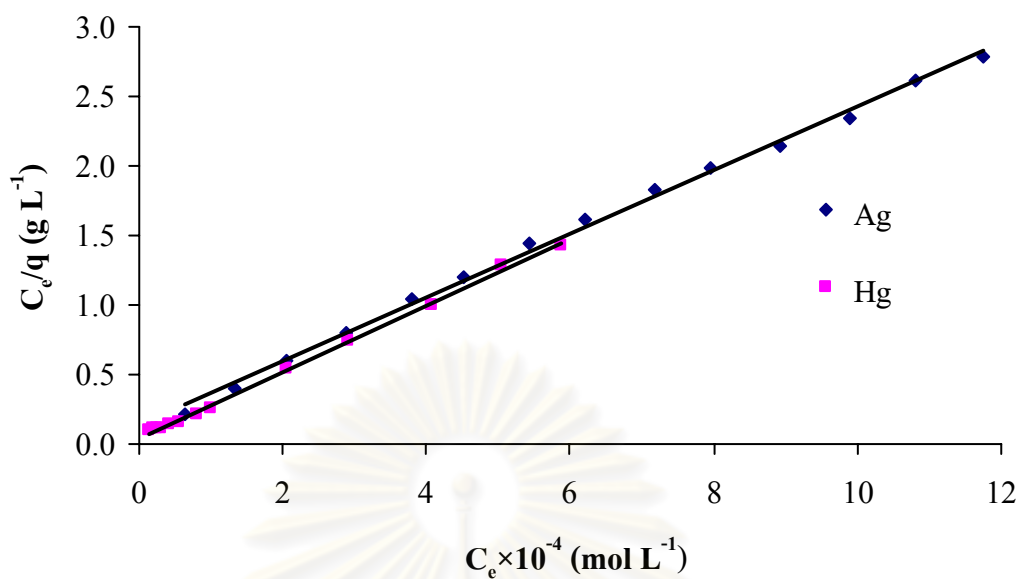
Figure 4.14 Langmuir isotherm plot of the adsorption of Hg(II) and Ag(I) ions onto MPs-PS-AEPE at $25.0 \pm 0.5^{\circ}$C.
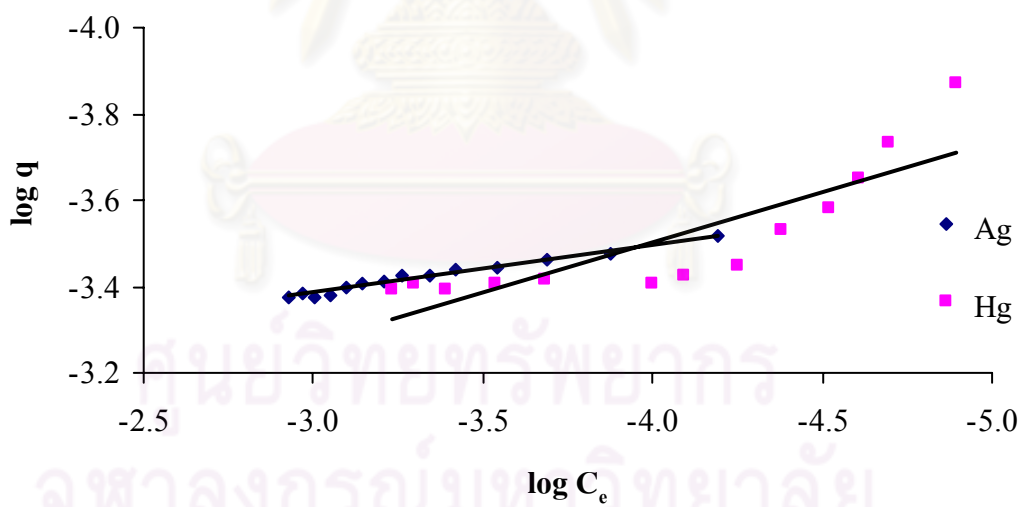
Figure 4.15 Fruendlich isotherm plot of the adsorption of Hg(II) and Ag(I) ions onto MPs-PS-AEPE at $25.0 \pm 0.5^{\circ}$C.

Table 4.12 The Langmuir isotherm parameters of the adsorption of Hg(II) and Ag(I) ions at $25.0 \pm 0.5^{\circ}$C

Metal	Linear equation	R^2	$b \times 10^4$ (L mol^{-1})	$q_{max,cal} \times 10^{-4}$ (mol g^{-1})	$q_{max,cal}$ (mg g^{-1})[a]	$q_{max,exp}$ (mg g^{-1})[b]	R_L
Hg(II)	y = 0.2392x + 0.0418	0.9983	5.72	4.18	83.86	82.38	0.017 – 0.106
Ag(I)	y = 0.2291x + 0.1358	0.9971	1.69	4.36	47.05	45.46	0.039 – 0.138

[a] The maximum adsorption capacity obtained from the calculation.

[b] The maximum adsorption capacity obtained from the experiment.

Table 4.13 The Freundlich isotherm parameters of the adsorption of Hg(II) and Ag(I) ions at $25.0 \pm 0.5^{\circ}$C

Metal	Linear equation	R^2	$K_f \times 10^{-3}$ (mol g^{-1})	K_f (mg g^{-1})	$1/n$	n
Hg(II)	y = 0.2314x – 2.5772	0.7262	2.65	531.29	0.2314	4.32
Ag(I)	y = 0.1108x – 3.0527	0.9780	0.89	95.48	0.1108	9.03

From the results shown in Table 4.12 and 4.13, the correlation coefficients (R^2) obtained by fitting the experimental data to the Langmuir model ($R^2 > 0.99$) are higher for both Hg(II) and Ag(I) adsorption, compared to the data fitting to the Freundlich model. These results indicate that the adsorption isotherm of Hg(II) and Ag(I) fit to Langmuir model better than Freundlich model. Therefore, the adsorption behavior of Hg(II) and Ag(I) on MPs-PS-AEPE follows Langmuir model assumptions. It was assumed that analytes are chemically adsorbed on the adsorbent surface. It could be confirmed by the Langmuir constant obtained from the calculation, which are high for adsorption of both metal ions onto MPs-PS-AEPE. Thus, it indicates that the main adsorption mechanism of Hg(II) and Ag(I) onto MPs-PS-AEPE surface is chemisorption via coordination of metal ions with the binding sites of AEPE that contain sulfur and nitrogen donor atom. The maximum adsorption capacity (q_{max}) of adsorbent for both Hg(II) and Ag(I) obtained from the experiment correspond to q_{max} obtained from the calculation of Langmuir model. The adsorption reached a saturation of adsorption capacity at high equilibrium concentration as shown Figure 4.11 with the monolayer coverage of Hg(II) and Ag(I) on the MPs-PS-AEPE surface. Moreover, the essential features of Langmuir isotherm model can be explained in term of a dimensionless constant separation factor or equilibrium parameter, R_L, given as equation 4.6 [162],

$$R_L = \frac{1}{1+bC_i} \qquad (4.6)$$

where b = Langmuir constant related to energy of adsorption (L mol^{-1})

C_i = initial concentration of metal ions (mol L^{-1})

In this experiment, the values of R_L obtained from Langmuir model are in the range of 0 to 1 (R_L = 0.017 – 0.138) indicating that the adsorption of both Hg(II)

and Ag(I) onto MPs-PS-AEPE are favorable with increasing of adsorption capacity at higher initial concentration [132, 138, 163, 164]. The parameter R_L is related to the type of isotherm as presented in Table 4.14.

Regarding the relatively high R^2 value obtained from Freundlich plot of Ag(I) adsorption, it seems that the surface of the adsorbent contains heterogeneous active sites i.e. AEPE and uncoated charged surface. At pH 5, the dominant species of Ag(I) are almost Ag^+ that can interact with the uncoated charged surface of MPs-PS-AEPE via ion exchange. In the adsorption of Ag, the ion exchange mechanism may occur along with the coordination. Hence, the adsorption behaviour for Ag ions may also follow Freundlich isotherm. Nevertheless, the R^2 value of linear fitting to Langmuir model is higher than Fruendlich model indicating that the adsorption of Ag mainly occurred via coordination at AEPE sites on the surface. On the other hand, when consider the adsorption of Hg(II), the dominant species of Hg(II) are $Hg(OH)_2$ at pH 7 that will not be adsorbed on uncoated surface of MPs-PS-AEPE via ion exchange mechanism. Therefore, Hg ions interact solely with AEPE sites and the behavior follows Langmuir model.

Table 4.14 The mean of R_L related to the type of isotherm [138, 165-168]

Value of R_L	Type of isotherm
$R_L > 1$	Unfavorable
$R_L = 1$	Linear
$0 < R_L < 1$	Favorable
$R_L = 0$	Irreversible

Finally, these results lead to the conclusion that the adsorption isotherm of Hg(II) and Ag(I) onto MPs-PS-AEPE follow Langmuir model and the maximum adsorption capacity of Hg(II) and Ag(I) onto MPs-PS-AEPE are 0.42 and 0.44

mmol g^{-1}, respectively. The maximum adsorption capacity of Ag(I) is slightly higher than that of Hg(II) probably due to the combination of coordination and ion exchange mechanism of Ag(I) adsorption onto MPs-PS-AEPE.

When compare the adsorption capacity of MPs-PS-AEPE to that of the adsorbents reported by other researchers (Table 4.15), the adsorbent prepared in this work has a fair adsorption capacity for both Hg(II) and Ag(I) ions.

Table 4.15 The maximum adsorption capacity of the modified materials for mercury(II) and silver(I) ions extraction
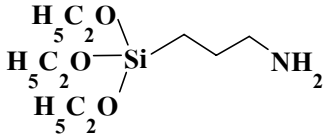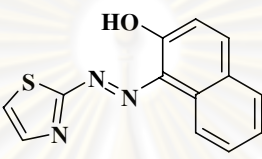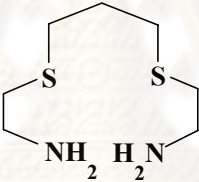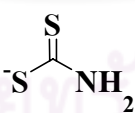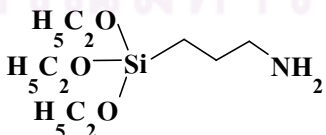
Solid support	Ligand	q_m (mmol g^{-1})	Ref.
Activated carbon	 3-aminopropyltriethoxysilane	0.37[a]	[168]
	 1-(2-thiazolylazo)-2-naphthol	0.011[a]	[169]
MCM-41	 2-(3-(2-aminoethylthio)propylthio) ethanamine	0.70[a]	[132]
Quartamin smectite	 Dithiocarbamate	0.32[a]	[170]
Montmorillonite	 3-aminopropyltriethoxysilane	1.77[a]	[171]

Table 4.15 The maximum adsorption capacity of the modified materials for mercury(II) and silver(I) ions extraction (continued)
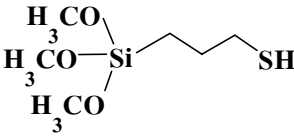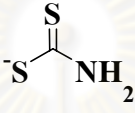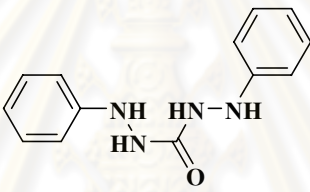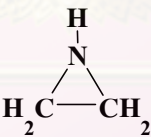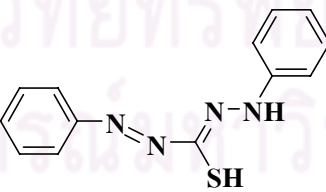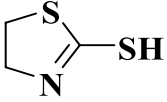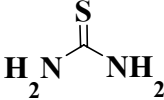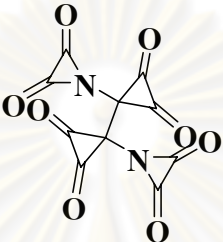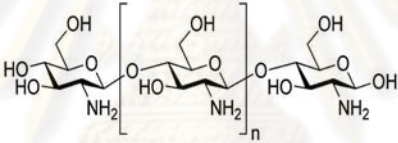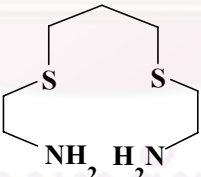
Solid support	Ligand	q_m (mmol g^{-1})	Ref.
Silica-coated magnetic nanoparticles	3-mercaptopropyltrimethoxysilane	0.42[a]	[10]
Polystyrene microspheres	Dithiocarbamate	0.17[a]	[163]
Silica	1,5 Diphenylcarbazide	0.03[a]	[172]
	Ethyleneimine	0.98[a]	[173]
	1,5-diphenylthiocarbazone	0.32[a]	[165]
	2-mercaptothiazoline	0.12[a]	[174]

Table 4.15 The maximum adsorption capacity of the modified materials for mercury(II) and silver(I) ions extraction (continued)

Solid support	Ligand	q_m (mmol g^{-1})	Ref.
Melamine resin	Thiourea	0.95^b	[175]
Magnetite	Tetraoxalyl ethylenediamine	0.51^b	[175]
	Chitosan	2.22^b	[166]
Polystyrene-coated magnetic particles	2-(3-(2-aminoethylthio)propylthio) ethanamine	0.42^a 0.44^b	**This work**

^{a} The maximum adsorption capacity in Hg(II) extraction

^{b} The maximum adsorption capacity in Ag(I) extraction

4.2.6 Adsorption kinetics and effect of adsorbent dosage

The adsorption kinetics was investigated by varying the extraction time in the range of 5 -180 minutes in this experiment. In addition, the amount of adsorbents was also varied in the range of 0.005 to 0.020 g. Each amount of adsorbent was added to 5 mL of Hg(II) solution (30 mg L^{-1}) or Ag(I) solution (100 mg L^{-1}). The results are shown in Figure 4.16 and 4.17. The experimental data were fitted to different adsorption kinetics models.

The results show that the % extraction was enhanced by increasing the extraction time. The adsorption equilibrium was attained in a short time when increased the adsorbent dose due to the increase of active sites number. On the other hand, the amount of metal ions adsorbed per unit mass or the adsorption capacity of MPs-PS-AEPE decreased due to the unsaturation of active sites of the higher adsorbent dose for the equal initial concentration [138, 176].

In order to investigate the kinetics of Hg(II) and Ag(I) adsorption onto MPs-PS-AEPE, the pseudo-first order [177] and pseudo second-order model [178-180] are commonly used. The equations of these two models are presented in equation 4.7 and 4.8, respectively,

$$\log(q_e - q_t) = \log q_e - \frac{k_1}{2.303}t \qquad (4.7)$$

$$\frac{t}{q_t} = \frac{1}{k_2 q_e^2} + \frac{t}{q_e} \qquad (4.8)$$

where q_e = adsorption capacity at equilibrium (mg g^{-1})

q_t = adsorption capacity at time t (mg g^{-1})

t = extraction time (minute)

k_1 = rate constant of the pseudo-first order model (min^{-1})

k_2 = rate constant of the pseudo-second order model (g mg^{-1} min^{-1})
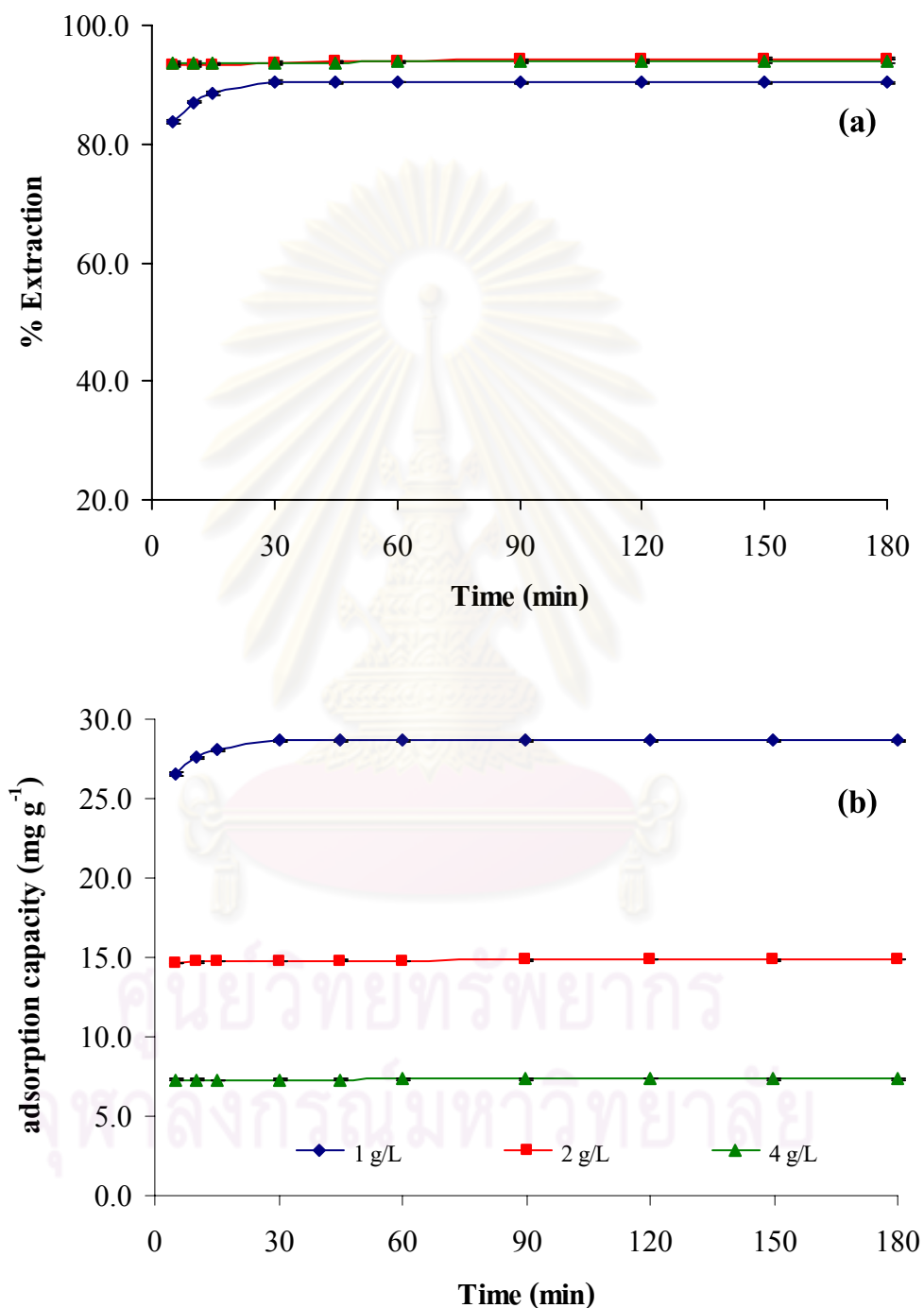
Figure 4.16 Effect of adsorbent dose at different extraction time on (a) adsorption efficiency of Hg(II) ions by MPs-PS-AEPE and (b) adsorption capacity of MPs-PS-AEPE for Hg(II) ions (initial concentration : 30 mg L^{-1}).
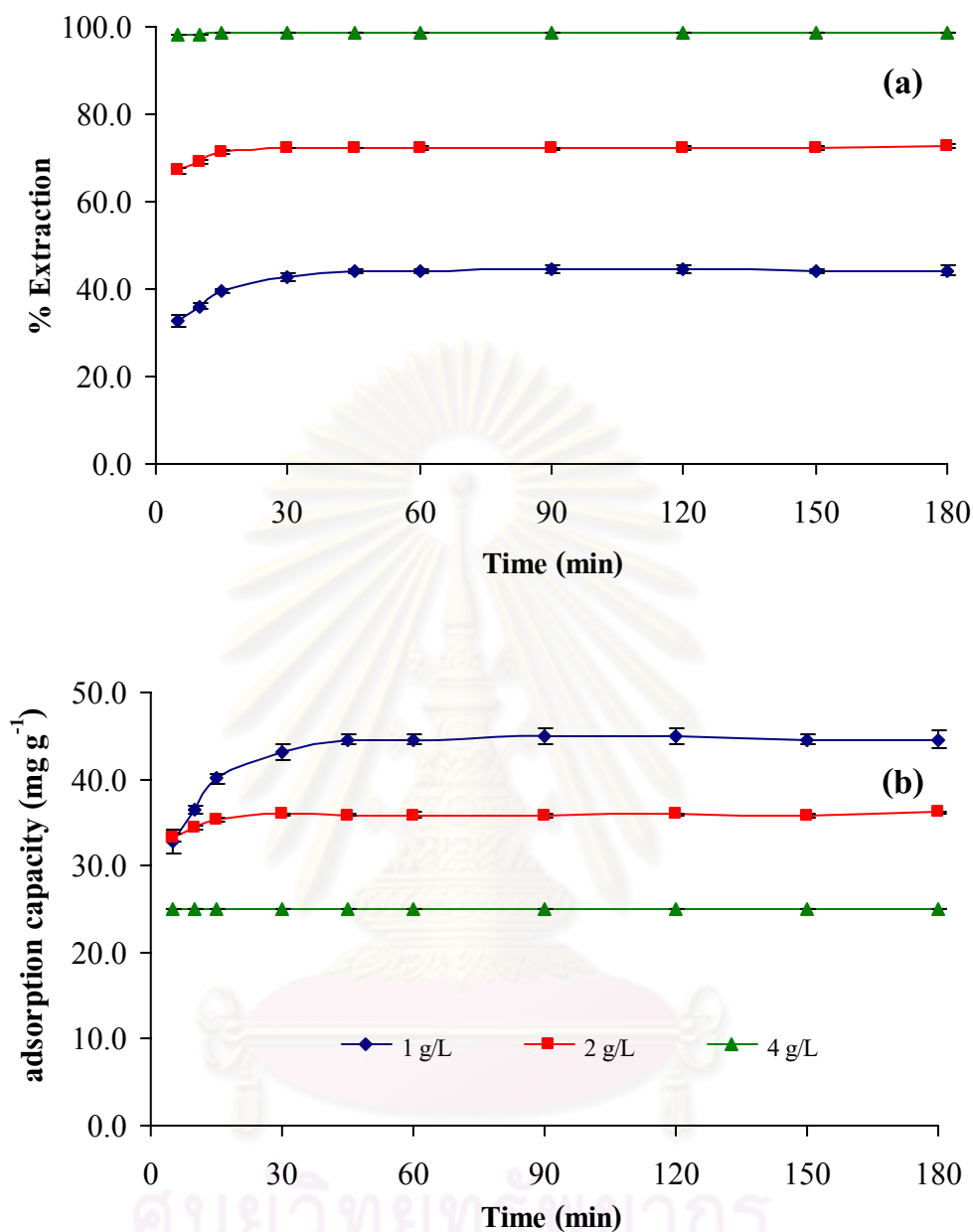
Figure 4.17 Effect of adsorbent dose at different extraction time on (a) adsorption efficiency of Ag(I) ions by MPs-PS-AEPE and (b) adsorption capacity of MPs-PS-AEPE for Ag(I) ions (initial concentration : 100 mg L^{-1}).

When the experimental data were plotted in form of $log\ (q_e\text{-}q_t)$ versus t, the rate constant (k_1) could be obtained from the slope of the linear line (Figure 4.18). Furthermore, by plotting t/q_t against t, the value of k_2 can be determined graphically

from the intercept of the linear plots as shown Figure 4.19. The value of q_e could also be obtained from the intercept and slope of the pseudo-first order plot and the pseudo-second order model plot, respectively. The results are summarized in Table 4.16.
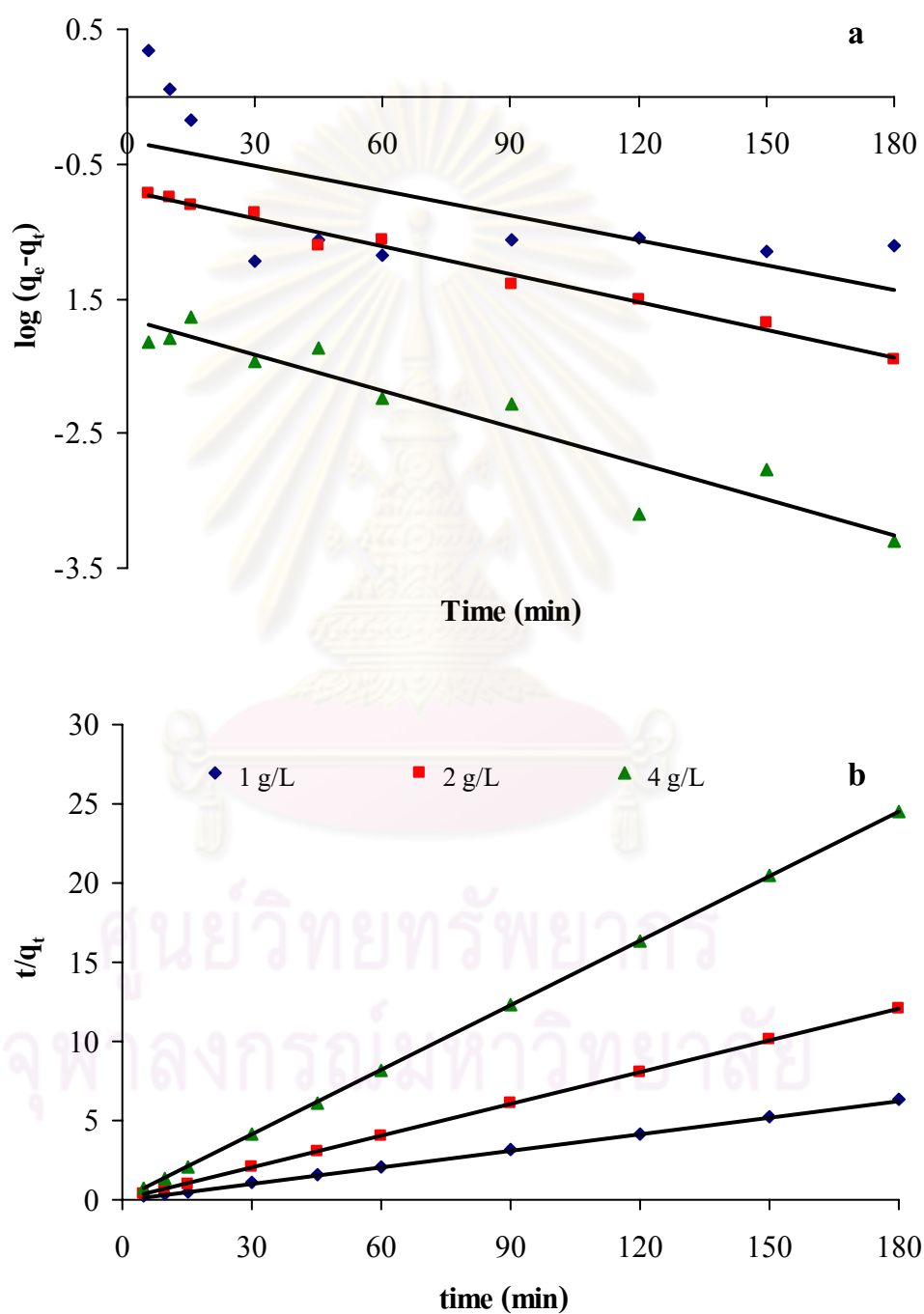
Figure 4.18 Kinetics plot of the extraction of Hg(II) ions onto MPs-PS-AEPE (a) pseudo-first order plot and (b) pseudo-second order plot.
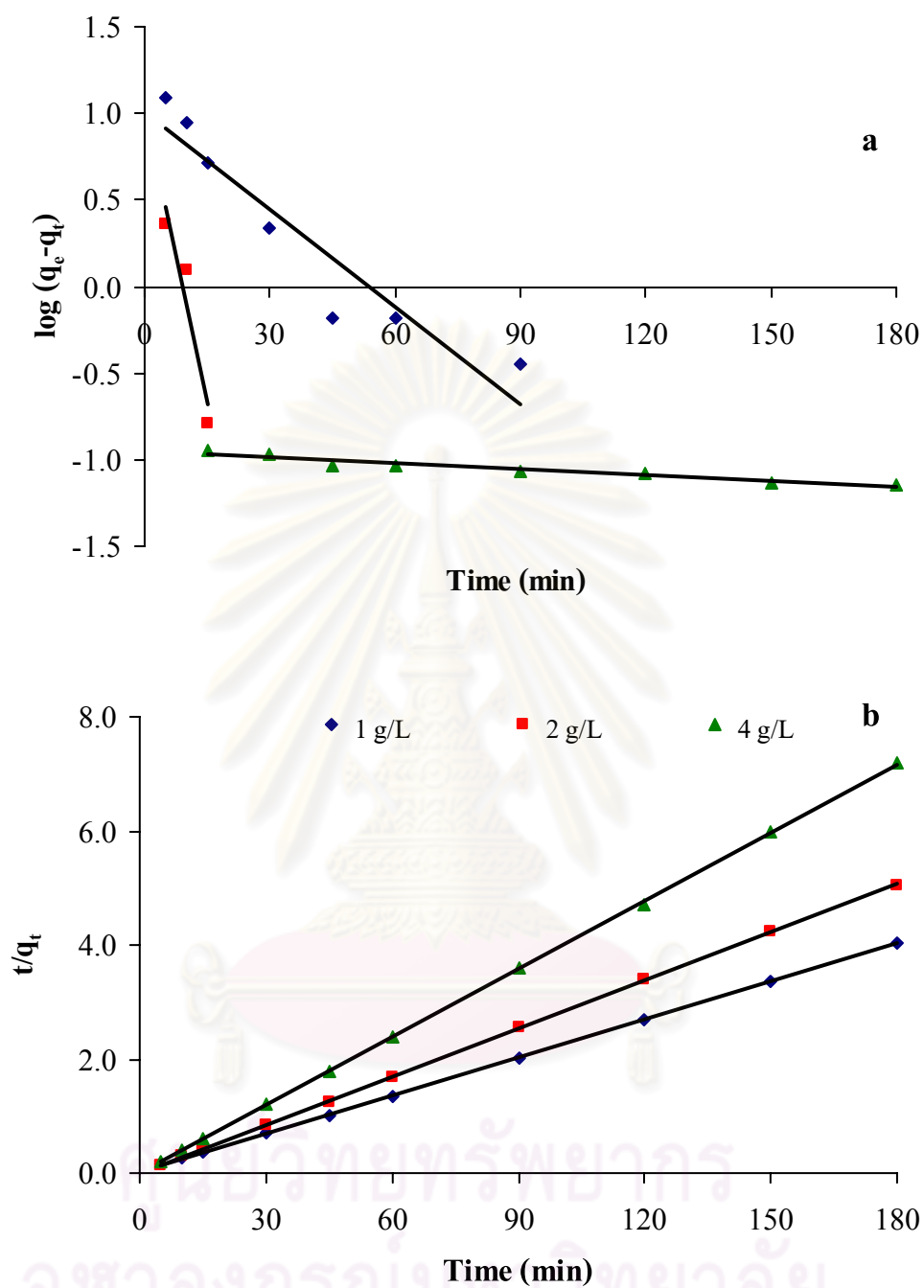
Figure 4.19 Kinetics plot of the extraction of Ag(I) ions onto MPs-PS-AEPE (a) pseudo-first order plot and (b) pseudo-second order plot.

Table 4.16 The kinetics parameter and constants for adsorption of Hg(II) and Ag(I) ions on MPs-PS-AEPE of various dose

Metal	Adsorbent dose (g)	$q_{e,exp}$ [a] (mg g^{-1})	Pseudo-first order model				Pseudo-second order model			
			Linear equation	$q_{e,cal}$ [b] (mg g^{-1})	$k_1 \times 10^{-2}$ (min^{-1})	R_1^2 [c]	Linear equation	$q_{e,cal}$ [b] (mg g^{-1})	$k_2 \times 10^{-2}$ (g mg^{-1} min^{-1})	R_2^2 [d]
	0.005	28.68	y = -0.0061x - 0.3293	0.47	1.40	0.4121	y = 0.0348x + 0.0086	28.74	14.08	1.000
Hg(II)	0.010	14.87	y = -0.0069x - 0.6988	0.20	1.59	0.9861	y = 0.0672x + 0.0128	14.88	35.28	1.000
	0.020	7.33	y = -0.0090x - 1.6451	0.02	2.07	0.9025	y = 0.1364x + 0.0050	7.33	310.08	1.000
	0.005	44.89	y = -0.0187x - 1.0090	10.21	4.31	0.8942	y = 0.0221x + 0.0322	45.25	1.52	0.9999
Ag(I)	0.010	36.14	y = -0.1148x - 1.0372	10.89	26.44	0.9106	y = 0.0281x + 0.0042	35.59	18.80	1.000
	0.020	25.05	y = -0.0011x - 0.9512	0.11	0.25	0.9366	y = 0.0398x + 0.0018	25.13	88.00	0.9999

[a]The adsorption capacity at equilibrium obtained by the experiments.

[b]The adsorption capacity at equilibrium obtained by the calculation using linear equation.

[c]The correlation coefficient of pseudo-first order model.

[d]The correlation coefficient of pseudo-second order model.

The kinetics parameters presented in Table 4.16 were calculated by using the linear equations obtained from the linear plot of pseudo-first order equation (eq.4.6) and the pseudo-second order model equation (eq.4.7). The results show that the correlation coefficients of pseudo-first order model (R_1^2) are in the range of 0.4121-0.9861 and 0.8942-0.9366 for Hg(II) and Ag(I) adsorption, respectively. Moreover, the adsorption capacity at equilibrium ($q_{e,cal}$) calculated from linear equation of pseudo-first order linear plot did not correspond to the adsorption capacity at equilibrium obtained from experiment ($q_{e,exp}$) for all adsorbent dose used in both Hg(II) and Ag(I) adsorption. In contrast, in the case of pseudo-second order model, the correlation coefficients (R_2^2) are in the range of 0.9999-1.000 for Ag(I) adsorption and equal to 1.000 for Hg(II) adsorption. The $q_{e,cal}$ values were very close to the $q_{e,exp}$ values. Obviously, the pseudo-second order kinetics model fit the experimental data better than the pseudo-first order kinetics model. By this model, it can be assumed that (i) the adsorption occurred via chemisorption by coordination or complexation between metal ions and active sites of adsorbent [180, 181], (ii) the adsorption followed a monolayer regime with monolayer coverage of metal ions on adsorbent surface without bond formation between each adsorbed metal ions, (iii) adsorption energy of each metal ion is equal and did not depend on the adsorbed metal ions on adsorbent surface and (iv) the adsorption rate occurred rapidly at the initial step of adsorption. Moreover, the rate constant of pseudo-second order (k_2) may be constant [162] or increased [180], depending on temperature and adsorbent dose used in the experiment.

In this experiment, k_2 increased with the increase of adsorbent dose. Therefore, the higher adsorbent dose is used, the faster adsorption equilibrium will be reached. From the comparison of k_2 values of Hg(II) adsorption and Ag(I) adsorption, the higher k_2 values was observed in Hg(II) adsorption corresponding to the results from adsorption isotherm experiment that the b value of Hg(II) adsorption is higher than that of Ag(I) adsorption. These results reveal that the modified AEPE coordinate with Hg(II) better than Ag(I). Finally, the results suggest that the pseudo-second order

adsorption mechanism is predominant for this adsorbent system and the overall rate of the adsorption process appears to be controlled by chemical adsorption with monolayer coverage of metal ions on surface [145, 146] that is in agreement with the results observed in adsorption isotherm study.

4.2.7 Metal ions desorption study

The desorption of Hg(II) and Ag(I) ions from the used MPs-PS-AEPE was studied using batch method. After adsorption, the used MPs-PS-AEPE was washed with DI water and then mixed with 5 mL of eluent. The concentrations of eluted metal ions were determined. Various parameters such as type of eluent and elution time were studied.

The metal ions desorption efficiency is presented in term of % desorption that was calculated from equation 4.9,

$$Desorption(\%) = \frac{n_{eluted}}{n_{adsorbed}} \times 100 \qquad (4.9)$$

where n_{eluted} = the amount of Ag(I) ions eluted from the adsorbent (mg)

$n_{adsorbed}$ = the amount of Ag(I) ions adsorbed on the adsorbent (mg)

4.2.7.1 Type of eluents

The desorption of metal ions was studied using different types and concentrations of eluent. The suitable eluent should be compatible with the used analytical technique. Thus, nitric acid (HNO_3) and thiourea, which are widely used and compatible with AAS technique, were selected as eluent. In this study, the criteria in the selection of suitable eluent is based on the adsorption mechanism, desorption

efficiency of eluent and adsorbent stability in the eluent regarding the Fe and Co leaching from adsorbents. The results are presented in Table 4.17. The concentrations of HNO_3 were 1 and 5% v/v in order to assure the protonation of chelation sites. Both 1 and 5% v/v HNO_3 solution could elute Ag(I) from MPs-PS-AEPE with low % desorption. This result can be attributed to the high affinity of Ag(I) toward sulfur active sites of AEPE [182]. Whereas, 1 % v/v HNO_3 could elute Hg(II) from MPs-PS-AEPE with moderate % desorption of 66.76 %. It could be explained that the chelating sites were protonated and the adsorbed $Hg(OH)_2$ was desorbed from adsorbent surface to the solution. Furthermore, Hg(II) species could be changed from $Hg(OH)_2$ to Hg^{2+} in acid solution. From the results of pH effect, chelating ligand AEPE prefers to form complex with $Hg(OH)_2$ species rather than Hg^{2+}. Thus, some Hg^{2+} is still adsorbed on MPs-PS-AEPE surface whereas most Hg^{2+} is desorbed by high acidic solution. Therefore, the use of HNO_3 as eluent would change the species $Hg(OH)_2$ to Hg^{2+} resulting in a decrease in adsorption efficiency and the moderate % percentage was observed.

The alternative way for desorption is the elution by complexing agent that can form complex with Hg(II) and Ag(I) with higher affinity than AEPE. Thiourea is a well known complexing agent and has high complex formation constant with various metal ions such as Ag(I), Au(III), Cu(I) and Hg(II) [166, 167, 183]. Therefore, thiourea was selected to elute Hg(II) and Ag(I) from MPs-PS-AEPE by mixing with HNO_3. The concentration of thiourea was 0.1, 0.5 or 1.0 M in both 1 and 5% v/v HNO_3 for elution of Ag(I) and only in 1 % v/v HNO_3 for elution of Hg(II). According to Hard and Soft Acids and Bases (HSAB) theory [142, 143], the sulfur and nitrogen atom of thiourea can polarize their lone pairs of electrons easily and act as a soft base, which would have a tendency to form complex with soft acids like Hg(II) and Ag(I) ions. In the presence of thiourea in acid solution, the synergism working effect will occur. The proton (H^+) from acid will protonate AEPE active sites and deprotonate thio form of

thiourea to thiol form at the end of reaction as shown in Figure 4.20 [175]. Therefore, Hg(II) and Ag(I) ions were released and formed complexes with thiourea.
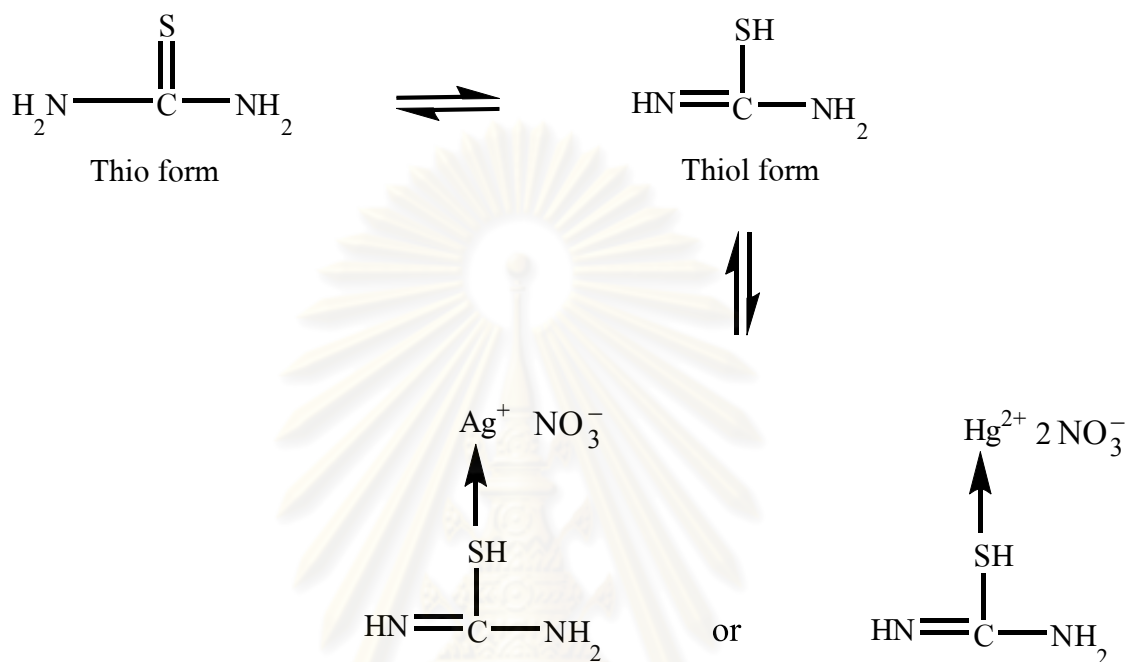
Figure 4.20 The tautomerization of thio form of thiourea moiety at the end of reaction and the complexation between thiol form and metal ions.

ศูนย์วิทยทรัพยากร
จุฬาลงกรณ์มหาวิทยาลัย

Table 4.17 Desorption of Hg(II) and Ag(I) from the used adsorbents

Type of eluents	% Desorption [a]	
	Hg(II)	Ag(I)
1% HNO$_3$	67.66 ± 2.79	6.61 ± 0.36
5% HNO$_3$	-[b]	9.12 ± 0.97
1% HNO$_3$ + 0.1 M Thiourea	95.58 ± 0.92	83.59 ± 0.98
1% HNO$_3$ + 0.5 M Thiourea	98.40 ± 0.11	85.23 ± 1.79
1% HNO$_3$ + 1.0 M Thiourea	98.20 ± 0.06	87.34 ± 0.29
5% HNO$_3$ + 0.1 M Thiourea	-[b]	84.77 ± 0.94
5% HNO$_3$ + 0.5 M Thiourea	-[b]	86.74 ± 1.47
5% HNO$_3$ + 1.0 M Thiourea	-[b]	90.00 ± 2.02

[a] Mean ± S.D. (n=3)

[b] There is no experiment.

The initial concentration of Hg(II) and Ag(I) were 100 and 50 mg L^{-1}, respectively.

The % desorption of Ag(I) increased from 83.59 to 90.00 % when thiourea in HNO$_3$ was used. From the *t-Test* statistic calculation, the concentration of HNO$_3$ did not affect the desorption efficiency, whereas, the concentration of thiourea affected the desorption efficiency when the results were tested with *ANOVA test*. In the case of Hg(II) desorption, the % desorption increased to 95.58, 98.40 and 98.20 % when used 0.1, 0.5 and 1.0 M thiourea in 1 % HNO$_3$ as eluent, respectively. From the statistic calculation, the increase in the thiourea concentration from 0.1 to 0.5 M in 1 % HNO$_3$ affected the desorption efficiency, whereas using thiourea concentration of 0.5 and 1.0 M in 1 % HNO$_3$ did not affect the desorption efficiency when the results were tested with *t-Test*. Therefore, 0.5 M thiourea in 1 % HNO$_3$ and 1.0 M thiourea in 1 % HNO$_3$ were selected as eluent for desorption of Hg(II) and Ag(I) ions from MPs-PS-AEPE, respectively. It should be noted that thiourea in HNO$_3$ can elute Hg(II) from

MPs-PS-AEPE better than Ag(I) due to higher affinity of thiourea toward Hg(II) (K_f = 3.0 × 10^{22} for [Hg[CS(NH$_2$)$_2$]$_2$] and K_f = 9.0 × 10^{32} for [Hg[CS(NH$_2$)$_2$]$_4$]) [184], compared to the complex formation between thiourea and Ag(I) (K_f = 4.0 × 10^{13} for [Ag[CS(NH$_2$)$_2$]$_3$]) [185].

4.2.7.2 Desorption time

In the case of Ag(I) desorption, the % desorption is not high enough. Consequently, the effect of desorption time was investigated using 1.0 M thiourea in 1% HNO_3 as eluent to obtain the suitable time that provides the maximum desorption. Desorption time was varied in the range of 15-180 minutes. The results are shown in Figure 4.21.
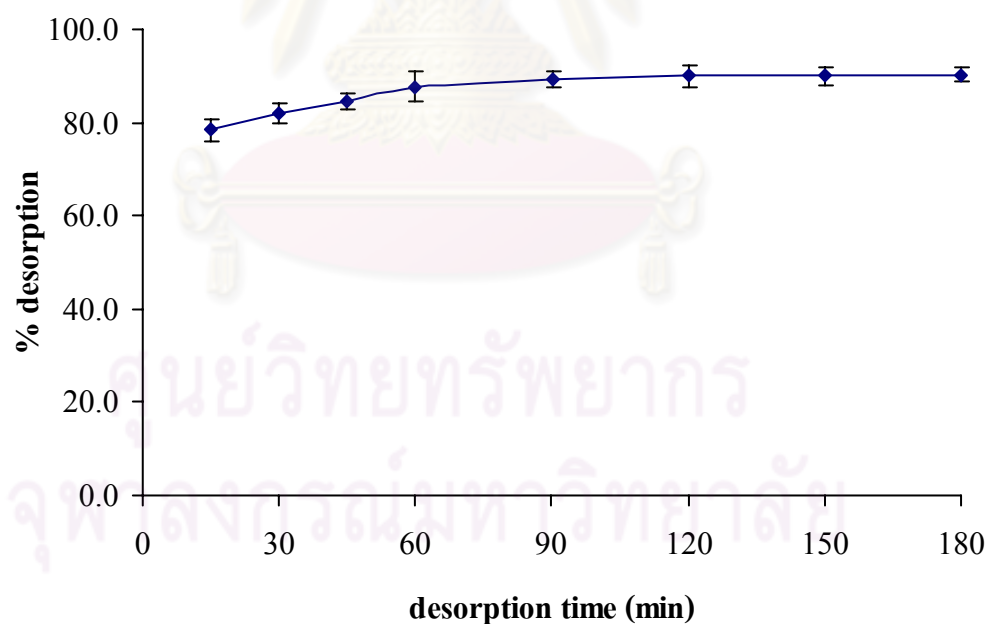
Figure 4.21 Effect of desorption time on desorption of Ag(I) from MPs-PS-AEPE.

The % desorption increased slightly by increasing time from 15 to 60 minutes. From 60 minutes onwards, the % desorption is relatively constant. Therefore, 1 hour desorption time was chosen for the regeneration of the adsorbents and used in adsorbent reusability experiment.

4.2.8 Reusability of adsorbent

The adsorbent reusability is an important and desired property of adsorbents. The reuse of adsorbent was investigated and the experiment was performed by using the same adsorbent for repeated cycles of adsorption/desorption. The initial concentration of Hg(II) and Ag(I) used in the adsorption were 100 and 50 mg L^{-1}, respectively. By using these initial concentrations, the adsorbent could extract the metal ions with the adsorption capacity close to their maximum adsorption capacity. The 0.5 M thiourea in 1 % HNO_3 and 1.0 M thiourea in 1 % HNO_3 were used as eluent for Hg(II) and Ag(I), respectively and 1 hour adsorption/desorption time was also used. The results are shown in Figure 4.22 and Table 4.18.
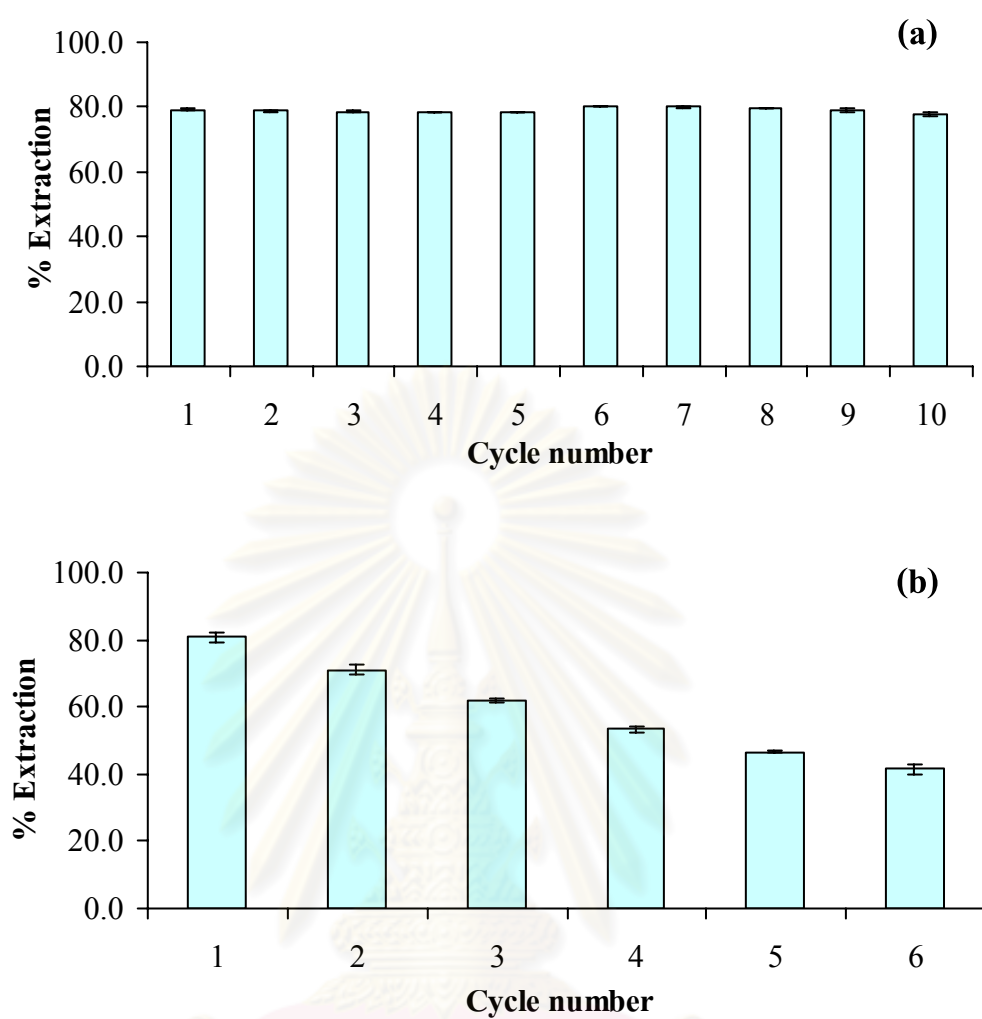
Figure 4.22 The % extraction of MPs-PS-AEPE toward (a) Hg(II) ions and (b) Ag(I) ions during repeated adsorption/desorption cycles.

Table 4.18 The adsorption capacity of Hg(II) and Ag(I) onto MPs-PS-AEPE during repeated adsorption/desorption cycles

Number of cycles	Adsorption capacity (mg g^{-1}) [a]	
	Hg(II)	Ag(I)
1	79.49 ± 0.18	42.15 ± 0.74
2	79.12 ± 0.06	37.15 ± 0.53
3	78.97 ± 0.19	32.35 ± 0.42
4	78.87 ± 0.11	27.91 ± 0.42
5	78.82 ± 0.11	24.39 ± 0.24
6	78.92 ± 0.13	21.62 ± 0.65
7	78.75 ± 0.06	-[b]
8	78.40 ± 0.20	-[b]
9	78.03 ± 0.57	-[b]
10	76.71 ± 0.50	-[b]

[a] adsorption capacity determined for each cycle, mean ± S.D. (n=3)

[b] There is no experiment.

The initial concentration of Hg(II) and Ag(I) were 100 and 50 mg L^{-1}, respectively.

It was found that the % extraction were not significantly different for Hg(II) after 10 cycles of extraction/desorption. These values are in the range of 77.93 and 80.18 % for 10 cycles. In the case of Ag(I), the % extraction decreased from 80.67 to 41.38 % after 6 cycles of extraction/desorption due to the reduction of the number of available active sites. Hg(II) was eluted from used MPs-PS-AEPE better than Ag(I) when using thiourea in HNO$_3$ as eluent. The MPs-PS-AEPE gave the highest extraction efficiency for Ag(I) extraction only for the first time application. On the other hand, the MPs-PS-AEPE could be used to extract Hg(II) at least 10 times.

4.3   Application to real water samples

Finally, MPs-PS-AEPE was applied to extract Hg(II) and Ag(I) ions in real water samples. In this experiment, the wastewater from the laboratory of Gem and Jewelry Institute of Thailand and the petrochemical industry plant were used as real samples of Ag(I) and Hg(II), respectively.

4.3.1 The wastewater from the laboratory of Gem and Jewelry Institute of Thailand

This wastewater contained a high concentration of silver (about 4,600 mg L^{-1}) at pH 1.7. It was diluted and adjusted the pH value to obtain a wastewater, which had the pH value and concentration of silver about 5.0 and 145 mg L^{-1}, respectively. The extraction experiment was performed by using 0.005, 0.010, 0.020 and 0.030 g of MPs-PS-AEPE and the extraction time of 60 minutes.

The results show that the extraction efficiency increased from 29.62 to 99.67 % by increasing MPs-PS-AEPE dose from 0.005 to 0.030 g (Figure 4.23).
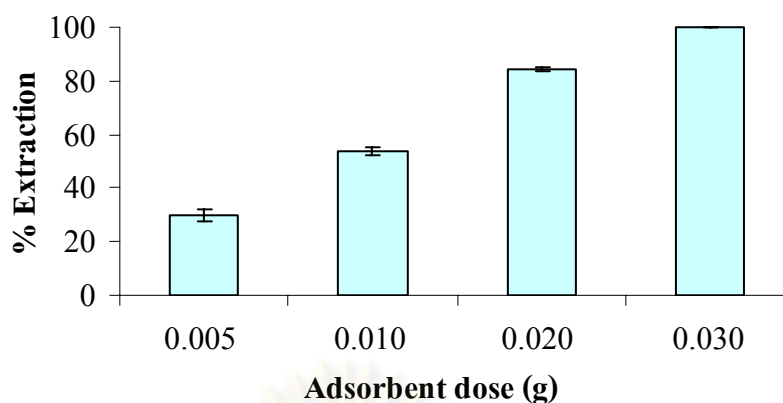
Figure 4.23 The extraction efficiency of Ag(I) ions in real wastewater sample at different doses of MPs-PS-AEPE. (Detection limit of silver = 0.006 mg L^{-1})

4.3.2 The wastewater from petrochemical industry plant

These wastewater samples had relatively low concentration of mercury (about 4.2 and 4.9 mg L^{-1}). The samples were digested using standard method ASTM3223 [134] to convert both organic and inorganic mercury compounds to the mercuric ions and cold-vapor atomic absorption spectrometer was used to determine Hg(II) concentration [135]. The extraction experiment was performed using 0.005 and 0.010 g of MPs-PS-AEPE and the extraction time of 60 minutes. The results show that the extraction efficiency is not different when increased MPs-PS-AEPE dose from 0.005 to 0.010 g for both samples (Table 4.19).

Table 4.19 The extraction efficiency of Hg(II) ions in real wastewater samples at different doses of MPs-PS-AEPE

Sample	Initial concentration (mg L^{-1})	Adsorbent dose (g)	% Extraction[a]
Refinery wastewater 1	4.9	0.005	99.50 $\pm$ 0.05
		0.010	99.66 $\pm$ 0.05
Refinery wastewater 2	4.2	0.005	99.49 $\pm$ 0.08
		0.010	99.77 $\pm$ 0.05

[a] Mean $\pm$ S.D. (n=3)

Detection limit of mercury was 5×10^{-4} mg L^{-1}.

The detection limit (LOD) was determined by measuring of signal of blank solution (n = 10) and then calculated from equation 4.10.

$$\text{signal}_{LOD} = \text{signal}_{blank} + 3(\text{S.D. of signal blank}) \qquad (4.10)$$

The signal of LOD was compared to the linear equation of calibration curve. The detection limit of mercury and silver in this experiment were 6×10^{-3} and 5×10^{-4} mg L^{-1}, respectively.

These results indicate that the MPs-PS-AEPE can be used to extract silver and mercuric ions in wastewater samples with high percentage extraction due to the presence of nitrogen and sulfur donor atom of chelating ligand AEPE on the adsorbent surface. Consequently, the MPs-PS-AEPE can be applied as adsorbent to extract the Hg(II) and Ag(I) ions in real wastewater samples.

CHAPTER V

CONCLUSION AND SUGGESTION

The cobalt ferrite magnetic particles were synthesized via co-precipitation between Co^{2+} and Fe^{3+} in basic solution. The polystyrene-coated magnetic particles were prepared by grafting of the initiator, which was synthesized via nucleophilic substitution reaction between 3-aminopropyltriethoxysilane and ethyl-2-bromo propionate, on the surface of magnetic particles, followed by polymerization of styrene via atom transfer radical polymerization process. Then, the syntheiszed chelating ligand 2-(3-(2-aminoethylthio)propylthio)ethanamine (AEPE) was attached on polystyrene-coated magnetic particles. The final product was characterized by XRD, FT-IR, TGA, SEM and surface area analyzer. The results from all characterization techniques confirmed the successful synthesis of the polystyrene-coated magnetic particles modified with 2-(3-(2-aminoethylthio)propylthio)ethanamine (MPs-PS-AEPE).

The MPs-PS-AEPE was applied as adsorbent for extraction of mercury(II) and silver(I) in aqueous solution using batch method. The effect of pH of metal ions solutions, extraction time, ionic strength, coexisting ions and adsorbent dose as well as the adsorption kinetic and adsorption isotherm were investigated. The adsorption behaviour of MPs-PS-AEPE for Hg(II) and Ag(I) ions in aqueous solution are summarized in Table 5.1.

The maximum adsorption capacity of Ag(I) is slightly higher than that of Hg(II) probably due to the combination of both ion exchange and coordination mechanism in the adsorption of Ag(I) ions onto the MPs-PS-AEPE. The adsorption of Hg(II) ions onto MPs-PS-AEPE occurred mainly via coordination. The MPs-PS-AEPE

show high affinity and selectivity toward Hg(II) and Ag(I) ions, confirmed by the results of ionic strength and coexisting ions effect.

Table 5.1 The adsorption behavior and suitable condition of the extraction of mercury(II) and silver(I) ions

Parameters	Metal ions adsorption	
	Hg(II)	Ag(I)
Solution pH	7-8	5-8
Ionic strength and coexisting ions	no effect	no effect
Adsorption isotherm	Langmuir	Langmuir
Adsorption kinetics	Pseudo-second order	Pseudo-second order
Maximum adsorption capacity (mmol g^{-1})	0.42	0.44

In the study of desorption and the reusability of MPs-PS-AEPE, the suitable eluents are 0.5 M thiourea in 1% HNO$_3$ and 1.0 M thiourea in 1% HNO$_3$ for Hg(II) and Ag(I) desorption, respectively. The MPs-PS-AEPE showed the highest extraction efficiency in the first time and at least 10 times for Ag(I) and Hg(II) extraction, respectively.

Moreover, the application to real wastewater samples from petrochemical industry plant and the Laboratory of Gem and Jewelry Institute of Thailand was investigated. The results showed that the MPs-PS-AEPE could be used as adsorbent to extract Hg(II) and Ag(I) ions in real wastewater samples.

Suggestion for future works

Because the MPs-PS-AEPE has high affinity and selectivity toward Hg(II) and Ag(I) ions, it should be applied in the preconcentration of these ions for the analysis of water sample contaminated by low level of these ions and the parameters of the preconcentration should be studied.

REFERENCES

[1] M. G. da Fonseca., M. M. de Oliveira., L. N. H. Arakaki. Removal of cadmium, zinc, manganese and chromium cations from aqueous solution by a clay mineral. Journal of Hazardous Materials. B137 (2006): 288–292

[2] N. Chiron., R. Guilet., E. Deydier. Adsorption of Cu(II) and Pb(II) onto a grafted silica:isotherms and kinetic models. Water Research. 37 (2003): 3079–3086.

[3] L. Mercier., T. J. Pinnavaia. Heavy Metal Ion Adsorbents Formed by the Grafting of a Thiol Functionality to Mesoporous Silica Molecular Sieves: Factors Affecting Hg(II) Uptake. Environmental Science & Technology. 32 (1998): 2749-2754.

[4] A. M. Starvin., T. P. Rao. Removal and recovery of mercury(II) from hazardous wastes using 1-(2-thiazolylazo)-2-naphthol functionalized activated carbon as solid phase extractant. Journal of Hazardous Materials. 113 (2004): 75–79.

[5] F. S. Zhang., J. O. Nriagu., H. Itoh. Mercury removal from water using activated carbons derived from organic sewage sludge. Water Research. 39 (2005):389–395.

[6] M. Ahmed., A. Asem., A. Hanaa., H. Dalia. Adsorption of Ag(I) on glycidyl methacrylate/*N,N*-methylene bis-acrylamide chelating resins with embedded iron oxide. Separation and Purification Technology. 48 (2006):281–287.

[7] A. Asem. Adsorption of silver(I) and gold(III) on resins derived from bisthiourea and application to retrieval of silver ions from processed photo films. Hydrometallurgy. 80 (2005): 98– 106.

[8] M. Ahmed., A. Asem., Z. Khalid. Recovery of gold(III) and silver(I) on a chemically modified chitosan with magnetic properties. Hydrometallurgy. 87 (2007):197–206.

[9]   Y. C. Chuang., D. W. Chen. Preparation and adsorption properties of monodisperse chitosan-bound Fe_3O_4 magnetic nanoparticles for removal of Cu(II) ions. Journal of Colloid and Interface Science. 283 (2005):446-451.

[10] C. Huang., B. Hu. Silica-coated magnetic nanoparticles modified with mercaptopropyltriethoxysilane for fast and selective solid phase extraction of trace amounts of Cd, Cu, Hg, and Pb in environmental and biological samples prior to their determination by inductively coupled plasma mass spectrometry. Spectrochimica Acta Part B. 63 (2008):437-444.

[11] W. Zheng., F. Gao., H. Gu. Magnetic polymer nanospheres with high and uniform magnetite content. Journal of Magnetism and Magnetic Materials. 288 (2005):403–410.

[12] Polysciences,Inc. Magnetic Microparticles : Properties and Advantages. Technical Data Sheet. 438 (2007):1-2.

[13] Classes of Magnetic Materials [online]. Avaiable from: http://www.irm. umn. edu/hg2m/ hg2m_b/hg2m_b.html. [2009, October 05]

[14] G. Wulfsberg. Inorganic Chemistry. University Science Books, 691, 2000.

[15] Spienl [online]. Avaiable from: http://wikis.lib.ncsu.edu/index.php/Spinel [2009, October 05]

[16] M. E. Fleet. The Structure of Magnetite. Acta Crytallographica B. 37 (1981): 917-920.

[17] G. K. Rozenberg. Structural characterization of temperature and pressure-induced inverse normal spinel transformation in magnetite. Physical Review B. 75 (2007):020102-020105.

[18] K. Maaz., A. Mumtaz., S. K. Hasanian., A. Ceylan. Synthesis and magnetic properties of cobalt ferrite $(CoFe_2O_4)$ nanoparticles prepared by wet chemical route. Journal of Magnetism and Magnetic Materials. 308 (2006):289-295.

[19] Y. Melikhov., J. E. Snyder., D. C. Jiles., A. P. Ring., J. A. Paulsen., C. C. H. Lo., K. W. Dennis. Temperature dependence of magnetic anisotropy in Mn-

substituted cobalt ferrite. Journal of Applied Physics. 99 (2006):08R102-08R102-3.

[20] C. N. Chinnasamy., B. Jeyadevan., K. Shinoda., K. Tohji., D. J. Djayaprawira., M. Takahashi., R. J. Joseyphus., A. Narayanasamy. Unusually high coercivity and critical single-domain size of nearly monodispersed $CoFe_2O_4$ nanoparticles. Applied Physics Letters. 83 (2003):2862.

[21] B. D. Cullity. Introduction to Magnetic Materials. Addision-Wesley, New York, 190, 1972.

[22] M. Grigorova., H. J. Blythe., V. Blaskov., V. Rusanov., V. Petkov., V. Masheva., D. Nihtianova., L. M. Martinez., J. S. Muñoz., M. Mikhov. Journal of Magnetism and Magnetic Materials. 183 (1998):163-172.

[23] H. Shenker. Magnetic anisotropy of cobalt ferrite ($Co_{1.01}Fe_{2.00}O_{3.62}$) and nickel cobalt ferrite ($Ni_{0.72}Fe_{0.20}Co_{0.08}Fe_2O_4$).Physical Review. 107 (1957):1246-1249.

[24] S. H. Xiao., W. F. Jiang., L. Y. Li., X. J. Li. Low-temperature auto-combustion synthesis and magnetic properties of cobalt ferrite nanopowder. Materials Chemistry and Physics. 106 (2007):82-87.

[25] C. Liu., B. Zou., A. J. Rondinone., Z. J. Zhang. Chemical control of superparamagnetic properties of magnesium and cobalt spinel ferrite nanoparticles through atomic level magnetic couplings. Journal of the American Chemical Society. 122 (2000):6263-6267.

[26] C. Liu., A. J. Rondinone., Z. J. Zhang. Synthesis of magnetic spinel ferrite $CoFe_2O_4$ nanoparticles from ferric salt characterization of the size-dependent superparamagnetic properties. Pure and Applied Chemistry. 72 (2000): 37-45.

[27] Q. Liu., J. Sunb., H. Longa., X. Suna., Z. Xub. Hydrothermal synthesis of $CoFe_2O_4$ nanoplatelets and nanoparticles. Materials Chemistry and Physics. 108 (2008):269-273.

[28] O. Carp., L. Patron., A. Leller. Coordination compounds containing urea as precursors for oxides-A new route of obtaining nanosized $CoFe_2O_4$. Materials Chemistry and Physics. 101 (2007):142-147.

[29] W. W. Wang. Microwave-induced polyol-process synthesis of $M^{II}Fe_2O_4$ (M = Mn, Co) nanoparticles and magnetic property. Materials Chemistry and Physics. 108 (2008):227-231.

[30] J. de Vincente., A. V. Delgado, R.C. Plaza, J.D.G. Duran and F.G. Caballero. Stability of cobalt ferrite colloidal particles. Effect of pH and applied magnetic fields .Langmuir. 16 (2000):7954-7961.

[31] G. Gnanaprakash., J. Philip., T. Jayakumar., B. Raj. Effect of digestion time and alkali addition rate on physical properties of magnetite nanoparticles. Journal of Physical Chemistry B. 111 (2007):7978-7986.

[32] L. Vayssieres, C. Chaneac, E. Tronc and J.P. Jolivet. Size tailoring of magnetite particles formed by aqueous precipitation: An example of thermodynamic stability of nanometric oxide particles. Journal of Colliod and Interface Science. 205 (1998):205-212.

[33] Technical data sheet. Magnetic microparticles. 438(2007):1-2.

[34] O. Hoboken. Bad Medicine: misconceptions and misuses revealed from distance healing to vitamin. New Jersey: John Wiley & Sons. (2003):1–253. ISBN 0-471-43499-X.

[35] Atom transfer radical polymerization [online]. Avaiable from: http://www. joensuu.fi/kemia/research/material/atrp.html [2009, October 05]

[36] K. Matyjaszewski., J. Xia. Atom transfer radiacl polymerization. Chemical Review. 101 (2001):2921-2990.

[37] T. E. Patten., K. Matyjaszewski. Atom-transfer radical polymerization and the synthesis of polymeric materials. Advanced Materials. 10 (1998): 901-905.

[38] K. Matyjaszewski. Transition metal catalysis in controlled radical polymerization: atom transfer radical polymerization. Chemistry-A European Journal. 5 (1999): 3095-3102.

[39] J. S. Wang., K. Matyjaszewski. Controlled "Living" radical polymerization. halogen atom transfer radical polymerization promoted by a Cu(I)/Cu(II) redox process. Macromolecules. 28 (1995): 7901.

[40] J. Xia., K. Matyjaszewski. Controlled "Living" radical polymerization. Atom transfer radical polymerization using multidentate amine ligands. Macromolecules. 30 (1997):7697-7700.

[41] F. Simal., A. Demonceau., A. F. Noels. Highly efficient ruthenium-based catalytic systems for the controlled free-radical polymerization of vinyl monomers. Angewandte Chemie International Edition. 38 (1999):538–540.

[42] T. Grimaud., K. Matyjaszewski. "Controlled/living" radical polymerization of methyl methacrylate by atom transfer radical polymerization. Macromolecules. 30 (1997):2216-2218.

[43] C. Granel., P. Dubois., R. Jerome., P. Teyssie. Controlled radical polymerization of methacrylic monomers in the presence of a *bis*(ortho-chelated) aryl nickel(II) complex and different activated alkyl halides. Macromolecules. 29 (1996):8576-8582.

[44] P. Lecomte, I. Drapier, P. Dubois, P. Teyssie, R. Jerome. Controlled radical polymerization of methyl methacrylate in the presence of palladium acetate, triphenylphosphine, and carbon tetrachloride. Macromolecules. 30 (1997): 7631-7633.

[45] K. Matyjaszewski., M. Wei., J. Xia., N. E. McDermott. Controlled "Living" radical polymerization of styrene and methyl methacrylate catalyzed by iron complexes. Macromolecules. 30 (1997):8161-8164.

[46] K. Matyjaszewski., J. L. Wang., T. Grimaud., D. A. Shipp. Controlled/"Living" atom transfer radical polymerization of methyl methacrylate using various initiation systems. <u>Macromolecules.</u> 31 (1998):1527-1534.

[47] K. Matyjaszewski., S. M. Jo., H. Paik., S. G. Gaynor. Synthesis of well-defined polyacrylonitrile by atom transfer radical polymerization. <u>Macromolecules.</u> 30 (1997): 6398-6400.

[48] S. M. Jo., S. G. Gaynor., K. Matyjaszewski. Homo- and ABA block polymerization of acrylonitrile, n-butyl acrylate, and 2-ethylhexyl acrylate using ATRP. <u>Polymer Preprints (American Chemical Society, Division of Polymer Chemistry).</u> 37 (1996):272-273.

[49] <u>Polystyrene cross - linked - properties and applications</u> [online]. Avaiable from: <u>http://www.azom.com/details.aspArticleID=2046.</u> [2009, September 24]

[50] <u>Polystyrene</u> [online]. Avaiable from: <u>http://www.3d-cam.com/materials/poly styrene.asp.</u> [2009, September 24]

[51] K. Davis., J. O'Malley., H. Paik., K. Matyjaszewski. Effect of the counter anion in atom transfer radical polymerization using alkyl (pseudo)halide initiators. <u>Polymer Preprints (American Chemical Society, Division of Polymer Chemistry).</u> 38 (1997):687-688.

[52] M. Nishimura., M. Kamigaito., M. Sawamoto. Living radical polymerization of styrene with transition metal dithiocarbamate/AIBN systems: Halogen-free living. <u>Polymer Preprints (American Chemical Society, Division of Polymer Chemistry).</u> 40 (1999): 470-471.

[53] J. Qiu., K. Matyjaszewski. Metal complexes in controlled radical polymerization. <u>Acta Polymerica</u> 48 (1997):169-180.

[54] T. Ando., M. Kamigaito., M. Sawamoto. Design of initiators for living radical polymerization of methyl methacrylate mediated by ruthenium(II) complex. <u>Tetrahedron.</u> 53 (1997):15445-15457.

[55] T. Nishikawa, M. Kamigaito, M. Sawamoto. Living radical polymerization in water and alcohols: suspension polymerization of methyl methacrylate with complex. Macromolecules. 32 (1999): 2204-2209.

[56] K. Matyjaszewski., D. A. Shipp., J. L. Wang., T. Grimaud., T. E. Patten. Utilizing halide exchange to improve control of atom transfer radical polymerization. Macromolecules. 31 (1998):6836-6840.

[57] V. Percec, B. Barboiu and H.-J. Kim. Arenesulfonyl halides: a universal class of functional initiators for metal catalyzed 'Living' radical polymerization or styrene(s), methacrylates and acrylates. Journal of the American Chemical Society. 120 (1998): 305-316.

[58] V. Percec., B. Barboiu. Living radical polymerization of styrene initiated by arenesulfonyl chlorides and Cu-I(bpy)(N)Cl. Macromolecules. 28 (1995): 7970-9972.

[59] V. Percec., H. J. Kim., B. Barboiu. Scope and limitations of functional sulfonyl chlorides as initiators for metal-catalyzed "Living" radical polymerization of styrene and methacrylates. Macromolecules. 30 (1997):8526–8528.

[60] V. Percec., B. Barboiu., T. K. Bera., M. Van der Sluis., R. B. Grubbs., J. M. J. Fréchet. Designing functional aromatic multisulfonyl chloride initiators for complex organic synthesis by living radical polymerization. Journal of Polymer Science Part A: Polymer Chemistry. *38* (2000):4776-4791.

[61] M. Kato., M. Kamigaito., M. Sawamoto., T. Higashimura. Polymerization of methyl methacrylate with the carbontetrachloride/dichloro tris-(triphenyl phosphine) ruthenium(II)/methylaluminum *bis*(2,6-di-tert-butylphenoxide) initiating system: Possibility of living radical polymerization. Macromolecules. 28 (1995):1721.

[62] H. Takahashi., T. Ando., M. Kamigaito., M. Sawamoto. Half-metallocene-type Ruthenium complexes as active catalysts for living radical polymerization of methyl methacrylate and styrene. Macromolecules. 32 (1999):3820-3823.

[63] T. Ando., M. Kamigaito., M. Sawamoto. Catalytic activities of Ruthenium(II) complexes in transition-metal-mediated living radical polymerization: polymerization, model reaction, and cyclic voltammetry. Macromolecules. 33 (2000):5825-5829.

[64] H. Takahashi, T. Ando, M. Kamigaito, M. Sawamoto. $RuH_2(PPh_3)_4$: An active catalyst for living radical polymerization of methyl methacrylate at or above room temperature. Macromolecules. 32 (1999):6461-6465.

[65] T. Otsu., T. Tazaki., M. Yoshioka. Living radical polymerization with reduced nickel/halide systems as a redox iniferter. Chemistry Express. 5 (1990):801-804.

[66] V. Percec., B. Barboiu., A. Neumann., J. C. Ronda., M. Zhao. Metal-catalyzed "living" radical polymerization of styrene initiated with arenesulfonyl chlorides. From heterogeneous to homogeneous catalysis of special interest. Macromolecules. 29 (1996):3665-3668.

[67] H. Uegaki., Y. Kotani., M. Kamigaito., M. Sawamoto. $NiBr_2(Pn\text{-}Bu_3)_2$-mediated living radical polymerization of methacrylates and acrylates and their block or random copolymerizations. Macromolecules. 31 (1998):6756-6761.

[68] T. E. Patten., K. Matyjaszewski. Copper(I)-Catalyzed Atom Transfer Radical Polymerizations. Accounts of Chemical Research. 32 (1999):895-903.

[69] J. Xia., S. G. Gaynor., K. Matyjaszewski. Controlled "Living" radical polymerization. Atom transfer radical polymerization of acrylates at ambient temperature. Macromolecules. 31 (1998):5958-5959.

[70] J. Xia., X. Zhang., K. Matyjaszewski. The effect of ligands on copper-mediated atom transfer radical polymerization. ACS Symposium Series. 760 (2000):207-223.

[71] K. Matyjaszewski., Y. Nakagawa., S. G. Gaynor. Synthesis of well-defined azido and amino-end-functionalized polystyrene by atom transfer radical

polymerization. Macromolecular Rapid Communications. 18 (1997):1057-1066.

[72] M. G. Da Fonseca., M. M. De Oliveira, L. N. H. Arakaki. Removal of cadmium, zinc, manganese and chromium cations from aqueous by a clay mineral. Journal of Hazadous Materials. B134 (2006):288-292.

[73] Water Quality Standards [online]. Pollution control Department, Ministry of Natural Resources and Environment. Avaiable from: http://www.pcd.go.th/ info_serv/en_reg_std_water01.html. [2009, September 29]

[74] L. J. Norrby. Why is mercury liquid or why do relativistic effects not get into chemistry textbooks. Journal of Chemical Education. 68 (1991): 110.

[75] Mercury in the Environment and Toxic Effects [online]. U.S. Geological Survey. Avaiable from: http://www.usgs.gov/themes/factsheet/146-00/ [2009, September 30]

[76] W. R. Knocke., L. H. Hemphill. Mercury(II) sorption by waste rubber. Water Research. 15 (1981):275-282.

[77] S. M. Wilhelm. Mercury in petroleum and natural gas: Estimation of emissions from production, processing, and combustion. United State Environmental Protection Agency: Research and Development. EPA/600/R-01/099 (September 2001).

[78] P. Chongprasith., W. Utoomprurkporn., W. Wilairatanadilok. Mercury situation in Thailand [online]. Avaiable from: http://www.marinepcd.org/hgtaskforce/ document/Mercury situation in Thailand.doc [2009, September 30]

[79] H. B. Bradl. Heavy metals in the environment. Vol.6. Germany: Elsevier, 2004.

[80] I. Herrerra., J. L. Gardea-Torresdey., K. J. Tiemann., J. R. Peralta-Videa., V. Armendariz., J. G. Parsons. Binding of silver(I) ions by Alfalfa biomass (*Medicago Sativa*): batch pH, time, temperature and ionic strength studies. Journal of Hazardous Substance Research. 4 (2003):1-14.

[81] S. Begum. Silver removal from aqueous solution by adsorption on concrete particles. Turkish Journal of Chemistry. 27 (2003):609-617.

[82] T. L. Ho. Hard and Soft Acids and Bases Principle in Organic Chemistry. New York. USA. Academic Press, Inc.1997.

[83] Adsorption process [online]. Avaiable from: http://www.owlnet.rice.edu/chbe 402/ Hirasaki/AdsorpIsotherm.pdf [2009, September 24]

[84] What is adsorption [online]. Avaiable from: http://www.icecoldservice.com/ pdf/ 001p.pdf. [2009, September 24]

[85] Description of sorption data [online]. Avaiable from: http://www.fzd.de/pls/ rois/Cms [2009, September 24]

[86] Adsorption process [online]. Avaiable from: http://pradthana.wordpress.com/ 2008/ 04/13/adsorption-process/ [2009, September 24]

[87] W. W. Eckenfelder. Application of adsorption to wastewater treatment. Tenessee. Envivo Press. (1981)

[88] I. Langmuir. The adsorption of gases on plane surfaces of glass, mica and platinum. Journal of American Chemical Society. 40 (1918): 1361-1403.

[89] H. Freundlich. Adsorption solution. Zeitschrift für Physikalische Chemie. 57 (1906): 384-470.

[90] S. Goldberg., L. J. Criscenti., D. R. Turner., J. A. Davis., K. J. Cantrell. Adsorption-desorption process in subsurface reactive transport modeling. Vadose Zone Journal. 6 (2007):407-435.

[91] B. C. Smith. Fundamentals of Fourier Transformation Infrared Spectroscopy Book Description [online] Available from: http://www.infibeam.com/ Books/info/Brian-C-Smith/Fundamentals-of-Fourier-Transform-Infrared-Spectroscopy/0849324610.html [2009, October 30]

[92] Fourier Transform Infrared Spectroscopy [Online]. West Coast Analytical Service. Available from: http://www.wcaslab.com/tech/tbftir.htm [2009, October 30]

[93] D. M. Moore., J. R. C. Reynolds. X-Ray Diffraction and the Identification and Analysis of Clay Mineral. New York. Oxford University Press. (1985)

[94] X-ray Diffraction From a Crystal Lattice, Bragg's Equation [Online]. Available from: http://www.bruker-axs.de/fileadmin/user_upload/xrfintro/sec1_8.html [2009, September 30]

[95] Y. Li., Y. Fan., J. Ma. Thermal, physical and chemical stability of porous plystyrene-type beads with different degrees of crosslinking. Polymer Degradation and Stability 73 (2001): 163-167.

[96] R. Keller., J. Mermet., M. Otto., H. Widmer. Analytical chemistry. Weinheim: Wiley-VCH, 1998.

[97] Scanning Electron Mircoscopy (SEM) [online]. Available from: http://www. photometrics.net/sem.html [2009, September 30]

[98] M. T. Postek. Handbook of charged particle optics. Boca Raton: CRD Press, 1997.

[99] Basic operating principles of the sorpmatic [online]. Avaiable from: http://saf. chem.ox.ac.uk/Instruments/BETsorpoptprin.html [2009, September 30]

[100] H. Tavallani., H. Norozikhah. Design of cold vapor system and assembled on atomic absorption spectrometer for mercury determination in several waste water samples. International Journal of ChemTech Research. 1 (2009):390-393.

[101] Particulate mercury in workplace atmosphere [online]. Avaiable from: www.osha.gov/.../inorganic/id145/id145.html [2009, September 30]

[102] Atomic absorption spectroscopy [online]. Avaiable from: http://www.gmu.edu/ departments/SRIF/tutorial/aas/aas.htm [2009, September 30]

[103] The use of atomic absorption spectroscopy (AAS), in detecting concentrations of metal ions in solutions and assess its impact on scientific understanding of the effects of trace elements [online]. Avaiable from: http://www.hsc.csu. edu.au/.../chem943/943net.html [2009, September 30]

[104] A. D. Arelaro., E. Lima., L. M. Rossi., P. K. Kiyohara., H. R. Rechenberg. Ion dependence of magnetic anisotropy in MFe_2O_4 (M=Fe, Co, Mn) nanoparticles synthesized by high-temperature reaction. Journal of Magnetism and Magnetic Materials. 320 (2008):335-338.

[105] X. Wen., J. Yang., B. He., Z. Gu. Preparation of monodisperse magnetite nanoparticles under mild conditions. Current Applied Physics. 8 (2008):535-541.

[106] S. Ayyappan., J. Philip., B. Raj. A facile method to control the size and magnetic properties of $CoFe_2O_4$ nanoparticles. Materials Chemistry and Physics. 115 (2009):712-717.

[107] Z. Zi., Y. Sun., X. Zhu., Z. Yang., J. Dai., W. Song. Synthesis and magnetic properties of $CoFe_2O_4$ ferrite nanoparticles. Journal of Magnetism and Magnetic Materials. 321(2009):1251-1255.

[108] Y. Cedeno-Mattei., O. Perales-Perez. Synthesis of high-coercivity cobalt ferrite nanocrystals. Microelectronics Journal. 40 (2009):673–676.

[109] Y. C. Chuang., D. W. Chen. Preparation and adsorption properties of monodisperse chitosan-bound Fe_3O_4 magnetic nanoparticles for removal of Cu(II) ions. Journal of Colloid and Interface Science. 283 (2005):446-451.

[110] C. Huang., B. Hu. Silica-coated magnetic nanoparticles modified with mercaptopropyltriethoxysilane for fast and selective solid phase extraction of trace amounts of Cd, Cu, Hg, and Pb in environmental and biological samples prior to their determination by inductively coupled plasma mass spectrometry. Spectrochimica Acta Part B. 63 (2008):437-444

[111] A. Kraus., K. Jainae., F. Unob., N. Sukpirom. Synthesis of MPTS-modified cobalt ferrite nanoparticles and their adsorption properties in relation to Au(III). Journal of Colloid and Interface Science. 338 (2009): 359-365.

[112] H. Zhang., Y. Tu., X. Wan., Q. Zhou. Atom-transfer radical polymerization to synthesize novel liquid crystalline diblock copolymers with polystyrene

and Mesogen-jacketed liquid crystal polymer segments. Journal of Polymer Research. 9 (2002):11–15.

[113] P. D. Iddon., K. L. Robinson., S. P. Armes. Polymerization of sodium 4-styrenesulfonate via atom transfer radical polymerization in protic media. Polymer. 45 (2008):759-768.

[114] G. Li., L. Shi., Y. An., W. Zhang., R. Ma. Double-responsive core–shell–corona micelles from self-assembly of diblock copolymer of poly(t-butyl acrylate-co-acrylic acid)-b- poly(N-isopropylacrylamide). Polymer. 47 (2006):4581-4587.

[115] Y. Gao., H. Li., X. Wang. Synthesis and characterization of syndiotactic polystyrene- graft-poly(glycidyl methacrylate) copolymer by atom transfer radical polymerization. European Polymer Journal. 43 (2007):1258–1266.

[116] H. Y. Acar., R. S. Gaaras., F. Syud., P. Bonitatebus. Superparamagnetic nanoparticles stabilized by PEGylate coating. Journal of Magnetism and Magnetic Materials. 293 (2005): 1-7.

[117] S. Lu., R. Qu., J. Forcada. Preparation of magnetic polymeric composite nanoparticles by seeded emulsion polymerization. Material Letters. 63 (2009): 770-772.

[118] Y. Boguslavsky., S. Margel. Synthesis and characterization of poly(divinyl benzene)-coated magnetic iron oxide nanoparticles as precursor for the formation of air-stable carbon-coated iron crystalline nanoparticles. Journal of Colloid and Interface Science. 317 (2008): 101-114.

[119] S. Liu., X. Wei., M. Chu., J. Peng., Y. Xu. Synthesis and characterization of iron oxide/polymer composite nanoparticles with pendent functional groups. Colliods and Surface B : Biointerfaces. 51 (2006): 101-106.

[120] C. P. Chen., B. T. Ko., S. L. Lin., M. Y. Hsu., C. Ting. Hydrophilic polymer supports grafted by poly(ethylene glycol)derivatives via atom transfer radical polymerization. Polymer. 47 (2006):6630-6635.

[121] Z. Lei., S. Bi. Preparation of polymer nanocomposites of core-shell structure via surface- initiated atom transfer radical polymerization. Material letters. 61 (2007):3531-3534.

[122] Y. Zhou., S. Wang., B. Ding., Z. Yang. Modification of magnetite nanoparticles via surface-initiated atom transfer radical polymerization (ATRP). Chemical Engineering Journal. 138 (2008):578–585.

[123] K. Zhang., J. Ma., B. Zhang., S. Zho., Y. Li., Y. Xu., W. Yu., J. Wang. Synthesis of thermoresponsive silica nanoparticle/PNIPAM hybrids by aqueous surface-initiated atom transfer radical polymerization. Material letters. 61(2007):949-952.

[124] Z. Lei., Y. Li., X. Wei. A facile two-step modifying process for preparation of poly(SStNa)-grafted Fe_3O_4/SiO_2 particles. Journal of Solid State Chemistry. 181 (2008): 480-486.

[125] Y. Sun., X. Ding., Z. Zheng., X. Cheng., X. Hu., Y. Peng. Surface initiated ATRP in the synthesis of iron oxide/polystyrene core/shell nanoparticles. European Polymer Journal. 43 (2007):762–772.

[126] L. Garamszegi., C. Donzel., G. Carrot., T. Q. Nguyen. Synthesis of thiol end-functional polystyrene via atom transfer radical polymerization. Reactive & Functional Polymers. 55 (2003):179–183.

[127] A. Postma., T. P. Davis., G. Moad. Approaches to phthalimido and end-functional polystyrene by atom transfer radical polymerization. Reactive & Functional Polymers. 66 (2006):137-147.

[128] Y. Wang., J. Chen., J. Xiang., H. Li., Y. Shen., X. Gao., Y. Liang. Synthesis and characterization of end-functional polymers on silica nanoparticles via a combination of atom transfer radical polymerization and click chemistry. Reactive & Functional Polymers. 69 (2009):393–399.

[129] G. Bayramoglu., E. Yavuz., B. F. Senkal., M. Y. Arica. Glycidyl methacrylate grafted on p(VBC) beads by SI-ATRP technique: Modified with hydrazine as

a salt resistance ligand for adsorption of invertase. <u>Colloids and Surfaces A: Physicochemical and Engineering Aspects.</u> 345 (2009):127–134.

[130] B. Tang., L. Yuan., T. Shi., L. Yu., Y. Zhu. Preparation of nano-size magnetic particles from spent pickling liquors by ultrasonic-assisted chemical co-precipitation. <u>Journal of Hazardous Meterials.</u> 163 (2009): 1173-1178.

[131] P. Baldrian., V. Merhautova., J. Gabriel., F. Nerud., P. Stopka., M. Hruby., M.J. Benes. Decolorization of synthetic dyes by hydrogen peroxide with heterogeneous catalysis by mixed iron oxides. <u>Applied Catalysis B: Environmental.</u> 66 (2006): 258–264.

[132] M. Puanngam., F. Unob. Preparation and use of chemically modified MCM-41 and silica gel as selective adsorbents for Hg(II) ions. <u>Journal of Hazadous Materials.</u> 154 (2008):578-587.

[133] ASTM D3223-95, Standard test method for total mercury in water (Cold-vapor AA). <u>ASTM International.</u> (2007).

[134] A. E. Greenberg., L. S. Clescerl., A. D. Eaton. Standard methods for the examination of water and wastewater. 18th ed. New York., USA., EPS Group. Inc. (1982)

[135] S. B. Choudhury., D. Ray., A. Chakravorty, Sulfur-ligated nickel oxidation states. Chemistry of a family of $Ni_zS_2N_4$ $(z = +2, +3, +4)$ complexes incorporating hexadentate thioether-imine-oxime binding. <u>Inorganic Chemistry.</u> 30 (1991): 4354–4360.

[136] M. Rajendran., R.C. Pullar., A.K. Bhattachraya., D. Das., S.N. Chintalapudi., C.K. Majumdar. Magnetic property of nanocrytalline $CoFe_2O_4$ powder prepared at room temperature: variation of crystalline size. <u>Journal of Magnetism and Magnetic Materials.</u> 232 (2001): 71–83.

[137] J. Wang., T. Deng., Y. Lin., C. Yang., W. Zhan. Synthesis and characterization of $CoFe_2O_4$ magnetic particles prepared by co-precipitation method: Effect of

mixture procedure of initial solution. Journal of Alloy and Compounds. 450 (2008): 532-539.

[138] Y. Ren., X. Wei., M. Zhang. Adsorption character for removal Cu(II) by magnetic Cu(II) ion imprinted composite adsorbent. Journal of Hazardous Meterials. 158 (2008): 14-22.

[139] X. M. Liu., S. Y. Fu., H. M. XiAO., C.J. Huang. Synthesis of nanocrystalLine spinel $CoFe_2O_4$ via a polymer-pyrolysis route. Physica B. 370 (2005): 14-21.

[140] T. Ozkaya., M. Toprak., A. Baykal. Synthesis of Fe_3O_4 nanoparticles at 100 $^\circ$C and its magnetic characterization. Journal of Alloys and Compounds. 472 (2009): 18-23.

[141] T. Phothitontimongkol., N. Siebers., N. Sukpirom., F. Unob. Preparation and characterization of novel organo-clay minerals for Hg(II) ions adsorption from aqueous solution. Applied Clay Science. 43 (2009): 343–349.

[142] T. L. Ho. Hard and Soft Acids and Bases Principle in Organic Chemistry. New York. USA. Academic Press, Inc.1997.

[143] R. G. Pearson. Hard and Soft Acids and Bases. Stroudsville, PA. Dowden, Hutahinson and Ross. 1973.

[144] S. H. Huang., D. H. Chen. Rapid removal of heavy metal cations and anions from aqueous solutions by an amino-functionalized magnetic nano-adsorbent. Journal of Hazardous Materials. 163 (2009): 174-179.

[145] G. McKay., Y. S. Ho. The sorption of lead (II) on peat. Water Research. 33(1999): 578 -584.

[146] G. McKay., Y. S. Ho. Pseudo-second-order model for sorption processes. Process Biochemistry. 34(1999): 451-465.

[147] J. L. Barriada., R. Herrero. Interaction of mercury with chitin: A physichemical study of metal binding by a natural biopolymer. Reactive & Functional Polymer. 68 (2008): 1609-1618.

[148] A. Bollen., A. Wenke., H. Biester. Mercury speciation analyses of $HgCl_2$-contaminated soil and groundwater – Implication for risk assessment and remediation strategies. Water Research. 42 (2008): 91-100.

[149] P. Michard., E. Guibal., T. Vincent., P. Le Cloirec. Sorption and desorption of uranyl ions by silica gel : pH, particle size and porosity effect. Microporous Materials. 5 (1996): 309-324.

[150] Major constituents of seawater [online]. Avaiable from: http://www.answers.com/topic/seawater. [2009, September 10]

[151] Artificial sea-water [online]. Avaiable from: http://www.freepatentsonline.com/5351651.html [2009, September 10]

[152] The chemical composition of seawater [online]. Avaiable from: http://www.seafriends.org.nz/oceano/seawater.htm [2009, September 10]

[153] A. Beerbower., W. B. Jensen. The HSAB principle and extended solubility theory. Inorganica Chimica Acta. 75 (1983): 193-197.

[154] D. Sarkar., M. E. Essington., K. C. Misra. Adsorption of mercury(II) by kaolonite. Soil Science Society of America Journal. 64 (2000): 1968-1975.

[155] J. A. Dean. Lange's Handbook of Chemistry, 13th ed., Mc Graw-Hill Book Co, Singpore, 1987.

[156] N. P. Brandon., P. A. Francis., J. Jeffrey., Q. Yin. Thermodynamics and electrochemical behaviour of Hg-S-Cl-H_2O system. Journal of Electro analytical Chemistry. 497 (2001): 18-32.

[157] D. G. Kinniburgh. General propose adsorption isotherm. Environmental Science and Technology. 20 (1986): 895-904.

[158] J. C. Igwe., A. A. Abia. Adsorption isotherm studies of Cd(II), Pb(II) and Zn(II) ions bioremediation from aqueous solution using unmodified and EDTA-modified maize cob. Ecletica Quimica. 32 (2007): 33-42.

[159] A. M. Donia., A. A. Atia., K. Z. Elvakeel. Selective separation of mercury(II) using magnetic chitosan resin modified with shiff 's base derived from

thiourea and gluteraldehyde . Journal of Hazardous Matterials. 151 (2008): 372-379.

[160] Y. Zhai., X. Wei., G. Zeng., D. Zhang., K. Chu. Studies of adsorbent derived from sewage sludge for the removal of Cd^{2+}, Ni^{2+} in aqueous solution. Separation and Purification Technology. 38 (2004): 191-196.

[161] M. Iqbal., A. Saeed. FTIR spectrophotometry, kinetics and adsorption isotherm modeling, ion exchange, and EDX analysis for understanding and mechanism of Cd^{2+} and Pb^{2+} removal by mango peel waste. Journal of Hazardous Matterials. 164 (2009): 161-171.

[162] V. Vadivelan., K. V. Kumar., Y. J. Koay. Equilibrium, kinetics, mechanism, and process design for the sorption of methylene blue onto rice husk. Journal of Colliod and Interface Science. 286 (2005): 90-100.

[163] A. Denizli., K. Kesenci., Y. Arica., E. Piskin. Dithiocarbamate-incorperated nanosize polystyrene microsphere for selective removal mercury ions. Reactive & Functional Polymer. 44 (2000): 235-243.

[164] M. Akgul., A. Karabakan., O. Acar., Y. Yurum. Removal of silver(I) from aqueous solutions with cliloptilonite. Micorporous & Mesoporous Materials. 94 (2006): 99-104.

[165] A. R. Cestari., E. F. S.Vieira., E. C. N. Lopes., E. G. Da Silva. Kinetics and equilibrium parameters of Hg(II) adsorption on silica-dithizone. Journal of Colliod and Interface Science. 272 (2004): 271-276.

[166] A. M. Donia., A. A. Atia., K. Z. Elvakeel. Recovery of gold(III) and silver(I) on a chemically modified chitosan with magnetic properties. Hydrometallurgy. 87 (2007): 197-206.

[167] C. P. Jordao., R. B. Alves Fernandes., K. De Lima Libiero., B. De Souza Nascimento., P. M. de Barros. Zn(II) adsorption from synthetic solution and kaolin wastewater onto vermicompose. Journal of Hazardous Matterials. 162 (2009): 804-811.

[168] J. Zhu., J. Yang., B. Deng. Enhanced mercury ion adsorption by amine-modified activated carbon. <u>Journal of Hazardous Matterials.</u> 16 (2009): 866-872.

[169] A. M. Donia., T. Prasada Rao. Removal and recovery of mercury(II) form hazardous waste using 1-(2-thiazolylazo)-2-naphthol functionalized activated carbon as solid phase extractant. <u>Journal of Hazardous Matterials.</u> B113 (2004): 75-79.

[170] R. Say., E. Birlik., Z. Erdemgil., A. Denizli., A. Ersoz. Removal of mercury species with dithiocarbamate-anchored polymer/organosmectite composites. <u>Journal of Hazardous Matterials.</u> 150 (2008): 560-564.

[171] D. L. Guerra., R. R. Viana., C. Airoldi. Adsorption of mercury ion on chemically modified clay. <u>Matterials Research Bullitin.</u> 44 (2009): 485-491.

[172] A. Khan., F. Mahmood., M. Y. Khokhar., S. Hahmed. Functionalized sol-gel material for extraction of mercury(II). <u>Reactive & Functional Polymer.</u> 66 (2006): 1014-1020.

[173] L. N. H. Aakaki., V. S. A. Filha., K. S. de Sousa., F. P. Aguiar., M. G. Da Fonceca., J. G. P. Espinola. Silica gel ethyleneimine and its adsorption capacity for divalent Pb, Cd, and Hg. <u>Thermochimica Acta.</u> 440 (2006): 176-180.

[174] D. Perez-Quintanilla., I. del Hirerro., F. Carlillo-Hermosilla., M. Farjado., I. Sierra. Adsorption of mercury ions by mercapto-functionalized amorphous silica. <u>Analytical and Bioanalytical Chemistry.</u> 384 (2006): 827-838.

[175] M. A. Abd El-Ghaffar., Z. H. Abdel-Wahab., K. Z. Elvakeel. Extraction and separation studies of silver(I) and copper(II) form their aqueous solution using chemically modified melamine resins. <u>Hydrometallurgy.</u> 96 (2009): 27-34.

[176] A. Shukla., Y. H. Zhang., P. Dubey., J. L. Margrave., S. S. Shula. The role of sawdust in the removal of unwanted materials from water. <u>Journal of Hazardous Matterials.</u> B95 (2002): 137-152.

[177] S. Lagergren. Zur theorie der sogenannten adsorption gelöster stoffe, Kungliga Svenska Vetenskapsakademiens. Handlingar. 24 (1898): 1-39.

[178] Y. S. Ho., G. McKay. A comparison of chemisorption kinetic models applied to pollutant removal on various sorbents. Transaction of the Instutition of Chemical Engeneers. B76 (1998): 332-340.

[179] Y. S. Ho., G. McKay. Kinetics models for the sorption of dye from aqueous solution by wood. Transaction of the Instutition of Chemical Engeneers. B76 (1998): 183-191.

[180] Y. S. Ho., G. McKay. The kinetics of sorption of divalent metal ions onto Sphagnum Moss Peat. Water research. 34 (2000): 735-742.

[181] W. S. Wan Nagh., A. Kamari., Y. J. Koay. Equilibrium and kinetics studies of adsorption of copper(II) on chitosan and chitosan/PVA beads. International Journal of Biological Macromolecules. 34 (2000): 155-161.

[182] A. M. Donia., A. A. Atia., K. Z. Elwakeel. Gold (II) recovery using synthetic chekating resins with amine, thio and amine/mercaptan functionalities. Separation & Purification Technology. 42 (2005): 111-116.

[183] P. Bombicz., I. Mutikainnen., M. Krunks., T. Leskela., J. Madarasz., L. Niinisto. Synthesis, vibrational spectra and X-ray structure of copper(I) thiourea complexes. Inorganica Chimica Acta. 357 (2004): 513-525.

[184] Polarography of thiourea [online]. Downloaded by Chulalongkorn University. Avaiable from: http://pubs.acs.org/doi/abs/10.1021/ac60139a020. [2009, August 11]

[185] The stability of complexes of silver with thiobases [online]. Avaiable from: http://www.ias.ac.in/j_archive/currsci/33/13/399-400/viewpage.html [2009, August 11]

APPENDIX

Table A.1 Absorbance of Hg(II) in 1% HNO$_3$ determined at 253.7 nm by CVAAS

Concentration (ppm)	Absorbance[a]
0.00	0.002 ± 0.001
0.05	0.154 ± 0.013
0.10	0.315 ± 0.024
0.15	0.472 ± 0.030
0.20	0.607 ± 0.022
0.25	0.719 ± 0.019
0.30	0.823 ± 0.024

[a] Mean ± S.D. (n=27)
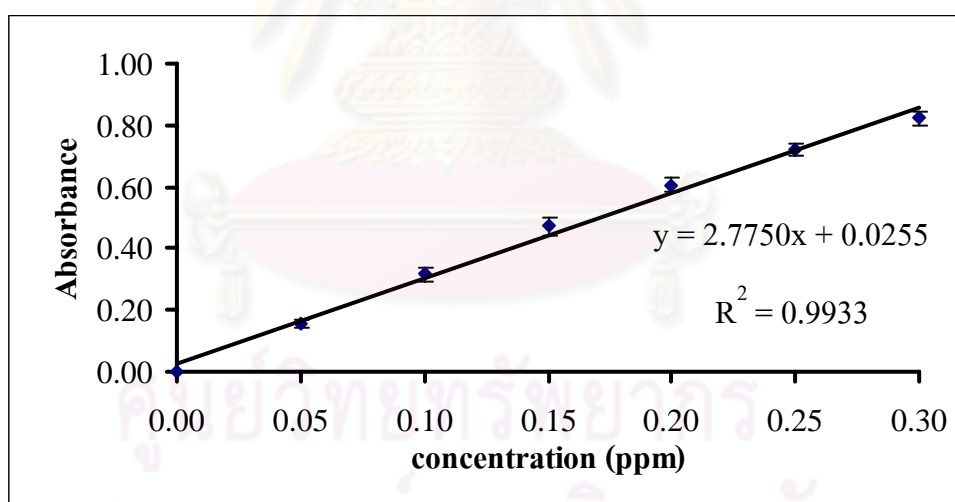
Figure A.1 Calibration curve of Hg(II) used in this work (average from all experiments)

Table A.2 Absorbance of Ag(I) in 1% HNO_3 determined at 328.1 nm by FAAS

Concentration (ppm)	Absorbance[a]
0.00	0.000 ± 0.000
0.50	0.026 ± 0.003
1.00	0.048 ± 0.005
1.50	0.070 ± 0.005
2.00	0.091 ± 0.007
2.50	0.113 ± 0.007
3.00	0.135 ± 0.009

[a] Mean $\pm$ S.D. (n=17)
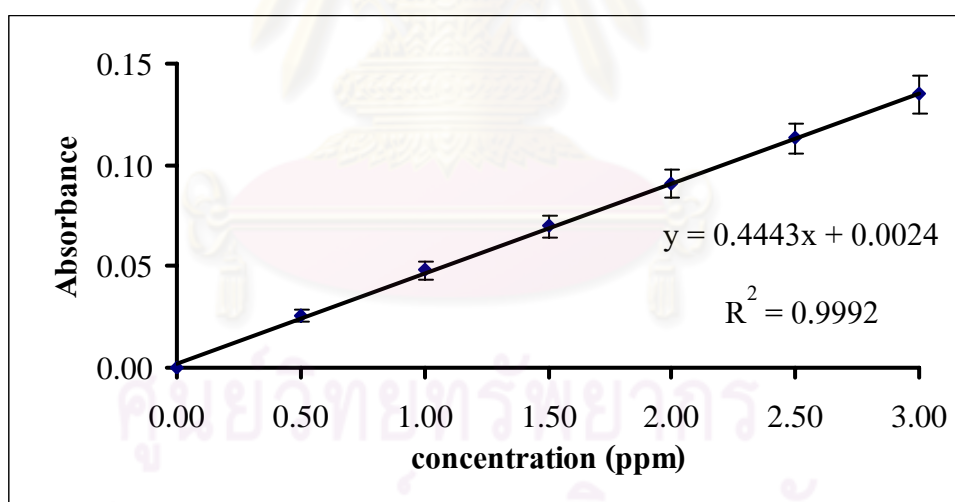

Figure A.2 Calibration curve of Ag(I) used in this work (average from all experiments)

Table A.3 The % extraction of Hg(II) and Ag(I) by different adsorbents and pH values related to Figure 4.9-4.10

Metals	MPs		MPs-PS		MPs-PS-AEPE	
	pH	%Extraction[a]	pH	%Extraction[a]	pH	%Extraction[a]
Hg(II)	1.11	4.55 ± 1.26	1.09	1.14 ± 0.47	1.07	53.26 ± 0.18
	2.09	5.55 ± 0.60	2.08	1.62 ± 0.24	2.07	53.98 ± 0.19
	3.08	6.04 ± 0.88	3.03	1.24 ± 0.40	3.06	54.72 ± 0.19
	4.02	9.56 ± 0.87	4.04	1.30 ± 0.80	4.05	56.47 ± 0.19
	5.08	11.86 ± 1.52	5.03	1.21 ± 0.50	5.06	59.34 ± 0.26
	6.06	19.06 ± 1.10	6.01	2.05 ± 0.34	6.11	64.60 ± 0.78
	7.06	20.28 ± 1.16	7.08	1.38 ± 0.57	7.11	89.51 ± 0.04
	7.63	19.21 ± 1.21	7.63	1.38 ± 0.49	7.65	89.83 ± 0.20
Ag(I)	1.01	2.03 ± 1.50	1.04	5.95 ± 3.96	1.02	62.48 ± 3.00
	2.28	8.20 ± 1.99	2.10	7.56 ± 1.67	2.27	70.40 ± 1.11
	3.30	10.31 ± 1.94	3.25	9.99 ± 1.12	3.23	78.76 ± 2.02
	4.10	20.00 ± 1.64	4.10	12.22 ± 1.44	4.12	80.84 ± 1.97
	5.17	27.88 ± 1.44	5.16	16.53 ± 2.01	5.15	85.88 ± 1.44
	6.10	25.92 ± 1.43	5.96	17.20 ± 1.87	6.06	85.73 ± 0.54
	7.04	23.27 ± 2.47	6.96	15.10 ± 0.98	6.91	85.36 ± 1.13
	7.64	25.42 ± 2.21	7.63	15.22 ± 1.91	7.64	84.11 ± 0.95

[a] Mean ± S.D. (n=3)

Table A.4 The % extraction of Hg(II) and Ag(I) by MPs-PS-AEPE at different times related to Figure 4.12

Time (min)	% Extraction[a]	
	Hg(II)	Ag(I)
5	83.75 ± 0.28	66.02 ± 1.32
10	86.97 ± 0.17	69.13 ± 0.77
15	88.48 ± 0.25	73.41 ± 1.55
30	90.40 ± 0.18	79.89 ± 1.02
45	90.34 ± 0.19	81.08 ± 0.77
60	90.40 ± 0.17	82.11 ± 1.02
90	90.34 ± 0.17	82.11 ± 1.11
120	90.33 ± 0.11	82.54 ± 1.11
150	90.38 ± 0.13	83.14 ± 1.55
180	90.33 ± 0.11	83.43 ± 1.11

[a] Mean ± S.D. (n=3)

Table A.5 The % desorption of Ag(I) at different times related to Figure 4.21

Desorption time (min)	% Desorption[a]
15	78.46 ± 2.40
30	81.87 ± 2.17
45	84.45 ± 1.80
60	87.07 ± 3.16
90	89.25 ± 3.12
120	89.93 ± 2.89
150	90.02 ± 1.90
180	90.25 ± 1.44

[a] Mean $\pm$ S.D. (n=3)

Table A.6 The % extraction and desorption of Hg(II) and Ag(I) related to Figure 4.22

Cycles	Hg(II)		Ag(I)	
	% Extraction[a]	%Desorption[a]	% Extraction[a]	%Desorption[a]
1	79.15 ± 0.18	99.25 ± 0.76	80.67 ± 1.42	84.70 ± 0.88
2	78.78 ± 0.08	98.67 ± 1.02	71.10 ± 1.24	73.80 ± 1.19
3	78.63 ± 0.19	98.38 ± 1.78	61.92 ± 0.81	66.72 ± 1.06
4	78.53 ± 0.11	98.44 ± 1.21	53.43 ± 0.81	59.75 ± 2.14
5	78.48 ± 0.11	99.60 ± 0.92	46.68 ± 0.47	53.73 ± 2.64
6	80.18 ± 0.13	99.14 ± 0.45	41.38 ± 1.24	48.73 ± 2.52
7	80.01 ± 0.08	95.91 ± 0.53	-[b]	-[b]
8	79.64 ± 0.20	93.27 ± 0.98	-[b]	-[b]
9	79.27 ± 0.58	92.35 ± 1.99	-[b]	-[b]
10	77.93 ± 0.51	89.42 ± 3.66	-[b]	-[b]

[a] Mean ± S.D. (n=3)

[b] There is no experiment.

VITA

Mr. Kunawoot Jainae was born on October 13, 1984 in Nakhonsithammarat, Thailand. He received his Bachelor degree of Science in Chemistry from Chulalongkorn University in 2006. After that, he has been a graduate student at the Program of Petrochemistry and Polymer Science, Faculty of Science, Chulalongkorn University and a member of Environmental Analysis Research Unit (EARU). During his postgraduate study, he was elected as the student president. In 14-16 January 2009, he attended Pure and Applied Chemistry International Conference held by Naresuan University in the title of "Synthesis of polystyrene-coated magnetic particles modified with 2-(3-(2-aminoethylthio)propylthio)ethanamine for Ag(I) extraction" by poster presentation. In 15-17 October 2009, he attended the 35th Congress on Science and Technology of Thailand held by Burapha University in the title of "Polystyrene-coated magnetic particles modified with 2-(3-(2-aminoethylthio)propylthio)ethanamine for Ag(I) extraction" by poster presentation. Furthermore, in 21-23 January 2010, he attended Pure and Applied Chemistry International Conference held by Ubonratchathani University in the title of "Mercury(II) extraction using polystyrene-coated magnetic particles modified with 2-(3-(2-aminoethylthio)propylthio) ethanamine as adsorbent" by poster presentation. He finished his postgraduate study with the Master degree of Science in 2009. His present address is 240/1 Rod-phai Road, Tambol Sichon, Amphur Sichon, Nakhonsithammarat, Thailand, 80120. Contact number is 085-839 5561.